European Commission

JRC TECHNICAL REPORTS

System Vicarious Calibration for Copernicus Ocean Colour Missions

Updated Requirements and Recommendations for a European Site

Giuseppe Zibordi, Frédéric Mélin and Marco Talone

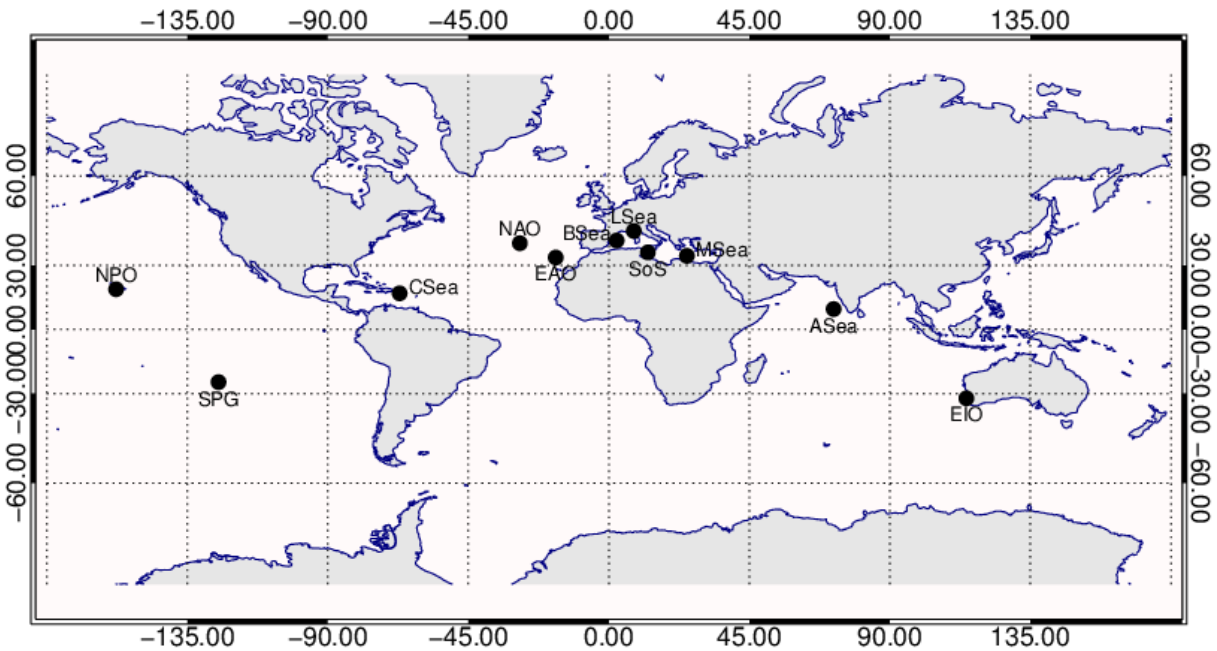

2017

EUR 28851 EN

Joint Research Centre

This publication is a Technical Report by the Joint Research Centre (JRC), the European Commission's science and knowledge service. It aims to provide evidence-based scientific support to the European policymaking process. The scientific output expressed does not imply a policy position of the European Commission. Neither the European Commission nor any person acting on behalf of the Commission is responsible for the use that might be made of this publication.

JRC Science Hub
https://ec.europa.eu/jrc

JRC108912

EUR 28851 EN

PDF	ISBN 978-92-79-75340-4	ISSN 1831-9424	doi:10.2760/145183
Print	ISBN 978-92-79-75341-1	ISSN 1018-5593	doi:10.2760/319494

Luxembourg: Publications Office of the European Union, 2017

© European Union, 2017

The reuse of the document is authorised, provided the source is acknowledged and the original meaning or message of the texts are not distorted. The European Commission shall not be held liable for any consequences stemming from the reuse.

How to cite this Report: Giuseppe Zibordi, Frédéric Mélin and Marco Talone, *System Vicarious Calibration for Copernicus Ocean Colour Missions: Updated Requirements and Recommendations for a European Site*, EUR 28851 EN, doi:10.2760/145183, 2017

All images © European Union 2017

Joint Research Centre

Contents

Acknowledgements …….. 2

Summary ……. 3

1. Introduction 5

2. System Vicarious Calibration 6

3. In situ Radiometry 9

4. Location for a European Site 12

5. Conclusions 16

References 18

List of abbreviations and definitions 20

Annex 1 20

System vicarious calibration for ocean colour climate change applications: Requirements for in situ data. Reprinted from *Remote Sens. Environ.* 159, 361–369 (2015) 20

Annex 2 33

Impact of spectral resolution of in situ ocean color radiometric data in satellite matchups analyses. Reprinted from *Optics Express* 25, A798-A812 (2017) 35

Annex 3 51

An evaluation of marine regions relevant for ocean colour system vicarious calibration. Reprinted from *Remote Sens. Environ.* 190, 122–136 (2017) 53

Acknowledgements

The content of this Report summarizes results published in peer review literature by the same authors in collaboration with a number of colleagues whose contribution is duly acknowledged. Specifically, grateful thanks are due to: K.J. Voss (University of Miami, Coral Gables, FL), B. C. Johnson (National Institute of Standards and Technology, Gaithersburg, MD), B. A. Franz (National Aeronautics and Space Administration, Greenbelt, MD), E. Kwiatkowska (Eumetsat, Darmstadt, Germany), J.-P. Huot (European Space Agency, Noordwijk, The Netherlands), M. Wang (National Oceanic and Atmospheric Administrations, College Park, MD) and D. Antoine (Curtin University, Perth, Australia).

Particular acknowledgments are due to K. J. Voss and B. C. Johnson who provided a number of suggestions improving the quality of this Report.

This Report, which is an update of the previous Report EUR28433, is a contribution to *Earth Observation Support to Copernicus Climate and Marine Services* (EOSS) funded by the Joint Research Centre (JRC).

Summary

The Copernicus Program has been established through the Regulation EU No377/2014 with the objective to ensure long-term and sustained provision of accurate and reliable data on environment and security through dedicated services. Among these, the Copernicus Marine Environment Monitoring Service and the marine component of the Climate Change Service, both rely on satellite ocean colour observations to deliver data on water quality and climate relevant quantities such as chlorophyll-a concentration used as a proxy for phytoplankton biomass.

Satellite ocean colour missions require in situ highly accurate radiometric measurements for the indirect calibration (so called System Vicarious Calibration (SVC)) of the space sensor. This process is essential to minimize the combined effects of uncertainties affecting the space sensor calibration and those resulting from the inaccuracy of processing algorithms and models applied for the generation of data products.

SVC is thus a fundamental element to maximize the return on investments for the Copernicus Program by delivering to the user science community satellite ocean colour data with accuracy granting achievement of target objectives from applications addressing environmental and climate change issues.

The long-term Copernicus Program foresees multiple ocean colour missions (i.e., the Sentinel-3 satellites carrying the Ocean and Land Colour Instrument (OLCI)). The need to ensure the highest accuracy to satellite derived data products contributing to the construction of Climate Data Records (CDRs), suggests the realization, deployment and sustain of a European in situ infrastructure supporting SVC for Sentinel-3 missions, fully independent from similar facilities established and maintained by other space agencies (e.g., that operated in the Pacific Ocean by US agencies). It is emphasized that the need to cope with long-term Copernicus objectives on data accuracy, implies very stringent requirements for the in situ infrastructure and location providing reference measurements for SVC. These requirements, in fact, are much higher than those imposed by SVC for a single mission.

The content of this Report, which is a revised version of a previous one (Zibordi et al. 2017), builds on the long-standing experience of the JRC on ocean colour radiometry. This experience counts on decadal field and laboratory measurements performed in support of validation and SVC applications, and additionally on activities comprehensively embracing measurement protocols, instruments characterization and the initiation of autonomous measurement infrastructures. Overall, this Report summarizes a number of recent investigations led by the JRC on SVC requirements for the creation of CDRs. The final objective is to consolidate in a single document the elements essential for the realization of a European SVC infrastructure in support of the Copernicus Program.

Briefly, the various Chapters summarize:

- General requirements for a long-term SVC infrastructure, which indicate the need for spatially homogenous oceanic optical properties, seasonal stability of marine and atmospheric geophysical quantities, negligible land perturbations, hyperspectral radiometry, and low measurement uncertainties;
- Spectral resolution requirements for in situ SVC hyperspectral measurements as a function of bandwidths and center-wavelengths of most advanced satellite sensors, which specify the need for sub-nanometre resolutions to allow for supporting any scheduled satellite ocean color sensor;
- Suitable SVC locations in European Seas showing the fitness of regions in the Eastern Mediterranean Sea to satisfy fundamental requirements.

1. Introduction

Understanding of climate change is a problem for multiple generations. One generation of scientists has to make provisions for the needs of successor generations, rather than focusing solely on its own immediate scientific productivity (C. Wunsch, R. W. Schmitt, and D. J. Baker. Climate change as an intergenerational problem. Proceedings of the National Academy of Sciences of the United States of America, 110, 4435 – 4436, 2013).

The spectral water-leaving radiance L_W or alternatively the derived remote sensing reflectance R_{RS}, quantify the light emerging from the sea retrieved from the top of the atmosphere radiance L_T detected by a satellite ocean colour sensor. L_W and R_{RS} are then the primary ocean colour data products applied to determine geophysical quantities such as the near-surface chlorophyll-a concentration (*Chla*) used as a proxy for phytoplankton biomass. Consequently, the accuracy of derived quantities depends on the accuracy of primary radiometric products.

Both L_w and *Chla* are listed among Essential Climate Variables (ECVs) by the World Meteorological Organization (WMO 2016). Requirements for L_w, defined for oceanic waters in the blue-green spectral bands, specify a 5% maximum uncertainty and additionally a radiometric stability better than 0.5% per decade. While the first requirement ensures the quantification of geophysical quantities with uncertainties suitable to support environmental applications, the requirement on stability is essential for the creation of long-term data records to address climate change investigations (Ohring 2005).

Uncertainties affecting the calibration of the satellite sensor together with uncertainties associated with the removal of atmospheric perturbations, both limit the capability to meet accuracy requirements of derived data products. The previous limitations are resolved through the so-called System Vicarious Calibration (SVC). This leads to the determination of gain-factors *g* (i.e., *g*-factors) applied to adjust the absolute radiometric calibration coefficients of satellite sensors. The *g*-factors are mission specific, and determined from the ratio of measured to simulated top-of-the atmosphere radiance. Where, specifically, simulated L_T values are computed relying on: *i*. highly accurate *in situ* L_w reference measurements; and *ii*. the same atmospheric models and algorithms as applied for the atmospheric correction of satellite data.

In situ reference radiometric measurements are thus central to SVC. The present Report, which is a revised version of a previous one (Zibordi et al. 2017), summarizes key elements to consider for the definition of an SVC site (i.e., infrastructure and region, both satisfying in situ measurement requirements for SVC) with specific reference to European seas and Copernicus ocean colour missions. Focus is given to *i.* fundamental requirements for in situ data, *ii.* specific radiometric needs in terms of spectral resolution of in situ radiometers and *iii*. the identification of potential European geographic regions relevant for SVC in support of the construction of data records from multiple satellite ocean colour missions.

This Report when compared to the previous version, includes an expanded number of potential SVC sites. Additionally, it includes integral copy of the journal articles summarized in the main chapters.

2. System Vicarious Calibration

By considering oligotrophic waters, Gordon and Clark (1981), Gordon et al. (1983) and Gordon (1987) indicated a 5% uncertainty for L_W in the blue spectral region to allow for the determination of *Chla* concentration with a 35% maximum uncertainty. Following the objectives of the Sea-viewing Wide Field-of-view Sensor (SeaWiFS) mission (Hooker et al. 1992), spectrally independent 5% uncertainties in satellite-derived L_W have become a science requirement for the ocean colour community. Achievement of such an uncertainty target is however challenged by the uncertainty affecting the absolute radiometric calibration of satellite optical sensors (i.e., approximately 2-3% (Butler et al. 2007, Eplee et al. 2011, Esposito et al. 2004) and by the uncertainty affecting the removal of atmospheric effects in L_T (i.e., also larger than a few percent (IOCCG 2010)).

SVC is commonly applied to solve the previous uncertainty issues. In fact, SVC leads to the determination of *g*-factors to adjust the absolute radiometric calibration coefficients of satellite sensors (Gordon 1998) through simulation of top-of-atmosphere L_T. As already stated, this process requires: *i*. highly accurate *in situ* L_W measurements; and *ii*. the same atmospheric models and algorithms as applied for the atmospheric correction of satellite data. The *g*-factors, given by the ratio of simulated to measured spectral L_T values, are applied to the top of atmosphere radiances L_T after full instrument calibration following pre-launch calibration and characterization, and successive corrections for temporal changes in radiometric sensitivity. Because of this, SVC minimizes the combined effects of: *i*. uncertainties due to the absolute pre-flight radiometric calibration and characterization; and *ii*. inaccuracy of the models and algorithms applied in the atmospheric correction process. Thus, assuming equivalent observation conditions characterizing both SVC and atmospheric correction processes, SVC forces the determination of satellite-derived L_W with an uncertainty comparable to that of the *in situ* reference L_W measurements. It is noted that re-computation of *g*-factors is required after any change in the models or algorithms applied for the atmospheric correction, or any significant change in instrument calibration or temporal response model.

As already anticipated in the introduction, current requirements for the generation of Climate Data Records (CDRs) of Essential Climate Variables (ECVs) such as satellite-derived L_W (WMO, 2016), include:

1. Radiometric uncertainty lower than 5% in the blue and green spectral regions in oceanic waters;
2. Radiometric stability better than 0.5% over a decade.

Different from the 5% maximum uncertainty requirement, which is commonly accepted by the satellite ocean colour community, the uncertainty required for *g*-factors to support the creation of CDRs through different missions still creates debates.

Uncertainty issues have been discussed (see Zibordi et al. 2015) using *g*-factors computed with various data sources within the framework of different investigations, but applying the same processing code (i.e., SeaDAS): *i*. the Marine Optical Buoy (MOBY, Clark et al. 1997); *ii*. the Buoy for the Acquisition of a Long-Term Optical Time Series (Bouée pour L'acquisition de Séries Optiques à Long Terme, BOUSSOLE, Antoine at al. 2008), iii. the multi-site and multi-instrument NASA bio-Optical Algorithm Data set (NOMAD, Werdell and Bailey 2005); iv. the Ocean Colour component of the Aerosol Robotic Network (AERONET-OC, Zibordi et al. 2009); v. the U.S. Joint Global Ocean Flux Study (JGOFS) Bermuda Atlantic Time-series Study (BATS, Werdell et a. 2007); and *vi*. the Hawaiian Ocean Time-series (HOT, Werdell et a. 2007).

Percent differences between *g*-factors determined from MOBY data and those from other data sources are summarized in Table 1.

Table 1. Relative percent differences $\Delta g(\lambda)$ between SeaWiFS *g*-factors determined for the various sensor bands at center-wavelengths λ from different data sources and those determined with Marine Optical Buoy (MOBy) data (adapted from Zibordi et al. 2015).

Data Source	$\Delta g(412)$ [%]	$\Delta g(443)$ [%]	$\Delta g(490)$ [%]	$\Delta g(510)$ [%]	$\Delta g(510)$ [%]	$\Delta g(670)$ [%]
BOUSSOLE	+0.33	-0.03	+0.43	+0.33	+0.14	-0.59
NOMAD	+0.26	+0.03	+0.49	-0.20	-0.04	-0.37
AAOT	+0.55	+0.11	+0.51	-0.05	+0.41	+0.93
HOT-ORM	-0.66	-0.45	-0.39	-0.03	+0.53	-0.11
BATS-ORM	-0.22	-1.11	-1.05	-0.41	+0.23	+0.02

The difference shown in Table 1 appears quite minor. However, an uncertainty of 0.3% affecting L_T (i.e., a value that often occurs in Table 1), may already challenge the 5% uncertainty requirement in satellite-derived L_W in the blue spectral region (with the rule of thumb that L_w is one order of magnitude lower than L_T). Additionally, a 0.3% uncertainty in L_T in the blue-green spectral regions, may introduce mission dependent biases of several percent in multi-mission CDRs. These biases would affect the radiometric stability of multi-mission satellite-derived products even when applying the same atmospheric correction code to the processing of data. Further, spectral differences affecting the values of Δg, may become the source of spectral inconsistencies in CDRs.

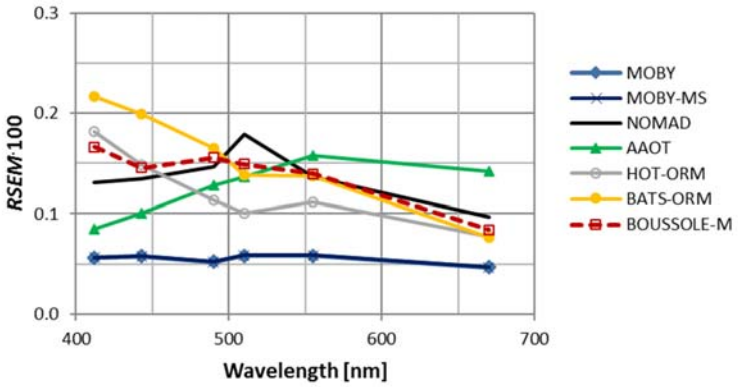

Figure 1. Plot of the standard percent error of the mean (*RSEM*) for the SeaWiFS *g*-factors (except BOUSSOLE-M) determined with the various data sources (adapted from Zibordi et al. 2015).

The stability requirement for the construction of CDRs from different satellite missions is hereafter discussed through the relative standard error of the mean (*RSEM*) of the *g*-factors *g* applied for the determination of the Δg values given in Table 1. Specifically, *RSEM* is computed as

$$RSEM = (\sigma_g/\mathrm{g})/\sqrt{N_y}$$

where σ_g is the standard deviation of *g* assumed invariant with time for each considered data source, and N_y is the scaled number of match-ups per decade (i.e., $N_y=10 \cdot N/Y$ where *N* is the number of actual matchups and *Y* the number of measurement years). It is specified that the scaling of the number of matchups over a decade, has been applied assuming an ideal continuous availability of measurements for each *in situ* data source during the considered period, regardless of the time-limited availability of some *in situ* data (which implies that continuous operation and delivery of measurements are required for any *in situ* SVC data source contributing to the creation of CDRs).

The RSEM spectra displayed in Fig.1 exhibit large differences across the various data sources. The relevance of these differences can be discussed through the 0.5% stability requirement over a decade. This requirement implies (standard) uncertainties lower than 0.05, 0.025 and 0.005% for *g*-factors determined in oligotrophic/mesotrophic waters in the blue, green and red spectral regions, respectively. By considering Fig. 1, the previous uncertainties are comparable to the *RSEM* values determined for MOBY in the blue-green spectral regions during approximately 10 years. Conversely, they are significantly lower than those determined from the other *in situ* data sources included in the analysis. These results suggest: *i*. the use of long-term highly consistent *in situ* data for SVC to minimize uncertainties in *g*-factors determined for different satellite missions; and *ii*. the inappropriateness of sole or multiple data sources referred to measurement conditions difficult to reproduce during the time frame of different missions.

In conclusion, the *RSEMs* determined with MOBY data suggest high measurement precision likely explained by very stable measurement conditions, systematic calibration and characterization of field radiometers, robust quality assessment of field measurements and quality control of data products. Conversely, the higher *RSEM* values resulting from the other data sources are likely explained by: *i*. measurement conditions perturbed by intra-annual changes in the marine and atmospheric optical properties or observation geometry; *ii*. instability of the *in situ* measurement system due to environmental perturbations or different performances of radiometer systems during successive deployments, or by the application of different measurement methods when considering in situ data sets resulting from multiple sources; *iii* or lastly a relatively small number of matchups N_y per decade. It is specified that the BOUSSOLE *RSEM* values displayed in Fig. 1 (i.e., BOUSSOLE-M) refer to *g*-factors determined for the Medium Resolution Imaging Spectrometer (MERIS).

The previous findings indicate that any element affecting the reproducibility of measurements and thus challenging the precision of *in situ* reference measurements, should be minimized. This would diminish the impact of perturbations that affect the random component of uncertainties for *g*-factors and thus increase the stability of CDRs from multi-mission satellite-derived data.

Overall, Zibordi et al. (2015) concluded that *the creation of ocean colour CDRs should ideally rely on:*

- *One main long-term in situ calibration system (site and radiometry) established and sustained with the objective to maximize accuracy and precision over time of g-factors and thus minimize possible biases among satellite data products from different missions;*
- *and unique (i.e., standardized) atmospheric models and algorithms for atmospheric corrections to maximize cross-mission consistency of data products at locations different from that supporting SVC.*

Additionally, accounting for the overall results presented in Zibordi et al. (2015) and in previous literature, *an ideal ocean colour SVC site should meet the following general requirements:*

- *Located in a region chosen to maximize the number of high-quality matchups by trading off factors such as best viewing geometry, sun-glint avoidance, low cloudiness, and additionally set away from any continental contamination and at a distance from the mainland to safely exclude any adjacency effect in satellite data;*
- *Exhibiting known or accurately modelled optical properties coinciding with maritime atmosphere and oligotrophic/mesotrophic waters, to represent the majority of world oceans and minimize relative uncertainties in computed g-factors;*
- *Characterized by high spatial homogeneity and small environmental variability, of both atmosphere and ocean, to increase precision of computed g-factors.*

3. In Situ Radiometry

The extremely high accuracy requirements of in situ radiometry supporting SVC, advocates the application of state-of-the-art measurement technologies, data reduction methods and quality assurance/control schemes. In view of meeting uncertainty targets, Zibordi et al. (2015) summarized the following wide-range requirements for *in situ* radiometric measurements:

i. *Hyperspectral field data with sub-nanometre resolution to allow system vicarious calibration of any satellite ocean colour sensor regardless of its center-wavelengths and spectral responses, and thus ensure minimization of inter-band uncertainties;*
ii. *State-of-the-art absolute calibration traceable to National Metrology Institutes (i.e., tentatively with target standard calibration uncertainty lower than 2% for radiance and stability better than 0.5% per deployment) and comprehensive characterizations of radiometers in terms of linearity, temperature dependence, polarization sensitivity and stray light effects, in view of minimizing measurement uncertainties and allowing for accurate determinations of uncertainty budgets;*
iii. *Application of quality assurance/control schemes minimizing effects of measurement perturbations like those (when applicable) due to infrastructure shading, radiometer self-shading, wave perturbations, bio-fouling, and additionally scheduling regular checks of in situ systems and frequent swap of radiometers, as best practice to maximize long-term accuracy and precision of in situ reference radiometric data;*
iv. *Data rate ensuring generation of matchups for any satellite ocean colour mission with time differences appropriate to minimize variations in bi-directional effects due to changes in sun zenith and daily fluctuations in the vertical distribution of phytoplankton.*

Any uncertainty resulting from the poor-application of previous requirements, may affect the comparability of matchups of in situ and satellite radiometric data at the basis of any SVC activity. For instance, differences between widths, shapes and center-wavelengths of corresponding in situ and satellite spectral bands, may become the source of uncertainties affecting *g*-factors. Spectral differences can certainly be minimized through in situ hyperspectral data. In fact, when compared to multispectral measurements, in situ hyperspectral data allow for determining L_W or R_{RS} in satellite sensor spectral bands with an accuracy increasing with the spectral resolution determined by the bandwidth $\Delta\lambda_B$ and the spectral sampling interval $\Delta\lambda_C$ (i.e., the distance between center-wavelengths of adjacent bands) of the in situ sensor. Thus, SVC ideally requires hyperspectral in situ radiometric data.

In view of contributing to the quantification of the uncertainty budget of in situ reference measurements, a recent work by Zibordi et al. (2017b) has investigated the impact of spectral resolution of in situ radiometric data in the determination of R_{RS} at bands representative of ocean colour sensors. The work focused on the visible spectral bands of the Ocean Land Colour Imager (OLCI) from the European Space Agency (ESA) operated onboard Sentinel-3 since 2016, and of the Plankton, Aerosol, Cloud, ocean Ecosystem (PACE) of the National Aeronautics and Space Administration (NASA) planned from 2022. Relative spectral response functions for OLCI and PACE-like bands are illustrated in Fig. 2 excluding any out-of-band response. Considering that PACE bands are not yet finalized, PACE-like bands have been ideally defined assuming 5 nm width Gaussian spectral response functions, and 5 nm spectral sampling interval. This solution leads to an oversampling of R_{RS} spectra with respect to the future PACE capabilities.

Uncertainty analysis have been performed in the 380–700 nm spectral region with in situ reference R_{RS} spectra from the Marine Optical Buoy (MOBy, Clark et al. (1997)) collected in ultra-oligotrophic waters with the Marine Optical System (MOS) characterized by a bandwidth $\Delta\lambda_B$ of 1 nm and a spectral sampling interval $\Delta\lambda_C$ of approximately 0.6 nm.

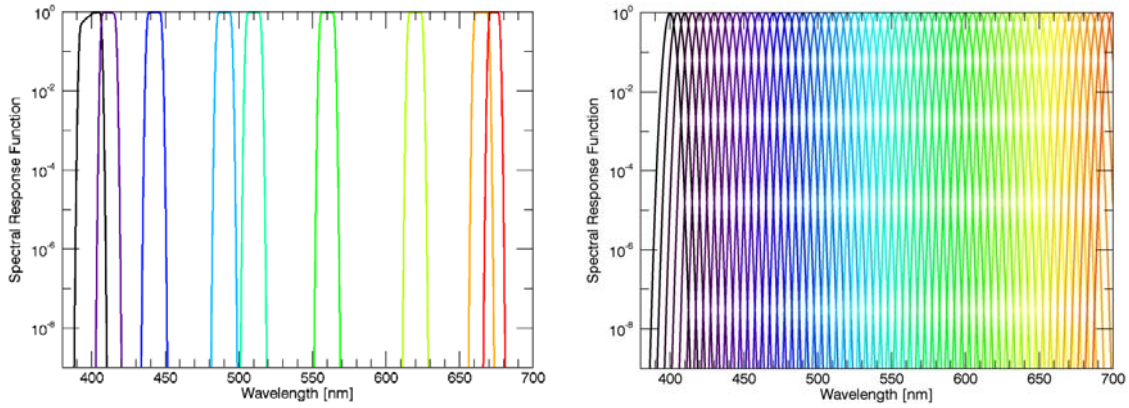

Figure 2. Relative spectral response functions of the visible OLCI sensor (*left panel*) exhibiting typical 10 nm bandwidth in the visible spectral region, and the PACE-like (*right panel*) bands with 5 nm bandwidth from the ultraviolet to near-infrared (after Zibordi et al. 2017b).

MOBy full resolution spectra have been applied to compute "exact" satellite R_{RS} for both OLCI and PACE-like bands, and additionally, to compute R_{RS} for ideal in situ hyperspectral radiometers characterized by Gaussian spectral response, various bandwidths $\Delta\lambda_B$ and different sampling intervals $\Delta\lambda_C$. These latter reduced resolution spectra have then been used to determine "equivalent" satellite R_{RS}. Percent differences ε between "equivalent" and "exact" R_{RS} determined for OLCI or PACE-like bands from full and reduced resolution in situ spectra, respectively, have allowed drawing conclusions on spectral resolution requirements for in situ radiometry supporting SVC.

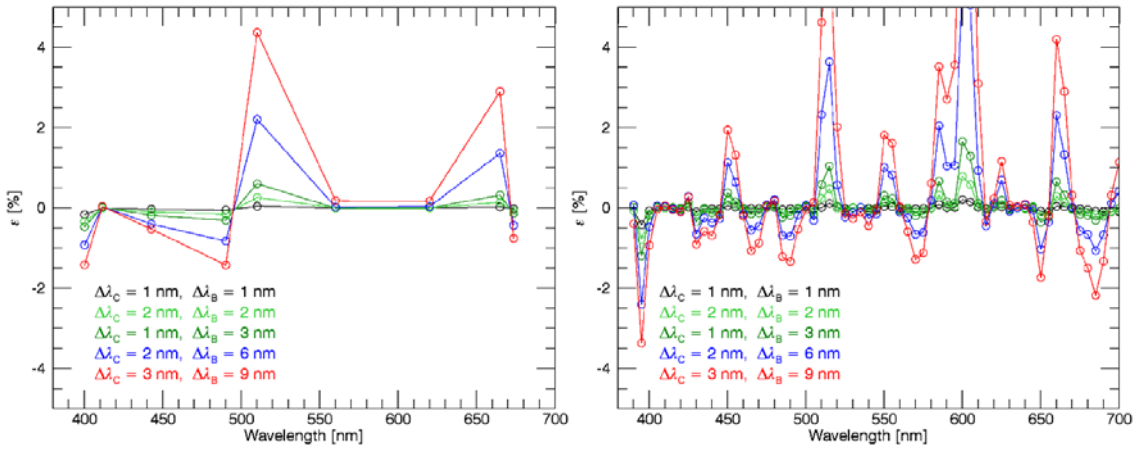

Figure 3. Percent differences ε between "equivalent" and "exact" R_{RS} determined for OLCI (*left panel*) or PACE-like (*right panel*) bands. Different colours refer to results for various bandwidths $\Delta\lambda_B$ and spectral sampling intervals $\Delta\lambda_C$ of the in situ hyperspectral sensor (after Zibordi et al. 2017b).

Results for OLCI bands (see Fig. 3, left panel) indicate values of ε increasing with bandwidth and sampling interval of the in situ sensor. The values of ε determined with $\Delta\lambda_B$ = 9 nm and $\Delta\lambda_C$ = 3 nm slightly exceed 4% at 510 nm. In the most favourable case given by $\Delta\lambda_B$ = 1 nm and $\Delta\lambda_C$ = 1, ε does not generally exceed 0.1%.

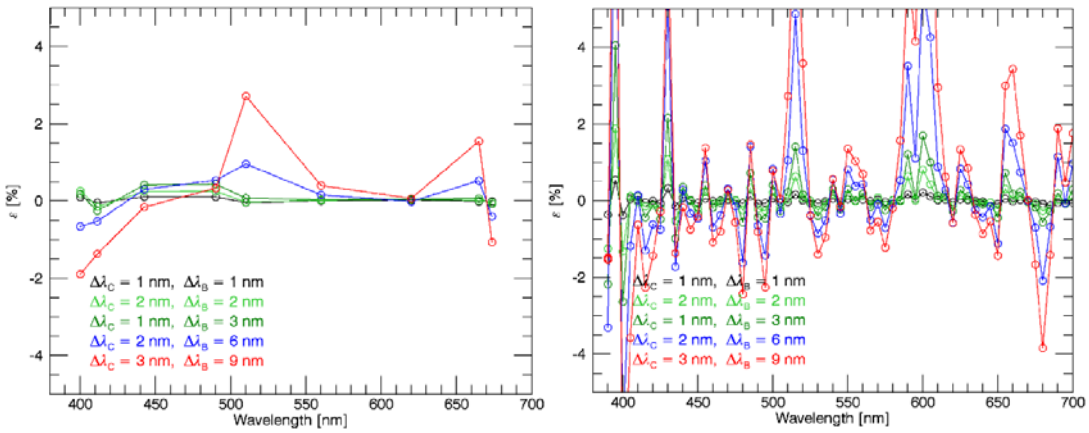

Figure 4. Percent differences ε between "equivalent" and "exact" L_W determined for OLCI (*left panel*) or PACE-like (*right panel*) bands. Different colours refer to results for various bandwidths $\Delta\lambda_B$ and spectral sampling intervals $\Delta\lambda_C$ of the in situ hyperspectral sensor (after Zibordi et al. 2017b).

The same analysis performed for PACE-like bands (see Fig. 3. right panel) shows values of ε more pronounced than those determined for OLCI in spectral regions exhibiting marked changes in the slope of R_{RS}. Specifically, ε determined with $\Delta\lambda_B$ = 9 nm and $\Delta\lambda_C$ = 3 nm indicates values exceeding 4%. With $\Delta\lambda_B$ = 2 nm and $\Delta\lambda_C$ = 2 nm, the percent differences are generally lower than 0.5%.

It is noted that the previous analysis has been performed using R_{RS} data, which are the target quantity for most ocean colour applications. However, SVC is often performed using L_W data (where $L_W = R_{RS} \cdot E_d$, with E_d downward irradiance at the sea surface) exhibiting lower uncertainty than R_{RS}.

The application of L_W instead of R_{RS} naturally leads to an increase in the spectral resolution requirements for in situ radiometry due to the higher spectral complexity of L_W with respect to R_{RS} spectra. Percent differences ε between "equivalent" and "exact" OLCI or PACE-like L_W are presented in Fig. 4. These values, when compared to those given in Fig. 3, show equivalence of L_W and R_{RS} for the spectral resolution requirements related to multispectral satellite sensors like OLCI. Conversely, the values of ε determined for the PACE-like bands, exhibit a marked increase in the blue spectral region.

In view of contributing to the definition of specifications for the spectral resolution of in situ radiometric measurements satisfying uncertainty and stability requirements for SVC, a value of ε < 0.5% (equivalent to the requirement for decadal radiometric stability), has been assumed in the blue-green spectral regions. It is mentioned that such a low value is mostly justified by the need to define a threshold well below the target uncertainty defined for SVC. Based on the previous analysis and assumptions, Zibordi et al. (2017b) produced the following conclusions for SVC applications relying on R_{RS} with a spectral sampling interval close or lower than half the spectral resolution (i.e., $\Delta\lambda_C \lesssim \Delta\lambda_B/2$) for in situ hyperspectral radiometers:

- *A spectral resolution better than 3 nm is required* to support *multispectral satellite sensors* (such as OLCI).
- *A spectral resolution better than 1 nm is devised* to support *hyperspectral satellite sensors* (such as PACE).

Obviously, a lower ε would imply more stringent requirements on spectral resolution of the in situ hyperspectral sensors. Additionally, the use of L_W instead of R_{RS}, also increases requirements ultimately indicating the need for sub-nanometre resolutions in the blue spectral region for hyperspectral satellite sensors such as PACE.

4. Location for a European Site

The work by Zibordi et al. (2015), besides indicating that *the creation of CDRs from independent ocean colour missions should ideally rely on the application of the same atmospheric correction process and on time-series of in situ radiometric data from a single reference SVC site*, recognizes that *strategies to support long-term climate investigations also recommend redundancy of in situ SVC measurement sites (IOCCG 2012). This implies establishing multiple SVC sites: i. relying on in situ radiometry systems equivalent in terms of data accuracy and long-term performance; ii. and located in regions also exhibiting ideal and likely similar measurement conditions.*

By recalling that an SVC site established to support the creation of satellite ocean colour CDRs should be maintained over decades, any proposed site should respond to basic requirements including the benefits of logistic support from nearby infrastructures.

In view of helping with future discussions on marine regions suitable for SVC, Zibordi and Mélin (2016) compared a number of established sites but also evaluated potential sites under consideration. The regions hosting established SVC sites include: the North Pacific Ocean (NPO) with the Marine Optical Buoy (MOBy) site managed by the US National Oceanic and Atmospheric Administration (NOAA; Clark et al. 1997); the Arabian Sea (ASea) with the Kavaratti Site managed by the Indian Space Research Organization (ISRO; Shukla et al. 2011); the Ligurian Sea (LSea) with the BOUée pour l'acquiSition d'une Série Optique à Long termE (BOUSSOLE) site managed by the French Laboratoire d'Océanographie de Villefranche (LOV; Antoine et al. 2008). The regions for which the setting up of new SVC sites has been matter of discussion within the scientific community comprise: the Mediterranean Sea (MSea) near the Island of Crete; the Caribbean Sea (CSea) near Puerto Rico Islands; the North Atlantic Ocean (NAO) near Azores Islands; the Eastern Indian Ocean (EIO) near Rottnest Island off Perth; the Strait of Sicily (SoS) near the Pantelleria Island; the Balearic Sea (BSea) in the proximity of the Balearic Islands; and the Eastern Atlantic Ocean (EAO) near Madeira Island.

Without excluding other candidate areas, all these regions satisfy the needs for: *i*. nearby islands or coastal locations essential to ensure maintenance services of the offshore SVC infrastructure; *ii*. distance from the coast to minimize adjacency effects in satellite data; and finally *iii*. waters representative of the most common oceanic conditions.

The ranking of SVC regions has been performed through the analysis of 5-year SeaWiFS Level-2 daily full-resolution products. Table 2 summarizes the mean m and standard deviation σ of the SeaWiFS marine/atmospheric data products. These data confirm the unique marine and atmospheric characteristics of the NPO region with respect to the other areas considered: maritime aerosols and oligotrophic waters exhibiting high intra-annual optical stability in addition to low sun zenith variations. Because of this, MOBY has been confirmed to be an ideal site for SVC in support of the creation of CDRs and its features are thus considered a reference to evaluate additional or alternative SVC sites.

Equivalence of measurement conditions across marine regions is expected to minimize differences in g-factors regardless of the geographic location of the SVC site. From Table 2, it is evident that the identification of multiple SVC sites may imply trading-off criteria related to the marine/atmospheric properties. For instance, MSea followed by EAO, CSea and EIO, mostly compare to NPO in terms of intra-annual stability and mean values of the considered marine bio-optical quantities (i.e., $k_d(490)$ and *Chla*). When looking at $R_{rs}(555)$, CSea, EIO and EAO show variabilities (quantified by σ) lower than those observed at NPO, while ASea and MSea exhibit slightly higher values.

For atmospheric optical quantities, the lowest temporal variability of the Ångström exponent α is observed at ASea and LSea. However, both regions exhibit values of α indicating contamination by non-maritime aerosols more marked for LSea (and also seen for MSea). Conversely, despite a lower intra-annual stability, EAO and EIO show mean values of α close to those of NPO.

Zibordi and Mélin (2017) addressed the suitability of different regions to support SVC by assuming in situ L_w measurements, or the derived R_{RS}, are regularly available at each location considered. Relying on this assumption, Table 3 presents the number of potential high quality matchups (i.e., applicable for SVC) between SeaWiFS and in situ data over a 5-year period, as identified through the application of very stringent criteria associated with oligotrophic conditions and a clear marine atmosphere: $Chla \leq 0.1$ µg l^{-1}, or $\tau_a(865) \leq 0.1$, or $\alpha \leq 1.0$, or all of them. The applied thresholds reflect the statistical values determined for the NPO reference region already identified as favourable for SVC (see Zibordi et al. 2015), and naturally identify cases characterized by oligotrophic conditions and maritime aerosols exhibiting a small seasonal variability and a low marine bio-optical complexity.

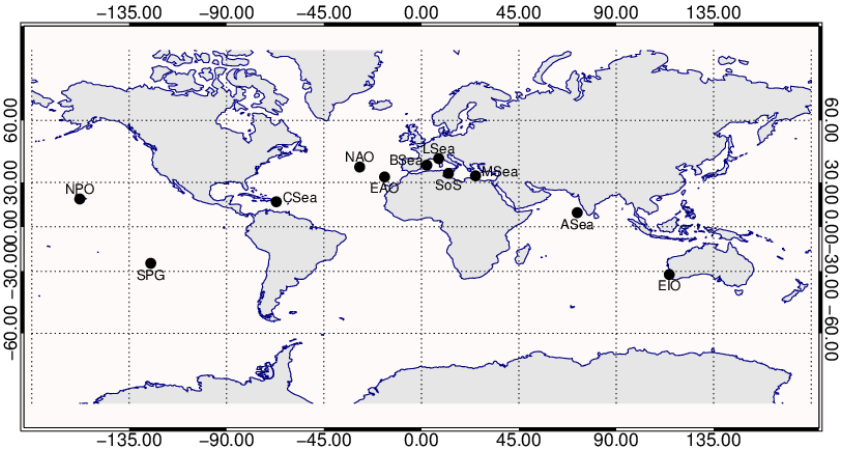

Figure 5. Map of the marine regions of interest (adapted from Zibordi and Mélin 2017).

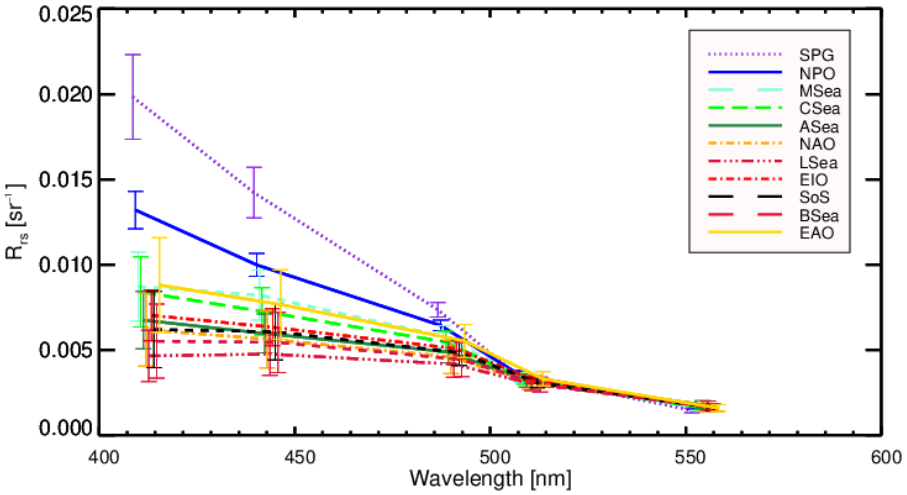

Figure 6. Mean values of R_{rs} determined with SeaWiFS Level-3 data from the entire mission at the 412-555 nm bands for the considered marine regions. Error bars indicate ±1σ. Spectra are incrementally shifted by 2 nm to increase readability of the figure. Data at 670 nm, which exhibit negligible values with respect to the spectral bands centered at shorter wavelengths, are not plotted. The South Pacific Gyre (SPG) spectrum is included as a virtual reference due to its highly oligotrophic waters likely ideal for SVC (adapted from Zibordi and Mélin 2017).

Table 2. Mean *m* and standard deviation σ of SeaWiFS Level-2 data products (*M*) non-flagged by the default SeaDAS exclusion flags: the remote sensing reflectance $R_{rs}(555)$ at the 555 nm center-wavelength is in units of $sr^{-1} \times 10^{-3}$, the diffuse attenuation coefficient $k_d(490)$ at the 490 center-wavelength is in units of m^{-1}, *Chla* is in units of μg l^{-1}, the aerosol optical depth $\tau_a(865)$ at the 865 nm center-wavelength and the Ångström exponent α are both dimensionless (adapted from Zibordi and Mélin 2017).

		$R_{rs}(555)$		$k_d(490)$		*Chla*		$\tau_a(865)$		α	
	M	*m*	σ	*m*	σ	*m*	σ	*m*	σ	*m*	σ
NPO	212	1.54	0.29	0.027	0.004	0.07	0.01	0.07	0.04	0.88	0.40
MSea	821	1.51	0.33	0.029	0.006	0.09	0.03	0.08	0.05	1.22	0.41
CSea	242	1.54	0.23	0.033	0.009	0.13	0.07	0.08	0.05	0.69	0.42
ASea	114	1.62	0.30	0.043	0.011	0.19	0.11	0.11	0.05	1.14	0.29
NAO	274	1.68	0.41	0.047	0.020	0.25	0.22	0.06	0.04	1.09	0.45
LSea	873	1.65	0.41	0.051	0.020	0.28	0.23	0.07	0.04	1.45	0.37
EIO	382	1.53	0.25	0.036	0.008	0.15	0.05	0.05	0.03	0.76	0.55
SoS	722	1.49	0.35	0.037	0.010	0.17	0.09	0.09	0.05	1.10	0.42
BSea	794	1.57	0.37	0.043	0.012	0.20	0.11	0.08	0.04	1.29	0.42
EAO	266	1.50	0.26	0.032	0.008	0.12	0.06	0.07	0.04	0.91	0.46

Results summarized in Table 3 derived from M_{CV} matchups (i.e., cases not affected by default SeaDAS flags and additionally characterized by high spatial homogeneity around the measurement site as detailed in Zibordi and Mélin 2017), show a dramatic decrease of the number of matchups when all quality criteria are applied. Despite the low number of overall potential matchups (i.e., M_{CV}=187) with respect to those available for other regions (e.g., M_{CV}=798 for MSea or 828 for LSea), NPO exhibits the highest number of high quality matchups (i.e., M_{Q1}=75). In addition to NPO, those regions showing an appreciable number of potential high quality matchups are MSea, EAO, CSea and EIO with M_{Q1} equal to 59, 55, 48 and 42, respectively.

The number of potential high quality matchups obtained for NPO is fully supported by those determined from the application of MOBy data to SeaWiFS SVC. In fact, the number of 15 high quality matchups per year determined for NPO is comparable to the approximately 17 per year (i.e., 150 over a 9-year period) actually identified by Franz et al. (2007) for MOBy. It is however recognized that the consistency of results across the various regions may be affected by geographical differences in the accuracy of satellite data products. A specific case is that of *Chla* likely overestimated at MSea, LSea, SoS and BSea as a result of the application of global bio-optical algorithms.

The numbers in Table 3 have been determined after applying the SeaDAS default exclusion flags in combination with spatial homogeneity tests. Nevertheless, the need for a statistically significant number of matchups per mission (e.g., Franz et al. 2007), may suggest to relax some of the thresholds applied to the geophysical quantities used for the quality tests. Results identified as M_{Q2} in Table 3 show that matchups in some regions can largely increase through the application of less restrictive criteria. Examples are SoS, EIO, CSea and EAO which exhibit typical *Chl*a values higher than those of regions such as NPO or MSea. Because of this, when relaxing the exclusion criteria and thus accepting mean values of $Chla \leq 0.2$ μg l^{-1} and also of $\tau_a(865) \leq 0.15$, the number of potential matchups largely increases for some regions (e.g., EIO and SoS).

Table 3. SeaWiFS Level-2 observations M_{CV} over the 5-year period considered, not affected by SeaDAS Level-2 default exclusion flags and passing the spatial homogeneity test applied to investigate cases for which the 5x5 elements representing each region exhibit mean: *Chla*≤0.1 μg l^{-1}, *Chla*≤0.2 μg l^{-1}, $\tau_a(865)$ ≤0.10, $\tau_a(865)$ ≤0.15 and $\alpha \leq 1.0$. M_{Q1} indicates the number of potential high quality matchups identified through the application of combined tests on mean *Chla*≤0.1 μg l^{-1}, mean $\tau_a(865)$ ≤0.1 and mean $\alpha \leq 1.0$ (M_{Q1}/year is the related number of potential high quality matchups per year). Conversely, M_{Q2} indicates results from the application of combined tests with mean *Chla*≤0.2 μg l^{-1}, mean $\tau_a(865)$ ≤0.15 and mean $\alpha \leq 1.0$ (M_{Q2}/year, indicates the related potential number of matchups of high quality per year) (adapted from Zibordi and Mélin 2017).

	M_{CV}	*Chla*≤0.1	*Chla*≤0.2	$\tau_a(865)\leq 0.10$	$\tau_a(865)\leq 0.15$	$\alpha \leq 1.0$	M_{Q1}(M_{Q1}/year)	M_{Q2}(M_{Q2}/year)
NPO	187	182	187	153	177	107	**75** (15.0)	**98** (19.6)
MSea	798	572	794	570	714	212	**59** (11.8)	**147** (29.4)
CSea	218	79	197	164	195	172	**48** (9.6)	**141** (28.2)
ASea	103	0	80	37	83	21	**0** (0.0)	**13** (2.6)
NAO	256	3	156	219	246	102	**1** (0.2)	**56** (11.2)
LSea	827	0	400	668	790	87	**0** (0.0)	**36** (7.2)
EIO	367	53	328	337	363	235	**42** (8.4)	**220** (44.0)
SoS	693	140	523	462	598	275	**10** (2.0)	**135** (27.0)
BSea	735	30	500	556	692	121	**4** (0.8)	**61** (12.2)
EAO	227	123	202	198	221	123	**55** (11.0)	**108** (21.6)

It is however reminded that the choice of relaxing selection criteria might affect the equivalence of multiple SVC sites. In fact, differences in the atmospheric optical quantities for the diverse regions could unevenly impact the precision of *g*-factors across missions relying on different SVC sites.

Zibordi and Mélin (2017) came to the conclusion that *the analysis on potential high quality matchups confirms the superior location of the MOBy site in the northern Pacific Ocean for SVC. While recognizing that no site is superior for all criteria reviewed in the analysis, it nonetheless suggests that the Eastern Mediterranean Sea near the Island of Crete exhibits best equivalence with NPO and could be considered a suitable choice for a European SVC complying with requirements for the creation of CDRs.*

When considering criteria less strict than those leading to best equivalence between NPO and MSea, the Eastern Indian Ocean region near Rottnest Island appears an excellent candidate for SVC. EIO also offers the unique advantage of being located in the southern hemisphere, which implies solar zenith cycles opposite to those characterizing SVC sites located in the northern hemisphere. Definitively, the existence of two sites operated in the two hemispheres would provide seasonal alternatives to SVC of satellite sensors heavily affected by glint perturbations.

It is finally further restated that the full analysis summarized above and the related conclusions, are strictly based on the assumption of MOBY (both region and radiometry) as the "ideal model" for SVC as a result of its demonstrated capability to deliver high precision *g*-factors with current atmospheric correction codes (see Zibordi et al. 2015). The suggestion of alternative SVC sites based on selection criteria less strict than those applied in Zibordi and Mélin (2017) is definitively workable, but it would imply the need to demonstrate their suitability to meet the uncertainties required for *g*-factors devoted to support climate applications.

5. Conclusions

The generation of satellite ocean colour data products meeting requirements for the construction of CDRs, implies the implementation of SVC to minimize uncertainties affecting the calibration of the satellite sensor and inaccuracies connected with the atmospheric correction process. This strictly applies to the Copernicus Programme delivering Marine and Climate services centred on satellite ocean colour data from the Sentinel-3 missions.

By relying on studies led by the JRC and benefitting of the collaboration of various international scientists, the present work has summarized requirements for SVC in support of the creation of CDRs from multiple satellite ocean colour missions. The following comprehensive recommendations should be considered while establishing a European SVC site.

Following Zibordi et al. (2015) and the references therein, *the creation of ocean colour CDRs should ideally rely on:*

- *One main long-term in situ calibration system (site and radiometry) established and sustained with the objective to maximize accuracy and precision over time of g-factors and thus minimize possible biases among satellite data products from different missions;*
- *and ii. unique (i.e., standardized) atmospheric models and algorithms for atmospheric corrections to maximize cross-mission consistency of data products at locations different from that supporting SVC.*

Additionally, an *ideal ocean colour SVC site should meet the following general requirements:*

- *Located in a region chosen to maximize the number of high-quality matchups by trading off factors such as best viewing geometry, sun-glint avoidance, low cloudiness, and additionally set away from any continental contamination and at a distance from the mainland to safely exclude any adjacency effect in satellite data;*
- *Exhibiting known or accurately modeled optical properties coinciding with maritime atmosphere and oligotrophic/mesotrophic waters, to represent the majority of world oceans and minimize relative uncertainties in computed g-factors;*
- *Characterized by high spatial homogeneity and small environmental variability, of both atmosphere and ocean, to increase precision of computed g-factors.*

When dealing with *in situ* radiometric measurements, Zibordi et al. (2015) provided the following general requirements:

- *Hyperspectral field data with sub-nanometre resolution to allow system vicarious calibration of any satellite ocean colour sensor regardless of its center-wavelengths and spectral responses, and thus ensure minimization of inter-band uncertainties;*
- *State-of-the-art absolute calibration traceable to National Metrology Institutes (i.e., tentatively with target standard calibration uncertainty lower than 2% for radiance and stability better than 0.5% per deployment) and comprehensive characterizations of radiometers in terms of linearity, temperature dependence, polarization sensitivity and stray light effects, in view of minimizing measurement uncertainties and allowing for accurate determinations of uncertainty budgets;*
- *Application of quality assurance/control schemes minimizing effects of measurement perturbations like those (when applicable) due to infrastructure shading, radiometer self-shading, wave perturbations, bio-fouling, and additionally scheduling regular checks of in situ systems and frequent swap of radiometers, as best practice to maximize long-term accuracy and precision of in situ reference radiometric data;*
- *Data rate ensuring generation of matchups for any satellite ocean colour mission with time differences appropriate to minimize variations in bi-directional effects due to changes in sun zenith and daily fluctuations in the vertical distribution of phytoplankton.*

In agreement with finding by Zibordi et al. (2017), assuming a spectral sampling interval close or lower than half the spectral resolution (i.e., $\Delta\lambda_C \lesssim \Delta\lambda_B/2$):

- *A spectral resolution better than 3 nm* is required for in situ hyperspectral sensors delivering R_{RS} measurements in support of SVC for *multispectral satellite sensors* (such as OLCI on Sentinel-3 satellites).
- *A spectral resolution better than 1 nm is required* for the in situ hyperspectral sensors delivering R_{RS} measurements in support of SVC for *hyperspectral satellite sensors* (such as PACE planned by NASA for 2022). *… Additionally, the use of L_W instead of R_{RS}, would increase requirements ultimately indicating the need for sub-nanometre resolutions in the blue spectral region for hyperspectral sensors such as PACE.*

In agreement with recommendations from the scientific community (IOCCG 2012), Zibordi et al. (2015) recognized that *strategies to support long-term climate investigations recommend redundancy of in situ SVC measurement sites (IOCCG 2012). This implies establishing multiple SVC sites:*

- *Relying on in situ radiometry systems equivalent in terms of data accuracy and long-term performance;*
- *Located in regions also exhibiting ideal and likely similar measurement conditions.*

With reference to general recommendations on SVC sites, Zibordi and Mélin (2017) evaluated the atmospheric and marine optical features of a number of potential SVC regions in European and non-European seas. By considering MOBy (region and radiometry) in the North Pacific Ocean as the "ideal model" for SVC due to its capability to deliver high precision *g*-factors with current atmospheric correction codes, and additionally recognizing that none of the considered potential sites is superior for all criteria reviewed in the analysis, they concluded *that the Eastern Mediterranean Sea near the Island of Crete exhibits best equivalence with the North Pacific Ocean and could be considered as a further site for SVC complying with requirements for the creation of CDRs.*

References

Antoine, D., Guevel, P., Deste, J. F. , Bécu, G. Louis, F., Scott, A. J. & Bardey, P. (2008a). The "BOUSSOLE" buoy-a new transparent-to-swell taut mooring dedicated to marine optics: design, tests, and performance at sea. *J. Atmos. Oceanic Technol.*, 25*,* 968–989 (2008).

Butler, J.J., Johnson, B. C., Rice, J. P., Brown, S. W. & Barnes, R. A. (2007). Validation of radiometric standards for the laboratory calibration of reflected-solar Earth-observing satellite instruments. In SPIE Conference Proceedings *Earth Observing Systems*, pp. 667707-667707. International Society for Optics and Photonics.

Clark, D. K., Gordon, H. R., Voss, K. J., Ge, Y., Broenkow, W. & Trees, C. (1997). Validation of atmospheric correction over the oceans. *J. Geophys. Res.*, 102(D14), 17209–17217.

Franz, B. A., Bailey, S. W., Werdell, P. J. & McClain, C. R. (2007). Sensor-independent approach to the vicarious calibration of satellite ocean colour radiometry. *Appl. Opt.*, 46, 5068–5082.

Gordon, H. R. (1987). Calibration requirements and methodology for remote sensors viewing the ocean in the visible. *Remote Sens. Environ.* 22, 103–126.

Gordon, H. R. (1998). In orbit calibration strategy for ocean colour sensors. *Remote Sens. Environ*. 63, 265– 278.

Gordon, H. R. & Clark, D. K. (1981). Clear water radiances for atmospheric correction of coastal zone colour scanner imagery," *Appl. Opt.* 20, 4175–4180.

Gordon, H. R., Clark, D. K., Brown, J. W., Brown, O. B., Evans, R. H. & Broenkow, W. W. (1983). Phytoplankton pigment concentrations in the Middle Atlantic Bight: Comparison of ship determinations and CZCS estimates. *Appl. Opt.* 22, 20–36 (1983).

IOCCG (2010). *Atmospheric Correction for Remotely-Sensed Ocean-Colour Products.* Wang, M. (Ed.), Reports of the International Ocean-Colour Coordinating Group, No.10, pp. 78, IOCCG, Dartmouth, Canada.

IOCCG (2012). *International Network for Sensor Inter-comparison and Uncertainty assessment for Ocean Color Radiometry (INSITU-OCR): Working toward consistency and accuracy in the development of essential climate variables from multiple missions.* White Paper available at *http://www.ioccg.org/groups/INSITU-OCR_White-Paper.pdf* .

Eplee Jr, R. E., Sun, J.-Q., Meister, G., Patt, F. S., Xiong, X. & McClain, C. R. (2011). Cross calibration of SeaWiFS and MODIS using on-orbit observations of the Moon. *Appl. Opt.* 50, 120-133.

Esposito, J. A., Xiong, X., Wu, A., Sun, J. & Barnes, W. L. (2004). MODIS reflective solar bands uncertainty analysis. In SPIE Conference Proceedings *Earth Observing Systems*, pp. 448-458. International Society for Optics and Photonics.

Hooker, S. B., Esaias, W. E., Feldman, G. C., Gregg, W. W., McClain, C. R. (1982). An overview of SeaWiFS and ocean colour. *NASA Tech. Memo.* 1992–104566, vol. 1, S.B. Hooker and E.R. Firestone (Eds.), NASA Goddard Space Flight Center, Greenbelt, MD.

Ohring, G., Wielicki, B., Spencer, R., Emery, B. & Datla, R. (2005). Satellite instrument calibration for measuring global climate change: Report of a workshop. *B. Am. Meteorol. Soc*. 86, 1303–1313.

Shukla, A.K., Babu, K.N., Prajapati, R.P., Suthar, N.M., Ajai Sinha, A., Saifee, A.M., Satashia, S.N., Arul Muthiah, M., Venkatesan, R., 2013. An ocean CAL-VAL site at Kavaratti in Lakshadweep for vicarious calibration of OCM-2 and validation of geophysical products—development and operationalization. Mar. Geod. 36, 203–218.

Werdell, P. J. & Bailey, S. W. (2005). An improved in-situ bio-optical data set for ocean colour algorithm development and satellite data product validation. *Remote Sens. Environ*. 98, 122– 140.

Werdell, P. J., Bailey, S. W., Franz, B. A., Morel, A. & McClain, C. R. (2007). On-orbit vicarious calibration of ocean colour sensors using an ocean surface reflectance model. *Appl. Opt.* 46, 5649-5666 (2007).

World Meteorological Organization (WMO), (2016). The Global Observing System for Climate: Implementation Needs. Report GCOS – 200 (available at http://unfccc.int/files/science/workstreams/systematic_observation/application/pdf/gcos_ip_10oct2016.pdf) .

Zibordi, G., Holben, B. N., Slutsker, I., Giles, D., D'Alimonte, D., Mélin, F., Berthon, J.-F., Vandemark, D., Feng, H., Schuster, G., Fabbri, B. E., Kaitala, S. & Seppälä, J. (2009). AERONET-OC: a network for the validation of ocean color primary radiometric products. *J. Atmos. Ocean. Technol*. 26, 1634–1651.

Zibordi, G., Mélin, F., Voss, K.J., Johnson, B.C., Franz, B.A., Kwiatkowska, E., Huot, J.P., Wang, M. and Antoine, D. (2015). System vicarious calibration for ocean color climate change applications: Requirements for in situ data. *Remote Sens. Environ.* 159, 361–369.

Zibordi, G., Mélin (2017). An evaluation of marine regions relevant for ocean color system vicarious calibration. *Remote Sens. Environ.* 190, 122–136.

Zibordi, G., Mélin, F., Talone M. (2017), System Vicarious Calibration for Copernicus Ocean Colour Missions: Requirements and Recommendations for a European Site, EUR 28433 EN, doi:10.2760/155759.

Zibordi, G., Talone, M., Voss K. J., Johnson, B. C. (2017b). Impact of spectral resolution of in situ ocean color radiometric data in satellite matchups analyses. *Optics Express* 25, A798-A812.

List of abbreviations and definitions

ASea	Arabian Sea
BOUSSOLE	BOUée pour l'acquiSition d'une Série Optique à Long termE
BSea	Balearic Sea
CDR	Climate Data Record
CSea	Caribbean Sea
EAO	Eastern Atlantic Ocean
ECV	Essential Climate Variable
EIO	Eastern Indian Ocean
EO	Earth Observation
JRC	Joint Research Centre
ISRO	Indian Space Research Organization
LOV	Laboratoire d'Océanographie de Villefranche
LSea	Ligurian Sea
MOBy	Marine Optical Buoy
MOS	Marine Optical System
MSea	Mediterranean Sea
NASA	National Aeronautics and Space Administration
NAO	North Atlantic Ocean
NOAA	National Ocean and Atmosphere Administration
NPO	North Pacific Ocean
OLCI	Ocean and Land Colour Instrument
PACE	Plankton, Aerosol, Cloud ocean Ecosystem
RSEM	Relative standard error of the mean
SeaDAS	SeaWiFS Data Analysis System
SeaWiFS	Sea Wide Field of View Sensor
SoS	Strait of Sicily
SVC	System Vicarious Calibration
Chla	Clorophyll-*a* concentration
g	*g*-factors (gain correction factors determined through SVC)
K_d	Diffuse attenuation coefficient
L_T	Top of the atmosphere radiance
L_W	Water-leaving radiance
M	Number of matchups passing the default SeaDAS exclusion flags
M_{CV}	M matchups passing spatial homogeneity tests
N	Number of matchups
Ny	Scale factor
R_{RS}	Remote sensing reflectance
Y	Number measurement years
α	Ångström exponent
τ_a	Aerosol optical thickness
σ	Standard deviation
Δg	Percent difference between *g*-factors determined with different in situ data
$\Delta\lambda_B$	Bandwidth of a spectral channel
$\Delta\lambda_C$	Spectral sampling interval of a hyperspectral radiometer

Annex 1

System vicarious calibration for ocean colour climate change applications: Requirements for in situ data. Reprinted from *Remote Sens. Environ.* 159, 361–369.

Remote Sensing of Environment 159 (2015) 361–369

Contents lists available at ScienceDirect

Remote Sensing of Environment

journal homepage: www.elsevier.com/locate/rse

System vicarious calibration for ocean color climate change applications: Requirements for in situ data

Giuseppe Zibordi [a,*], Frédéric Mélin [a], Kenneth J. Voss [b], B. Carol Johnson [c], Bryan A. Franz [d], Ewa Kwiatkowska [e], Jean-Paul Huot [f], Menghua Wang [g], David Antoine [h,i]

[a] European Commission, Joint Research Centre, Ispra, Italy
[b] Physics Department, University of Miami, Coral Gables, FL, USA
[c] Sensor Science Division, National Institute of Standards and Technology, Gaithersburg, MD, USA
[d] National Aeronautics and Space Administration, Goddard Space Flight Center, Greenbelt, MD, USA
[e] EUMETSAT, Remote Sensing and Products Division, Darmstadt, Germany
[f] European Space Agency, Noordwijk, The Netherlands
[g] National Oceanic and Atmospheric Administrations, Center for Satellite Applications and Research, College Park, MD, USA
[h] Sorbonne Universités, Université Pierre et Marie Curie, Paris 06, UMR 7093, Laboratoire d'Océanographie de Villefranche, Villefranche-sur-Mer, France
[i] Department of Imaging and Applied Physics, Remote Sensing and Satellite Research Group, Curtin University, Perth, WA, Australia

ARTICLE INFO

Article history:
Received 13 October 2014
Received in revised form 16 December 2014
Accepted 22 December 2014
Available online 29 January 2015

Keywords:
Ocean color
System Vicarious Calibration
Climate Data Record

ABSTRACT

System Vicarious Calibration (SVC) ensures a relative radiometric calibration to satellite ocean color sensors that minimizes uncertainties in the water-leaving radiance L_w derived from the top of atmosphere radiance L_T. This is achieved through the application of gain-factors, *g*-factors, to pre-launch absolute radiometric calibration coefficients of the satellite sensor corrected for temporal changes in radiometric sensitivity. The *g*-factors are determined by the ratio of simulated to measured spectral L_T values where the former are computed using: *i.* highly accurate in situ L_w reference measurements; and *ii.* the same atmospheric models and algorithms applied for the atmospheric correction of satellite data. By analyzing basic relations between relative uncertainties of L_w and L_T, and *g*-factors consistently determined for the same satellite mission using different in situ data sources, this work suggests that the creation of ocean color Climate Data Records (CDRs) should ideally rely on: *i.* one main long-term in situ calibration system (site and radiometry) established and sustained with the objective to maximize accuracy and precision over time of *g*-factors and thus minimize possible biases among satellite data products from different missions; and additionally *ii.* unique (i.e., standardized) atmospheric model and algorithms for atmospheric correction to maximize cross-mission consistency of data products at locations different from that supporting SVC. Finally, accounting for results from the study and elements already provided in literature, requirements and recommendations for SVC sites and field radiometric measurements are streamlined.

© 2015 The Authors. Published by Elsevier Inc. This is an open access article under the CC BY-NC-ND license (http://creativecommons.org/licenses/by-nc-nd/4.0/).

1. Introduction

In recent decades, measurements of ocean color from earth-orbiting satellite sensors have demonstrated high value for a number of applications ranging from regional water quality assessment (e.g., Attila et al., 2013) to global climate change investigations (e.g., Behrenfeld et al., 2006). Confidence in results from these applications, however, depends on accuracy of the satellite-derived data products. The primary ocean color product is the spectral water-leaving radiance L_w, i.e., the radiance emerging from the sea that is retrieved from the total radiance L_T detected by the satellite, whose accuracy determines those of satellite-derived data products. These include the spectral distribution of the normalized water-leaving radiance L_{WN} (i.e., the water-leaving radiance that would occur with no atmosphere, the sun at the zenith and at the mean sun–earth distance) or of the equivalent remote sensing reflectance R_{RS}, applied to determine geophysical quantities such as the near-surface chlorophyll-a concentration (*Chla*).

Early accuracy requirements for satellite ocean color data products generally refer to the work of Gordon and Clark (1981), Gordon et al. (1983) and Gordon (1987). By considering oligotrophic waters, they indicated a 5% uncertainty for L_w in the blue spectral region to allow for the determination of *Chla* concentration with a 35% maximum uncertainty. Subsequently, spectrally independent uncertainties of 5%, with a 1% inter-band uncertainty, were included among the objectives of the Sea-viewing Wide Field-of-view Sensor

* Corresponding author. Tel.: +39 0332 785902.
E-mail address: giuseppe.zibordi@jrc.ec.europa.eu (G. Zibordi).

http://dx.doi.org/10.1016/j.rse.2014.12.015
0034-4257/© 2015 The Authors. Published by Elsevier Inc. This is an open access article under the CC BY-NC-ND license (http://creativecommons.org/licenses/by-nc-nd/4.0/).

(SeaWiFS) mission (Hooker, Esaias, Feldman, Gregg, & McClain, 1982). These target uncertainties were later retained for successive missions and have become a science requirement for the ocean color community.

Achievement of the spectrally independent 5% uncertainty target in satellite-derived L_w is mostly challenged by the accuracy of the absolute radiometric calibration of satellite optical sensors and additionally by uncertainties in the quantification of the large atmospheric perturbations affecting L_T. In particular, current uncertainties of approximately 2-3% (Butler, Johnson, Rice, Brown, & Barnes, 2007, Eplee et al., 2011, Esposito, Xiong, Wu, Sun, & Barnes, 2004) in the absolute radiometric calibration of satellite sensors in the visible spectral region and the additional uncertainties affecting the atmospheric correction process generally larger than a few percent (IOCCG 2010), may lead to large differences among multi-mission L_w data (Zibordi, Mélin, & Berthon, 2006).

These limitations can be resolved through the so-called System Vicarious Calibration (SVC) that determines vicarious adjustment gain-factors g (hereafter g-factors) for absolute radiometric calibration coefficients of satellite sensors (Gordon, 1998) through simulation of top-of-atmosphere L_T using: *i.* highly accurate in situ L_w reference measurements; and *ii.* the same atmospheric models and algorithms as applied for the atmospheric correction of satellite data. The g-factors, determined by the ratio of simulated to measured spectral L_T values, aim at minimizing the combined effects of: *i.* uncertainties due to the absolute pre-flight radiometric calibration and characterization of the satellite sensor after correction for sensitivity change with time; and *ii.* inaccuracy of the models and algorithms applied in the atmospheric correction to determine L_w from L_T. Clearly, the SVC process allows the determination of L_w with the lowest uncertainty when satellite observation conditions are equivalent to those characterizing the data applied for the calculation of g-factors (i.e., when the mean biases removed through SVC and those affecting the atmospheric correction processes are identical and fully compensate each other). It must be emphasized that the system nature of SVC requires re-computing g-factors after any change in the models or algorithms applied for the atmospheric correction, or any significant change in instrument absolute or temporal calibration knowledge.

By considering uncertainty requirements for satellite-derived L_w applicable for the construction of Climate Data Records (CDRs), which serve as core climate benchmark observations, the present work investigates the calibration needs for L_T with the objective of discussing requirements for in situ L_w data suitable for the determination of g-factors.

2. System vicarious calibration requirements

Vicarious calibration broadly refers to the indirect calibration of satellite sensors through simulation of top-of-atmosphere data (Koepke, 1982). Generic vicarious calibration methods based on atmospheric models and algorithms different from those applied for the operational data processing cannot reduce absolute uncertainties in derived radiometric calibration factors below a few percent (IOCCG, 2013). This may lead to very large uncertainties in satellite-derived L_w (see Section 2.1). Consequently, unlike SVC that minimizes uncertainties in retrieved L_w (Gordon, 1998), generic vicarious calibration methods are best applied for the quality check of pre-launch absolute radiometric calibrations of satellite ocean color sensors.

In view of supporting the discussion on accuracy and precision needs for g-factors from SVC, the following subsections will review: *i.* requirements for the construction of CDRs from satellite-derived L_w; and *ii.* legacy requirements for in situ L_w reference measurements.

2.1. Requirements for CDRs of L_w

CDRs of Essential Climate Variables (ECVs) are intended to support climate change investigations through time-series of core benchmark observations with enough accuracy to allow the detection of long-term trends embedded in large natural variations (Leroy, Anderson, & Ohring, 2008).

Requirements for the generation of a CDR of satellite-derived L_{WN} from L_w (WMO 2011), which is the fundamental satellite ocean color ECV, include:

1. Radiometric uncertainty lower than 5% in the blue and green spectral regions (downscaled with respect to the spectrally independent 5% uncertainty target listed among the objectives of several ocean color missions);
2. Stability better than 0.5% over a decade.

The requirement on uncertainty is essential to understand climate-driven processes and changes, while the requirement on stability is essential to confidently determine long-term changes or trends (Ohring, Wielicki, Spencer, Emery, & Datla, 2005).

As already anticipated, the strict requirement of 5% maximum uncertainty for L_w determined from L_T at relevant wavelengths, requires the application of SVC. While this need is commonly accepted by the satellite ocean color community, the accuracy and precision required for g-factors for different missions supporting the creation of CDRs appears less consolidated.

To strictly address such a need, the relationship linking uncertainties in L_w and L_T is hereafter investigated through the use of the measurement equation. Specifically, in the absence of atmospheric gaseous absorption and sun glint and foam perturbations, the top-of-atmosphere radiance L_T can be related to L_w through the following simplified model

$$L_T = L_R + L_A + L_w t_d \tag{1}$$

where L_R and L_A indicate the Rayleigh and aerosol atmospheric radiance contributions, and t_d is the diffuse atmospheric transmittance that varies with atmospheric path-length and constituents. By assuming the values of L_R and L_A are exactly determined for any given observation condition, following the Guide to the Expression of Uncertainty in Measurement (JCGM, 2008) Zibordi and Voss (2014) provided equations relating absolute uncertainties of L_T, $u(L_T)$, to those of L_w, $u(L_w)$, and also linking relative uncertainties $u(L_T)/L_T$ to $u(L_w)/L_w$. In agreement with their work, $u(L_T)$ and $u(L_T)/L_T$ are given by

$$u(L_T) = u(L_w)t_d \tag{2}$$

and

$$\frac{u(L_T)}{L_T} = \frac{u(L_w)}{L_w} t_d \frac{L_w}{L_T}. \tag{3}$$

For the purpose of this study centered on SVC, the uncertainties related to the atmospheric correction process do not influence the determination of L_w because both SVC and the atmospheric correction rely on the same robust atmospheric models and algorithms. Thus, to a first approximation Eq. (2) indicates that the absolute uncertainties $u(L_T)$ and $u(L_w)$ are solely related by the factor t_d. Differently, Eq. (3) shows that relative uncertainties $u(L_T)/L_T$ and $u(L_w)/L_w$ are additionally related by the ratio L_w/L_T. Because of this, while the relation between absolute uncertainties only slightly varies with the atmospheric optical properties through t_d, the dependence between relative uncertainties is highly variable with both marine and atmospheric optical properties, which affect the term $t_d \cdot L_w/L_T$. Thus, while satellite-derived L_w may exhibit similar absolute uncertainties for data collected over different water types, the corresponding relative uncertainties may largely differ as a function of L_w and L_T. Considering that requirements for satellite ocean color CDRs are provided in relative terms (e.g., see Ohring et al., 2005; WMO 2011), the following analysis only focuses on relative uncertainties.

Rearranging Eq. (3) as a function of $u(L_T)/L_T$, for which a realistic spectrally independent radiometric uncertainty of 2% is assumed together with an ideal value of $t_d = 1$, $u(L_w)/L_w$ would be approximately 20%, 40% and 200% for L_w/L_T equal to 0.10, 0.05 and 0.01, respectively. These uncertainty values, which may tentatively refer to blue, green and red wavelengths in oligotrophic waters, show the impossibility of meeting science requirements when only relying on current absolute radiometric calibration uncertainties, even assuming an exact quantification of the atmospheric perturbations.

Conversely, the application of Eq. (3) assuming $t_d = 1$ and a spectrally independent uncertainty of 5% for L_w, implies values of $u(L_T)/L_T$ as low as 0.5%, 0.25% and 0.05% for L_w/L_T equal to 0.10, 0.05 and 0.01, respectively. These values provide an estimate for the required spectral uncertainties of absolute radiometric calibrations for satellite ocean color sensors and further confirm that: *i.* even assuming that the uncertainties in $u(L_w)/L_w$ due to atmospheric correction are negligible, the sole uncertainties currently affecting in-flight absolute radiometric calibration are an impediment to meet ocean color science requirements for CDRs; and that *ii.* SVC is the only viable alternative to overcome limitations due to uncertainties in absolute radiometric calibration and atmospheric correction. It is additionally observed that, even accounting for future developments in absolute radiometric calibration, that are expected to considerably reduce uncertainties (Cramer, Lykke, Woodward, & Smith, 2013; Levick et al., 2014), SVC will still remain an essential component of any ocean color mission to minimize effects of inaccurate atmospheric corrections.

2.2. Legacy requirements for SVC sites and data

Early indications on the appropriateness of SVC sites for global missions (mostly derived from Gordon (1998)) include:

i. Cloud free, very clear and maritime atmosphere with aerosol optical thickness $\tau_a < 0.1$ in the visible, which maximizes the potential number of satellite and in situ coincident data (i.e., matchups) and additionally optimizes the performance of the atmospheric correction process;
ii. Horizontally uniform L_w over spatial scales of a few kilometers to increase the comparability between satellite and in situ data at different spatial resolutions;
iii. Mesotrophic waters to minimize the effects of in situ L_w measurement uncertainties in the blue spectral region (this requirement has been considered less stringent with respect to the previous two, leading to consider oligotrophic waters as an appropriate alternative);
iv. Coincident aerosol measurements to assess the atmospheric correction process.

In situ L_w data applicable for SVC are expected to have low uncertainty through the application of state-of-the-art instrumentation, data reduction and quality assurance/control. Indications, mostly derived from Clark et al. (2003), include the need for:

i. Hyper-spectral measurements to cover any ocean color spectral band regardless of its center-wavelengths and spectral responses;
ii. Fully characterized in situ radiometers to minimize uncertainties and allow their comprehensive quantification;
iii. Traceability of data to the International System of Units (SI) to ensure consistency with community shared measurement methods and standards.

Also, in the case of global data products contributing to the construction of CDRs, SVC should be applied using in situ L_w from measurement sites representative of the most common satellite observation conditions, i.e., the world oceans. The determination of regional *g*-factors has also been proposed for areas exhibiting unique optical features (Franz, Bailey, Werdell, & McClain, 2007). It is, however, recognized that this solution is mostly intended to support local applications where accurate in situ L_w data exist.

Ultimately, the limited number of highly accurate in situ data and their high costs challenge SVC at large. This has generated debates on the suitability of a number of data sources for SVC and also motivation for various studies to explore legacy requirements. These studies have produced a number of *g*-factors for the same satellite sensor relying on equivalent versions of the atmospheric correction code, but using L_w from different sources. As will be shown later, results offer the great opportunity to investigate differences among actual *g*-factors in view of discussing implications for the creation of CDRs.

3. Literature data

Among in situ systems specifically designed to support SVC for satellite ocean color sensors, only two ensured almost continuous data collection across a number of satellite ocean color missions. These are: *i.* the Marine Optical Buoy (MOBY) developed by the National Oceanic and Atmospheric Administration (NOAA) and the National Aeronautics and Space Administration (NASA) for the SeaWiFS and the Moderate Resolution Imaging Spectroradiometer (MODIS) (Clark et al., 1997); and *ii.* the Buoy for the Acquisition of a Long-Term Optical Time Series (Bouée pour L'acquisition de Séries Optiques à Long Terme, BOUSSOLE), developed for the Medium Resolution Imaging Spectrometer (MERIS) by the Laboratoire d'Océanographie de Villefranche (LOV) in collaboration with a number of agencies (Antoine et al., 2008).

Aside from MOBY and BOUSSOLE (Bailey, Hooker, Antoine, Franz, & Werdell, 2008, Eplee et al., 2001, Franz et al., 2007), a number of alternative data sources were considered for SVC of SeaWiFS data (see Table 1). These included in situ data sets obtained by combining measurements from a variety of instruments and reduction schemes (Bailey et al., 2008), data from specific coastal areas commonly applied for regional investigations (Mélin & Zibordi, 2010), as well as modeled data (Werdell, Bailey, Franz, Morel, & McClain, 2007). Derived *g*-factors, consistently determined by applying the scheme detailed in Franz et al. (2007) and the SeaWiFS Data Analysis System (SeaDAS, Fu et al., 1996) software package (version 5), are summarized in Table 2.

In agreement with Franz et al. (2007) and with specific reference to SeaWiFS center-wavelengths, *g*-factors are assumed fixed and equal to unity at 865 nm, while the value at 765 nm is computed by imposing a pure maritime aerosol model for locations in the oligotrophic gyres of the southern hemisphere. Spectral *g*-factors in the visible, which are those listed in Table 2, are successively determined from the average of individual factors computed imposing in situ reference water-leaving radiances as target values for the satellite-derived L_w. It is important to note that the averaging reduces the effects of random contributions to uncertainties in *g*-factors, but it does not remove the effects of any bias.

Recalling that unity *g*-factors indicate no correction, the values in Table 2 exhibit high consistency with differences generally within a few tenths of percent. The standard deviation, σ_g, gives an indication of the precision affecting the SVC process as mostly resulting from in situ radiometer stability or varying observation conditions. It is noted that the number of matchups used for SVC in all cases is larger than the approximate 40 estimated by Franz et al. (2007) to determine sufficiently precise *g*-factors for SeaWiFS using MOBY data. However, it is expected that such a number, implicitly referred to SeaWiFS-MOBY matchups, may change when considering observation conditions different from those offered by the MOBY site or satellite sensor performances different from those of SeaWiFS.

General elements on the various data sources utilized for the determination of the *g*-factors listed in Table 2 are summarized in the following sub-sections.

Table 1
General elements on the various sources utilized for SVC of SeaWiFS data: measurement method, spectral features and site location (see text for additional details).

Data source	L_w method	Spectral features	Site
MOBY	In-water, fixed depths	Hyper-spectral	Pacific Ocean (Hawaii)
MOBY-MS	In-water, fixed depths	Reduced resolution	Pacific Ocean (Hawaii)
BOUSSOLE	In-water, fixed depths	Multi-spectral	Ligurian Sea
NOMAD	Various	Various	Various
AAOT	Above-water	Multi spectral	Adriatic Sea
HOT-ORM	Modeled	User definable	Pacific Ocean (Hawaii)
BATS-ORM	Modeled	User Definable	Atlantic Ocean (Bermuda)

3.1. MOBY and MOBY-MS

Since 1997, MOBY has been deployed approximately 11 nautical miles from Lanai (Hawaii) in 1200 m water depth (Clark et al., 1997, Clark et al., 2002). The site was selected based on requirements for an ideal SVC location and accounting for the need to ensure economical and convenient access to shore facilities.

The main components of the MOBY system are: *i.* a spar buoy tethered to a moored buoy; and *ii.* a hyper-spectral radiometer operating in the 340–955 nm spectral region with 1 nm resolution, coupled via fiber optics to a number of radiance and irradiance collectors. These collectors ensure measurements of in-water downward irradiance and upwelling radiance at 1, 5 and 9 m depth. Above-water downward irradiance is additionally measured at 2.5 m above the sea surface. The MOBY radiometer system undergoes regular characterizations and calibrations to guarantee high accuracy and traceability of data to the US National Institute of Standards and Technology (NIST). Internal system sources allow daily monitoring of radiometric stability. By statistically combining uncertainty contributions including those related to the calibration source and its transfer, radiometric stability during deployments, and environmental effects, Brown et al. (2007) showed the capability of reducing uncertainties to approximately 3% in the 412–666 nm spectral interval for upwelling radiance L_u used to determine L_w.

A total of 166 MOBY-SeaWiFS matchups fulfilling strict SVC criteria (Bailey & Werdell, 2006, Franz et al., 2007) over a 7-year period, were applied by Bailey et al. (2008) to produce the SeaWiFS *g*-factors. Criteria for the inclusion of SeaWiFS data resulting from the average of L_w values from the 5×5 pixels centered at the MOBY site, are: no processing flag raised (e.g., indicating cloud contamination, glint perturbations, navigation problems or failure of the atmospheric correction); satellite viewing angle less than 56°; sun zenith angle less than 70°; *Chla* lower than 0.2 μg l^{-1}; τ_a in the near infrared lower than 0.15; and coefficient of variation less than 0.15 for L_{WN} in the blue-green spectral regions and for τ_a in the near-infrared. It is anticipated that similar matchup selection criteria were applied to the other datasets included in this review.

The qualified matchups were constructed by convolving MOBY hyperspectral L_w data with the actual SeaWiFS spectral band responses. Bailey et al. (2008) also considered the parallel case of MOBY L_w averaged over 10 nm bandwidths with center-wavelengths corresponding to those of SeaWiFS. These *g*-factors, referred to as MOBY-Multispectral (MOBY-MS), provide the unique opportunity to look into changes only due to differences in spectral resolution. In fact the radiometer system and measurement conditions are exactly the same for both hyperspectral and derived multispectral data.

3.2. Boussole

BOUSSOLE, operated in the Ligurian Sea since 2003, has been deployed at approximately 32 nautical miles from the coast in 2440 m water depth and relies on a moored buoy optimized to maximize its vertical stability and minimize the shading effects of its superstructure (Antoine, Guevel, et al., 2008). Optical instrumentation on the buoy includes 7-band commercial radiometers with 10 nm bandwidth in the 400–700 nm spectral region. In-water upwelling radiance, upward irradiance, and downward irradiance are measured with radiometers deployed at 4 and 9 m depths, while the downward irradiance is also measured at 4 m above the sea surface. Spectrally independent uncertainty values of approximately 6% have been declared for the normalized remote sensing reflectance determined from L_w (Antoine et al., 2008). Since 2008, BOUSSOLE is also equipped with hyperspectral radiometers to measure the in-water upwelling radiance and downward irradiance, and the above-water downward irradiance. Data from these instruments, which are not part of this study, will be relevant for vicarious calibration activities of future missions.

A significant difference characterizes the extrapolation methods applied to subsurface radiometric data from MOBY and BOUSSOLE. While MOBY values are simply determined from the linear fit of log-transformed radiometric measurements with respect to depth, BOUSSOLE sub-surface values result from the propagation of the 4 and 9 m depth values to the surface through models. This latter data reduction scheme, requiring estimates of *Chla*, takes into account Raman effects and the related nonlinearity of the log-transformed radiometric measurements with depth. Differences between the linear fits of log-transformed radiometric measurements and modeled values, are within a few percent at 412 nm but increase up to several tens percent at 670 nm (Antoine, D'Ortenzio, et al., 2008).

Table 2
Values of *g*-factors (g) and related standard deviations (σ_g) determined for SeaWiFS at its center-wavelengths. *N* indicates the number of matchups used for their determination, and *Y* the approximate number of measurement years.

Data source	*Y*	*N*	$g(412)$	$\sigma_g(412)$	$g(443)$	$\sigma_g(443)$	$g(490)$	$\sigma_g(490)$	$g(510)$	$\sigma_g(510)$	$g(555)$	$\sigma_g(555)$	$g(670)$	$\sigma_g(670)$
MOBY[a]	7	166	1.0368	0.009	1.0132	0.009	0.9918	0.008	0.9982	0.009	0.9993	0.009	0.9729	0.007
MOBY-MS[a]	7	166	1.0401	0.009	1.0136	0.009	0.9949	0.008	0.9937	0.009	0.9958	0.009	0.9691	0.007
BOUSSOLE[a]	3	46[d]	1.0402	0.005	1.0129	0.027	0.9961	0.033	1.0015	0.031	1.0007	0.021	0.9672	0.006
NOMAD[a]	7	64	1.0395	0.013	1.0135	0.013	0.9967	0.014	0.9962	0.017	0.9989	0.013	0.9693	0.009
AAOT[b]	5	99	1.0425	0.012	1.0143	0.014	0.9969	0.018	0.9977	0.019	1.0034	0.022	0.9819	0.020
HOT-ORM[c]	7	176	1.0300	0.015	1.0086	0.012	0.9879	0.009	0.9979	0.008	1.0046	0.009	0.9718	0.006
BATS-ORM[c]	7	241	1.0345	0.018	1.0020	0.016	0.9814	0.013	0.9941	0.011	1.0016	0.011	0.9731	0.006

[a] Bailey et al. (2008).
[b] Mélin and Zibordi (2010).
[c] Werdell et al. (2007).
[d] 5 matchups at 412 nm, only.

BOUSSOLE data were also considered by Bailey et al. (2008) for the determination of SeaWiFS *g*-factors. Specifically, 46 matchups were identified from approximately a 3-year data record by relaxing the inclusion criteria on *Chla* (0.25 instead of 0.20 μg l^{-1}). However, only 5 matchups were available for the 412 nm center-wavelength due to unavailability of that spectral band during some deployments.

3.3. Nomad

The NASA bio-Optical Algorithm Data set (NOMAD, Werdell & Bailey, 2005) includes multi-site and multi-source data resulting from the reprocessing and strict quality control of radiometric measurements from the SeaWiFS Bio-Optical Archive and Storage System (SeaBASS). The variety of measurement methods, instruments, calibration and also data reduction schemes, make it difficult to assign well-defined uncertainties to the NOMAD radiometric data set.

The SeaWiFS *g*-factors determined from NOMAD (Bailey et al., 2008) were computed using 64 matchups fulfilling SVC selection criteria — out of a total of 1039. These field radiometry data result from overall 3475 quality controlled measurements out of 15400 from 1350 field campaigns included in SeaBASS. These numbers clearly indicate the difficulty of supporting SVC with in situ L_w data from repositories constructed for applications more focused on validation and development rather than vicarious calibration.

3.4. AAOT

In contrast with MOBY and BOUSSOLE data, which are collected with systems specifically designed to support SVC, time-series data from a number of globally distributed coastal sites established to support satellite ocean color validation activities are accessible through the Ocean Color component of the Aerosol Robotic Network (AERONET-OC, Zibordi et al., 2009). AERONET-OC field radiometers perform multispectral L_w measurements at a number of ocean color bands with center-wavelengths in the 410–1020 nm spectral region and 10 nm bandwidth. Data collection, reduction and quality control rely on standardized methods (Zibordi et al., 2009) assuring cross-site consistency to data products. Among AERONET-OC sites, the Acqua Alta Oceanographic Tower (AAOT, often indicated as 'Venise'), located in the northern Adriatic Sea at approximately 8 nautical miles from the main land, since 2002 has provided an almost uninterrupted series of data largely applied for the validation of multi-mission ocean color radiometric data (e.g., Mélin et al. 2011, Zibordi & Voss, 2014, Zibordi et al., 2006). Uncertainties of 5% in the blue-green and 8% in the red spectral regions have been quantified for the AAOT fully quality assured normalized water-leaving radiance determined from L_w (Gergely & Zibordi, 2014).

AERONET-OC data from the AAOT were used by Mélin and Zibordi (2010) for the determination of regional SeaWiFS *g*-factors. Specifically, 99 qualified matchups were identified from a 5-year data set by relaxing some selection criteria (e.g., accepting *Chla* up to 3 μg l^{-1} and coefficient of variation up to 0.20 in the blue-green spectral region for satellite data). A particular effort was devoted to correct in situ L_w spectra for the effects of differences in center-wavelengths with respect to SeaWiFS bands.

Results from the study give insight on the relevance of coastal vicarious calibration sites for regional investigations and additionally provide elements to evaluate their suitability for global applications. Still, the spatial and inter-annual variability of both atmospheric and water optical properties in the region do not support the selection of the AAOT as a SVC site for the creation of CDRs.

3.5. HOT-ORM and BATS-ORM

Ocean Reflectance Models (ORM) are an additional source of radiance spectra (Morel & Maritorena, 2001) expected to be of suitable accuracy for oceanic waters. Even though these models are mostly relevant for bio-optical investigations or as diagnostic tools, their usefulness for SVC has been investigated by Werdell et al. (2007) to verify their fitness for historical satellite ocean color sensors (i.e., CZCS and OCTS) for which an extensive time-series of in situ radiometric measurements do not exist.

The SeaWiFS *g*-factors determined using ORM methodology include those relying on the *Chla* time-series from the U.S. Joint Global Ocean Flux Study (JGOFS) Bermuda Atlantic Time-series Study (BATS) and Hawaiian Ocean Time-series (HOT). Specifically, ORM-BATS *g*-factors were determined using 241 matchups from 1998 to 2004, while ORM-HOT *g*-factors were computed for the same period with 176 matchups (Werdell et al., 2007). Comprehensive uncertainty estimates for modeled L_w were not provided.

4. Analysis and discussion

It shall be noted that the *g*-factors in Table 2 were determined with an earlier version of the SeaDAS processor (i.e., version 5) based on an atmospheric model and pre-launch absolute calibration factors (specifically at 412 nm) different from those currently in use. Because of this, the *g*-factors in Table 2 need to be considered outdated for present SeaWiFS data processing. Still, they are the result of a unique combination of investigations and remain a convenient data set to explore effects of differences among *g*-factors in the creation of CDRs. Making use of these data, the following analysis focuses on percent differences between *g*-factors determined from MOBY data, g^{MOBY}, and those from other data sources, *g*, computed as

$$\Delta g = 100\frac{g - g^{MOBY}}{g^{MOBY}}. \quad (4)$$

The choice of the *g*-factors from MOBY as the reference is justified by its ideal location (exhibiting oligotrophic waters and maritime aerosol, in addition to annual cycles of small amplitude) and an extensive characterization of field radiometers and careful examination of radiometric uncertainties. This choice, however, has not to be interpreted as implicitly advocating the use of MOBY for SVC of any satellite ocean color mission.

For completeness it is also mentioned that the HOT-ORM and BATS-ORM *g*-factors included in Table 2, were discussed by Werdell et al. (2007) with respect to the older MOBY *g*-factors determined by Franz et al. (2007) on the basis of 150 match-ups. Those *g*-factors exhibit spectrally averaged differences of −0.09% with respect to the more recent values by Bailey et al. (2008) used in the current analysis. Still, the changes in the values of Δ*g* for HOT-ORM and BATS-ORM resulting from the application of the *g*-factors from Franz et al. (2007) instead of those from Bailey et al. (2008), does not affect the following discussion and conclusions.

The Δ*g* values in Table 3 from the same data source (i.e., inter-band) or across data sources (i.e., intra-band) are generally lower than ±0.5%.

At a first scrutiny, the values of Δ*g* determined for the AAOT and HOT-ORM appear to slightly differ from those determined for a more ideal site like BOUSSOLE or from a very large pool of data like NOMAD. Also interesting are the values of Δ*g* determined for MOBY-MS, which clearly indicate the appreciable effects of non-matching spectral bands or SeaWiFS out-of-band responses, and consequently the importance of in situ hyperspectral L_w data.

Excluding HOT-ORM and BATS-ORM, the values of Δ*g* exhibit high intra-band consistency between 412 and 490 nm, while they show a larger spread between 510 and 670 nm. Excluding a few spectral values particularly from HOT-ORM (i.e., 412 nm), BATS-ORM (i.e., 443 and 490 nm), AAOT (i.e., 412 and 670 nm) and BOUSSOLE (i.e., 670 nm), Δ*g* is generally lower than ±0.5% for all the data sources.

In view of more quantitatively investigating differences in *g*-factors, Eq. (3) is applied to compute $u(L_T)/L_T$ as a function of $u(L_w)/L_w$

Table 3
Relative percent differences Δg between SeaWiFS g-factors at different center-wavelengths determined using Eq. (4) applied to data in Table 2. The values in bold indicate Δg exceeding $\pm 0.3\%$ in the blue-green spectral regions and $\pm 0.1\%$ in the red.

Data source	Δg (412)	Δg (443)	Δg (490)	Δg (510)	Δg (555)	Δg (670)
MOBY-MS	**+0.32**	+0.04	**+0.31**	**−0.45**	**−0.35**	**−0.39**
BOUSSOLE	**+0.33**	−0.03	**+0.43**	**+0.33**	+0.14	**−0.59**
NOMAD	+0.26	+0.03	**+0.49**	−0.20	−0.04	**−0.37**
AAOT	**+0.55**	+0.11	**+0.51**	−0.05	**+0.41**	**+0.93**
HOT-ORM	**−0.66**	**−0.45**	**−0.39**	−0.03	**+0.53**	**−0.11**
BATS-ORM	−0.22	**−1.11**	**−1.05**	**−0.41**	+0.23	+0.02

accounting for actual mean spectral values of the term $t_d \cdot L_w/L_T$ determined using 1997–2010 SeaWiFS data for three different locations: the MOBY site in the Pacific Ocean with mean satellite-derived *Chla* of 0.08 ± 0.02 μg l^{-1} representing oligotrophic waters (O); the BOUSSOLE site in the Ligurian Sea with mean *Chla* of 0.36 ± 0.37 μg l^{-1} representing mesotrophic waters (M); and the AAOT coastal site in the northern Adriatic Sea with mean *Chla* of 1.74 ± 1.40 μg l^{-1} representing coastal waters moderately dominated by sediments (C). When considering all three water types (see Fig. 1), $t_d \cdot L_w/L_T$ exhibits a large range of mean values spanning from approximately 0.07-0.14 at 490 nm, 0.06-0.22 at 555 nm and 0.01-0.12 at 670 nm. These differences are mostly due to site dependent changes in L_w and L_A, both contributing to L_T (see Eq. (1)).

As already stated in Section 2.1, the following analysis assumes the uncertainties related to the atmospheric correction process do not affect the determination of satellite-derived L_w because of the use of the same atmospheric models and algorithms for SVC and for atmospheric correction.

Fig. 2 summarizes results from the application of Eq. (3) using identical spectrally independent relative uncertainties for in situ L_w (i.e., 5%). The derived values of $u(L_T)/L_T$ exhibit a significant spectral dependence and, as expected, are smaller when $t_d \cdot L_w/L_T$ is smaller (i.e., in correspondence with the lower values of L_w). Specifically, the lowest $u(L_T)/L_T$ are observed for mesotrophic waters with values included in the range of approximately 0.2-0.5% in the blue-green spectral regions, and dropping below 0.1% at 670 nm. The values observed for the oligotrophic waters are higher in the blue spectral region with values approaching 0.7%. In agreement with the higher values of L_w, $u(L_T)/L_T$ computed for the coastal waters reach 1.1% at 555 nm and 0.6% at 670 nm. It is mentioned that differences in the observation conditions at the various sites or in the spectral values of $u(L_w)/L_w$, may lead to $u(L_T)/L_T$ different from those presented in Fig. 2. Additionally, the relative combined uncertainty value of L_T determined from a number N of in situ L_w data obtained with

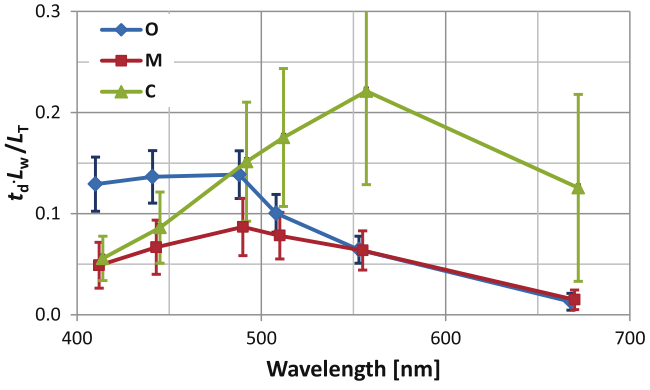

Fig. 1. Spectral values of $t_d \cdot L_w/L_T$ for oligotrophic (O), mesotrophic (M) and coastal (C) waters. Mean values and standard deviations σ (indicated by the vertical error bars), result from the analysis of 814, 1487 and 1045 SeaWiFS data extractions, respectively. The center-wavelengths between spectra have been shifted by ±2 nm to increase readability.

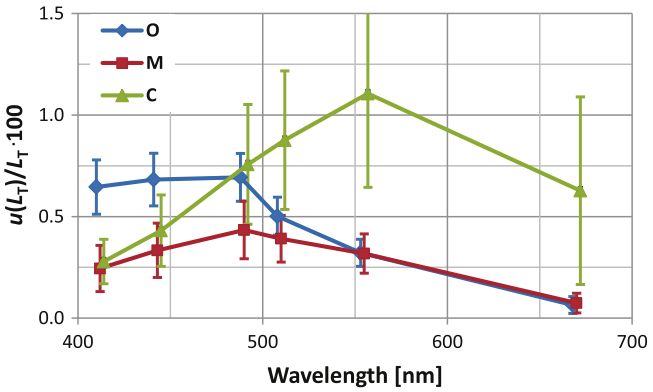

Fig. 2. Relative uncertainties $u(L_T)/L_T$ determined assuming a spectrally independent 5% uncertainty value for L_w with the mean values of $t_d \cdot L_w/L_T$ given in Fig. 1 for different water types: oligotrophic (O), mesotrophic (M) and coastal (C). The vertical bars refer to values determined with $t_d \cdot L_w/L_T \pm \sigma$.

equivalent observation conditions would decrease with respect to the value of $u(L_T)/L_T$ from an individual L_w due to the statistical averaging of the random component of uncertainties.

Rearranging Eq. (3), relative uncertainties in satellite-derived L_w, can be investigated as a function of $u(L_T)/L_T$. By assigning a spectrally independent value of 0.3% to $u(L_T)/L_T$ (i.e., a value that occurs often for $|\Delta g|$ in Table 3), results displayed in Fig. 3 indicate that the 5% uncertainty requirement in satellite-derived L_w generally cannot be met in the red for oligotrophic and mesotrophic waters, and is challenging in the blue mostly at 412 nm for mesotrophic and coastal waters. Because of this, the 0.3% value assigned to $u(L_T)/L_T$, could be considered a rough upper threshold for the uncertainties of g-factors allowing to meet the 5% science requirement for $u(L_w)/L_w$ in the blue-green spectral regions. The same $u(L_w)/L_w$ values displayed in Fig. 3 also indicate that the application to different missions of g-factors determined with independent in situ data sources and exhibiting typical differences of 0.3% in the blue-green spectral regions with respect to the values obtained with an identical in situ data source, may introduce mission dependent biases of several percent in multi-mission CDRs. These biases would hinder stability requirements in satellite-derived products even when applying the same atmospheric correction code to the processing of data from different missions. This result is confirmed by practical assessments presented in Werdell et al. (2007) showing that for deep waters $\Delta g \sim 0.3\%$ may lead to biases of 4% in L_w at 555 nm.

In addition, the spectral differences affecting the values of Δg from the same data source or across data sources (see Table 3), may lead to significant spectral inconsistencies in CDRs. These inconsistencies (i.e., substantial inter-band spectral changes of Δg) would affect the

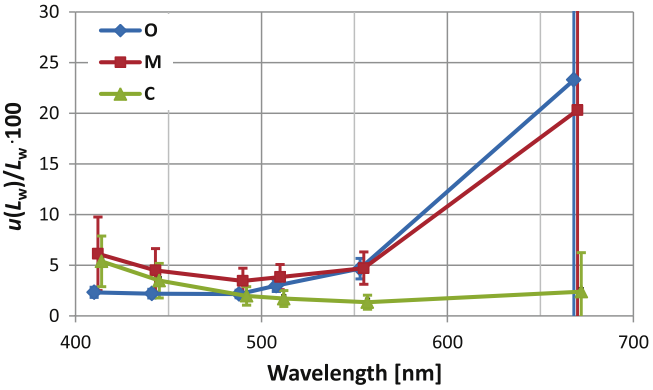

Fig. 3. Relative uncertainties $u(L_w)/L_w$ determined assuming a spectrally independent 0.3% uncertainty value for L_T and the mean values of $t_d \cdot L_w/L_T$ given in Fig. 1 for different water types: oligotrophic (O), mesotrophic (M) and coastal (C). The vertical bars refer to values determined with $t_d \cdot L_w/L_T \pm \sigma$.

capability of meeting the 1% inter-band uncertainty for L_w included in some mission objectives and likely the 3% stability requirement for an ECV like *Chla* (WMO 2011), which is commonly derived from spectral ratios of L_w.

A statistical index that can be of interest to discuss stability requirements for the construction of CDRs from different satellite missions, is the relative standard error of the mean (*RSEM*) of *g*-factors, *g*, determined from

$$RSEM = \left(\sigma_g/g\right)/\sqrt{N_y} \quad (5)$$

with σ_g standard deviation of *g* assumed invariant with time for each considered data source, and N_y the scaled number of match-ups per decade (i.e., $N_y = 10 \cdot N/Y$ where *N* is the number of actual matchups and *Y* the number of measurement years).

The scaling of the number of matchups over a decade, that forces the assumption of continuous availability of measurements for each in situ data source during the considered period, is only applied to facilitate the comparability of *RSEM* values for data which were available for a limited number of years at the time of their application for SVC. Nevertheless, continuous operation and delivery of measurements are required for any in situ SVC data source contributing to the creation of CDRs.

In view of supporting such a discussion on stability requirements through actual numbers, Fig. 4 displays *RSEM* values computed using the data in Table 2.

The notably low values of *RSEM* determined with the MOBY and MOBY-MS data suggest high measurement precision likely explained by very stable measurement conditions, systematic calibration and characterization of field radiometers, robust quality assessment of field measurements and quality control of data products. The higher *RSEM* values resulting from the other data sources are likely explained by a number of factors including (but not restricted to): *i.* measurement conditions perturbed by time-dependent changes in the marine and atmospheric optical properties or observation geometry; *ii.* instability of the in situ measurement system when challenged by environmental perturbations during deployments (e.g., bio-fouling) or by variable performance of radiometer systems operated during successive deployments, or even by different measurement methods when considering a combined data set; *iii* or a relatively small of number of matchups N_y per decade.

The large *RSEM* values determined for BOUSSOLE, which refer to field radiometric measurements performed during the early deployment phase of the buoy system, are due to large σ_g and a relatively small number of matchups. Successive improvements in quality assurance and control of the radiometric measurements have led to a great reduction of σ_g. This is shown by the BOUSSOLE-M *RSEM* values also displayed in Fig. 4, and computed applying recent σ_g of *g*-factors determined for the Medium Resolution Imaging Spectrometer (MERIS). These updated values of σ_g, which refer to a 7-year measurement period, vary between 0.006 and 0.012 with *N* ranging from 15 to 42.

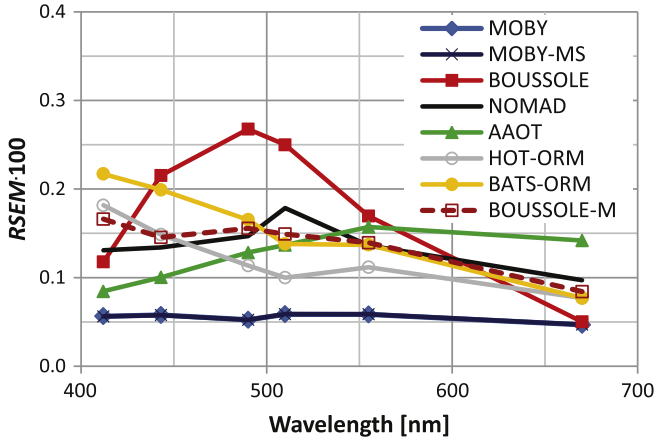

Fig. 4. Plot of the relative standard error of the mean (*RSEM*) for the SeaWiFS *g*-factor given in Table 2 and additionally for MERIS *g*-factors determined with BOUSSOLE data (i.e., BOUSSOLE-M).

Overall, the previous findings suggest that any element affecting reproducibility of measurements and observation conditions with time, and thus challenging the precision of in situ reference measurements, should be minimized to lessen perturbations affecting the random component of uncertainties for *g*-factors and thus the stability requirement for CDRs resulting from the combination of multi-mission satellite-derived data. In addition, frequent swaps of radiometer systems exhibiting similar measurement uncertainties should be considered an important best practice. In fact, the measurement uncertainties would average over the number of deployments occurring during each satellite mission. This is expected to increase the probability of achieving equivalent precision for *g*-factors applicable to the processing of satellite data from independent missions.

To conclude, the 0.5% stability requirement over a decade (WMO 2011) entails maximum uncertainties of approximately 0.05, 0.025 and 0.005% in *g*-factors, assuming generic values of 0.10, 0.05 and 0.01 for the term $t_d \cdot L_w/L_T$. These uncertainties are comparable to the *RSEM* values determined for MOBY in the blue-green spectral regions over a period of approximately 10 years, while they are significantly lower than those determined from the other in situ data sources (see Fig. 4). This result further indicates: *i.* the need for long-term highly consistent in situ data applicable to SVC in view of minimizing any appreciable perturbation that may affect the determination of *g*-factors over time for different or successive satellite missions; and *ii.* caution in using data from sole or multiple sources, which may refer to measurement conditions difficult to reproduce for successive missions.

Additionally, the application of mission-independent atmospheric models and algorithms for the atmospheric correction process is critical.

5. Summary and recommendations

SVC does not literally lead to the absolute radiometric calibration of the satellite sensor. Rather, assuming equivalent observation conditions characterizing both SVC and atmospheric correction processes, SVC forces the determination of satellite-derived L_w with an uncertainty comparable to that of the in situ reference L_w applied for the indirect calibration process. This is achieved through vicarious adjustment gain-factors (i.e., *g*-factors), which are applied to the top of atmosphere radiances L_T after full instrument calibration (e.g., following pre-launch absolute calibration and characterization, and additionally, corrections for temporal changes in radiometric sensitivity as determined through the sensor-specific on-orbit calibration system).

The investigation presented in this work highlights that the relative uncertainty that may affect *g*-factors, to a first approximation depends on the term $t_d \cdot L_w/L_T$ and on the uncertainties affecting in situ L_w data. This finding and differences among *g*-factors determined for the SeaWiFS spectral bands using various data sources, but relying on the same atmospheric models and atmospheric correction algorithms, provide suggestions on the suitability of in situ L_w data sources for SVC devoted to support the construction of CDRs. Specifically, when considering the blue and green center-wavelengths commonly applied for the determination of *Chla*, satellite-derived L_w resulting from the application of *g*-factors differing by as little as 0.3% can result in spectral biases close to 5%. These biases are several times higher than the 0.5% target stability value per decade indicated for satellite ocean color data products expected to contribute to CDRs. Thus, in view of avoiding inconsistencies in long-term data records resulting from the combination of satellite products from multiple missions, a careful evaluation of sites and in situ measurements supporting SVC is needed. In particular, the determination of *g*-factors by combining match-ups from multiple

sites, which is often a viable solution to shorten the otherwise long time needed to accumulate a relatively large number of matchups satisfying early mission needs or mission-specific objectives, has to be regarded as a potential source of artifacts for CDRs. In fact, even assuming equivalent uncertainties for in situ data from different sources and a single atmospheric correction code, differences in *g*-factors may result from a diverse performance of the atmospheric correction process at different sites due to differences in satellite observing geometries or marine and atmospheric optical properties. Further, differences in the performance of various in situ radiometer systems may also affect the accuracy and precision of *g*-factors through those of the in situ L_w data and thus also affect the stability requirements of CDRs.

In view of defining strategies for the upcoming satellite ocean color missions, the previous findings and considerations suggest that the creation of ocean color CDRs should ideally rely on: *i*. one main long-term in situ calibration system (site and radiometry) established and sustained with the objective to maximize accuracy and precision over time of *g*-factors and thus minimize possible biases among satellite data products from different missions; and *ii*. unique (i.e., standardized) atmospheric models and algorithms for atmospheric corrections to maximize cross-mission consistency of data products at locations different from that supporting SVC.

Accounting for results from this study and any element already provided in literature, it is expected that an ideal ocean color SVC site should meet the following general requirements:

1. Located in a region chosen to maximize the number of high-quality matchups by trading off factors such as best viewing geometry, sun-glint avoidance, low cloudiness, and additionally set away from any continental contamination and at a distance from the mainland to safely exclude any adjacency effect in satellite data;
2. Exhibiting known or accurately modeled optical properties coinciding with maritime atmosphere and oligotrophic/mesotrophic waters, to represent the majority of world oceans and minimize relative uncertainties in computed *g*-factors;
3. Characterized by high spatial homogeneity and small environmental variability, of both atmosphere and ocean, to increase precision of computed *g*-factors.

Any field radiometer system supporting SVC should rely on advanced in situ measurement technologies, data reduction methods and quality assurance/control schemes to minimize relative standard uncertainties in in situ L_w to within state-of-the-art values. In particular, uncertainty target values should be 3–4% in the blue-green spectral regions and, even though not relevant for GCOS, tentatively below 5% in the red, with inter-band uncertainties lower than 1%. In particular, accounting for findings from this study and from literature and without advocating the adoption of any existing SVC radiometry system, the fulfillment of the following wide-range requirements for in situ radiometric measurements should be considered of utmost importance:

i. Hyperspectral field data with sub-nanometer resolution to allow system vicarious calibration of any satellite ocean color sensor regardless of its center-wavelengths and spectral responses, and thus ensure minimization of inter-band uncertainties;
ii. State-of-the-art absolute calibration traceable to National Metrology Institutes (i.e., tentatively with target standard calibration uncertainty lower than 2% for radiance and stability better than 0.5% per deployment) and comprehensive characterizations of radiometers in terms of linearity, temperature dependence, polarization sensitivity and stray light effects, in view of minimizing measurement uncertainties and allowing for accurate determinations of uncertainty budgets;
iii. Application of quality assurance/control schemes minimizing effects of measurement perturbations like those (when applicable) due to infrastructure shading, radiometer self-shading, wave perturbations, bio-fouling, and additionally scheduling regular checks of in situ systems and frequent swap of radiometers, as best practice to maximize long-term accuracy and precision of in situ reference radiometric data;
iv. Data rate ensuring generation of matchups for any satellite ocean color mission with time differences appropriate to minimize variations in bi-directional effects due to changes in sun zenith and daily fluctuations in the vertical distribution of phytoplankton.

In addition to requirements for establishing an ideal SVC site and generating in situ radiometric data with the needed accuracy and precision, the supplementary capability of continuously characterizing both the atmospheric (e.g., τ_a) and water (e.g., inherent) optical properties would provide additional important elements for the quality assurance of matchups applicable to determine *g*-factors.

It is reminded that strategies for the construction of CDRs also suggest establishing and maintaining secondary in situ long-term systems with performance equivalent to the main one in terms of data accuracy, precision and measurement conditions. This recommendation is enforced by the fundamental need to allow for redundancy ensuring fault-tolerance to SVC and additionally to provide optimal means for continuous verification and validation of satellite primary data products including the capability to accurately investigate systematic effects induced by different observation conditions (i.e., viewing and illumination geometry, atmosphere and water types).

It is finally mentioned that the need to standardize the atmospheric correction process for multi-mission data contributing to CDRs is a requirement as relevant as the availability of in situ data from one ideal SVC site. This operational need, however, should not be seen as an impediment to further advance atmospheric models and atmospheric correction algorithms.

Acknowledgments

The authors would like to express appreciation to the International Ocean Color Coordination Group (IOCCG) for promoting a number of initiatives stimulating discussions on satellite ocean color system vicarious calibration which encouraged this study.

This work is dedicated to the memory of Dennis Clark whose commitment to Ocean Color led to the design, implementation and long-term operation of MOBY.

The contents of this paper reflect the views of the authors and should not be interpreted as an official statement of policy, decision, or position on behalf of any of the organizations mentioned.

References

Antoine, D., D'Ortenzio, F., Hooker, S. B., Bécu, G., Gentili, B., Tailliez, D., et al. (2008). Assessment of uncertainty in the ocean reflectance determined by three satellite ocean color sensors (MERIS, SeaWiFS and MODIS-A) at an offshore site in the Mediterranean Sea (BOUSSOLE project). *Journal of Geophysical Research, 113*(C7), C07013.

Antoine, D., Guevel, P., Deste, J. F., Bécu, G., Louis, F., Scott, A. J., et al. (2008a). The "BOUSSOLE" buoy-a new transparent-to-swell taut mooring dedicated to marine optics: Design, tests, and performance at sea. *Journal of Atmospheric and Oceanic Technology, 25*, 968–989.

Attila, J., Koponen, S., Kallio, K., Lindfors, A., Kaitala, S., & Ylöstalo, P. (2013). MERIS Case II water processor comparison on coastal sites of the northern Baltic Sea. *Remote Sensing of Environment, 128*, 138–149.

Bailey, S. W., Hooker, S. B., Antoine, D., Franz, B. A., & Werdell, P. J. (2008). Sources and assumptions for the vicarious calibration of ocean color satellite observations. *Applied Optics, 47*, 2035–2045.

Bailey, S. W., & Werdell, P. J. (2006). A multi-sensor approach for the on-orbit validation of ocean color satellite data products. *Remote Sensing of Environment, 102*, 12–23.

Behrenfeld, M. J., O'Malley, R. T., Siegel, D. A., McClain, C. R., Sarmiento, J. L., Feldman, G. C., et al. (2006). Climate-driven trends in contemporary ocean productivity. *Nature, 444*(7120), 752–755.

Brown, S. W., Flora, S. J., Feinholz, M. E., Yarbrough, M. A., Houlihan, T., Peters, D., et al. (2007). The Marine Optical BuoY (MOBY) radiometric calibration and uncertainty

budget for ocean color satellite sensor vicarious calibration. *SPIE Conference Proceedings Remote Sensing* (pp. 67441M). International Society for Optics and Photonics.

Butler, J. J., Johnson, B. C., Rice, J. P., Brown, S. W., & Barnes, R. A. (2007). Validation of radiometric standards for the laboratory calibration of reflected-solar Earth-observing satellite instruments. *SPIE conference proceedings earth observing systems* (pp. 667707). International Society for Optics and Photonics.

Clark, D. K., Feinholz, M. E., Yarbrough, M. A., Johnson, B. C., Brown, S. W., Kim, Y. S., et al. (2002). *Overview of the radiometric calibration of MOBY. SPIE proceedings earth observing systems VI, 4483*. (pp. 64–76).

Clark, D. K., Gordon, H. R., Voss, K. J., Ge, Y., Broenkow, W., & Trees, C. (1997). Validation of atmospheric correction over the oceans. *Journal of Geophysical Research*, *102*(D14), 17209–17217.

Clark, D. K., Yarbrough, M. A., Feinholz, M., Flora, S., Broenkow, W., Kim, Y. S., et al. (2003). A radiometric buoy for performance monitoring and vicarious calibration of satellite ocean color sensors: Measurement and data analysis protocols. In J. L. Mueller, G. S. Fragion, & V. R. Mc Clain (Eds.), *Ocean optics protocols for satellite ocean color sensor validation* (NASA/TM-2003-211621/Rev4-Vol. VI, Greenbelt, MD).

Cramer, C. E., Lykke, K. R., Woodward, J. T., & Smith, A. W. (2013). Precise measurement of lunar spectral irradiance at visible wavelengths. *Journal of Research of the National Institute of Standards*, *118*, 396–402.

Eplee, R. E., Robinson, W. D., Bailey, S. W., Clark, D. K., Werdell, P. J., Wang, M., et al. (2001). Calibration of SeaWiFS. II. Vicarious techniques. *Applied Optics*, *40*, 6701–6718.

Eplee, R. E., Jr., Sun, J. -Q., Meister, G., Patt, F. S., Xiong, X., & McClain, C. R. (2011). Cross calibration of SeaWiFS and MODIS using on-orbit observations of the moon. *Applied Optics*, *50*, 120–133.

Esposito, J. A., Xiong, X., Wu, A., Sun, J., & Barnes, W. L. (2004). MODIS reflective solar bands uncertainty analysis. *SPIE conference proceedings earth observing systems* (pp. 448–458). International Society for Optics and Photonics.

Franz, B. A., Bailey, S. W., Werdell, P. J., & McClain, C. R. (2007). Sensor-independent approach to the vicarious calibration of satellite ocean color radiometry. *Applied Optics*, *46*, 5068–5082.

Fu, G., Scheiber, B. D., Settle, K. J., Darzi, M., McClain, C. R., & Arrigo, K. R. (1996). SeaDAS: A processing package for ocean color satellite imagery. *Proceedings twelfth int. conf. on interactive inform. and processing systems for meteorol., oceanogr., and hydrol* (pp. 451–456).

Gergely, M., & Zibordi, G. (2014). Assessment of AERONET L_{WN} uncertainties. *Metrologia*, *51*, 40–47.

Gordon, H. R. (1987). Calibration requirements and methodology for remote sensors viewing the ocean in the visible. *Remote Sensing of Environment*, *22*, 103–126.

Gordon, H. R. (1998). In orbit calibration strategy for ocean color sensors. *Remote Sensing of Environment*, *63*, 265–278.

Gordon, H. R., & Clark, D. K. (1981). Clear water radiances for atmospheric correction of coastal zone color scanner imagery. *Applied Optics*, *20*, 4175–4180.

Gordon, H. R., Clark, D. K., Brown, J. W., Brown, O. B., Evans, R. H., & Broenkow, W. W. (1983). Phytoplankton pigment concentrations in the Middle Atlantic Bight: Comparison of ship determinations and CZCS estimates. *Applied Optics*, *22*, 20–36.

Hooker, S. B., Esaias, W. E., Feldman, G. C., Gregg, W. W., & McClain, C. R. (1982). In S. B. Hooker, & E. R. Firestone (Eds.), *An overview of SeaWiFS and ocean color. NASA Tech. Memo. 1992–104566, vol. 1*, . Greenbelt, MD: NASA Goddard Space Flight Center.

IOCCG (2010). Atmospheric correction for remotely-sensed ocean-colour products. In M. Wang (Ed.), *Reports of the international ocean-colour coordinating group, no.10* (pp. 78). Dartmouth, Canada: IOCCG.

IOCCG (2013). In-flight calibration of satellite ocean-colour sensors. In R. Frouin (Ed.), *Reports of the international ocean-colour coordinating group, no.14* (pp. 106). Dartmouth, Canada: IOCCG.

Joint Committee for Guides in Metrology (JCGM) (2008). Evaluation of measurement data—Guide to the expression of uncertainty in measurement. *Joint Committee for Guides in Metrology*, *100*.

Koepke, P. (1982). Vicarious satellite calibration in the solar spectral range by means of calculated radiances and its application to Meteosat. *Applied Optics*, *21*, 2845–2854.

Leroy, S. S., Anderson, J. G., & Ohring, G. (2008). Climate signal times and constrains on climate benchmark accuracy requirements. *Journal of Climate*, *21*, 841–846.

Levick, A. P., Greenwell, C. L., Ireland, J., Woolliams, E. R., Goodman, T. M., Bialek, A., et al. (2014). Spectral radiance source based on supercontinuum laser and wavelength tunable bandpass filter: The spectrally tunable absolute irradiance and radiance source. *Applied Optics*, *53*, 3508–3519.

Mélin, F., & Zibordi, G. (2010). Vicarious calibration of satellite ocean color sensors at two coastal sites. *Applied Optics*, *49*, 798–810.

Mélin, F., Zibordi, G., Berthon, J. -F., Bailey, S., Franz, B., Voss, K. J., et al. (2011). Assessment of MERIS reflectance data as processed with SeaDAS over the European Seas. *Optics Express*, *19*, 25657–25671.

Morel, A., & Maritorena, S. (2001). Bio-optical properties of oceanic waters: A reappraisal. *Journal of Geophysical Research*, *106*(C4), 7163–7180.

Ohring, G., Wielicki, B., Spencer, R., Emery, B., & Datla, R. (2005). Satellite instrument calibration for measuring global climate change: Report of a workshop. *Bulletin of the American Meteorological Society*, *86*, 1303–1313.

Werdell, P. J., & Bailey, S. W. (2005). An improved in-situ bio-optical data set for ocean color algorithm development and satellite data product validation. *Remote Sensing of Environment*, *98*, 122–140.

Werdell, P. J., Bailey, S. W., Franz, B. A., Morel, A., & McClain, C. R. (2007). On-orbit vicarious calibration of ocean color sensors using an ocean surface reflectance model. *Applied Optics*, *46*, 5649–5666.

World Meteorological Organization (WMO) (2011). Systematic observation requirements for satellite-based data products for climate 2011. *Update supplemental details to the satellite-based component of the implementation plan for the global observing system for climate in support of the UNFCCC (2010 update). Report GCOS — 154*. World Meteorological Organization.

Zibordi, G., Holben, B. N., Slutsker, I., Giles, D., D'Alimonte, D., Mélin, F., et al. (2009). AERONET-OC: A network for the validation of ocean color primary radiometric products. *Journal of Atmospheric and Oceanic Technology*, *26*, 1634–1651.

Zibordi, G., Mélin, F., & Berthon, J. -F. (2006). Comparison of SeaWiFS, MODIS, and MERIS radiometric products at a coastal site. *Geophysical Research Letters*, *L06617*. http://dx.doi.org/10.1029/2006GL025778.

Zibordi, G., & Voss, K. J. (2014). In situ optical radiometry in the visible and near infrared. In G. Zibordi, C. Donlon, & A. Parr (Eds.), *Optical radiometry for ocean climate measurement*. Academic Press.

Annex 2

Impact of spectral resolution of in situ ocean color radiometric data in satellite matchups analyses. Reprinted from *Optics Express* 25, A798-A812.

Impact of spectral resolution of *in situ* ocean color radiometric data in satellite matchups analyses

GIUSEPPE ZIBORDI,[1,*] MARCO TALONE,[1] KENNETH J. VOSS,[2] AND B. CAROL JOHNSON[3]

[1] *European Commission, Joint Research Centre, 21027 Ispra, Italy*
[2] *University of Miami, Coral Gables, Florida 33124, USA*
[3] *Sensor Science Division, National Institute of Standards and Technology, Gaithersburg, MD, USA*
* giuseppe.zibordi@ec.europa.eu

Abstract: The spectral resolution requirements for *in situ* remote sensing reflectance R_{RS} measurements aiming at supporting satellite ocean color validation and system vicarious calibration (SVC) were investigated. The study, conducted using sample hyperspectral R_{RS} from different water types, focused on the visible spectral bands of the Ocean Land Color Imager (OLCI) and of the Plankton, Aerosol, Cloud, ocean Ecosystem (PACE) satellite sensors. Allowing for a ±0.5 % maximum difference between *in situ* and satellite derived R_{RS} solely due to the spectral band characteristics of the *in situ* radiometer, a spectral resolution of 1 nm for SVC of PACE is needed in oligotrophic waters. Requirements decrease to 3 nm for SVC of OLCI. In the case of validation activities, which exhibit less stringent uncertainty requirements with respect to SVC, a maximum difference of approximately 1% between *in situ* and satellite derived data indicates the need for a spectral resolution of 3 nm for both OLCI and PACE in oligotrophic waters. Conversely, spectral resolutions of 6 nm for PACE and 9 nm for OLCI appear to satisfy validation activities in optically complex waters.

© 2017 Optical Society of America

OCIS codes (280.0280) Remote sensing and sensors; (120.0120) Instrumentation, measurement, and metrology.

References and links

1. World Meteorological Organization (WMO), *The Global Observing System for Climate: Implementation needs.* Report GCOS – 200 (2016) (available at http://unfccc.int/files/science/workstreams/systematic_observation/application/pdf/gcos_ip_10oct2016.pdf).
2. H. R. Gordon, "Calibration requirements and methodology for remote sensors viewing the ocean in the visible," Remote Sens. Environ. **22**, 103–126 (1987).
3. G. Zibordi, G., J.F. Berthon, F. Mélin, D. D'Alimonte, and S. Kaitala, "Validation of satellite ocean color primary products at optically complex coastal sites: Northern Adriatic Sea, Northern Baltic Proper and Gulf of Finland," Remote Sens. Environ. **113**(12), 2574–2591 (2009).
4. F. Mélin, and G. Sclep, "Band shifting for ocean color multi-spectral reflectance data," Opt. Express **23** (3), 2262–2279 (2015).
5. M. R. Wernand, S. J. Shimwell, and J. C. De Munck, "A simple method of full spectrum reconstruction by a five-band approach for ocean colour applications," Int. J. Remote Sens. **18**(9), 1977–1986 (1997).
6. Z. Lee, S. Shang, C. Hu, and G. Zibordi, "Spectral interdependence of remote-sensing reflectance and its implications on the design of ocean color satellite sensors," Appl. Opt. **53**(15), 3301–3310 (2014).
7. B. C. Johnson, S. Flora, S. Brown, D. Clark, M. Yarbrough, and K. Voss, "Spectral resolution requirements for vicarious calibration of ocean color satellites". Presented at the Ocean Color Research Team Meeting, Seattle (2007), available at http://oceancolor.gsfc.nasa.gov/cms/DOCS/ScienceTeam/OCRT_Apr2007/Posters/.
8. D. K. Clark, H. R. Gordon, K. J. Voss, Y. Ge, W. Broenkow, and C. Trees, "Validation of atmospheric correction over the oceans," J. Geophys. Res. **102**(17), 209–17 (1997).
9. S. W. Brown, S. J. Flora, M. E. Feinholz, M. A. Yarbrough, T. Houlihan, D. Peters, K. Y. S. Kim, J. L. Mueller, B. C. Johnson, and D. K. Clark, "The Marine Optical BuoY (MOBY) radiometric calibration and uncertainty budget for ocean color satellite sensor vicarious calibration," in SPIE Conference Proceedings *Remote Sensing,* pp. 67441M–67441M. International Society for Optics and Photonics (2007).
10. G. Zibordi, J-F. Berthon, F. Mélin, and D. D'Alimonte, "Cross-site consistent in situ measurements for satellite ocean color applications: The BiOMaP radiometric dataset," Remote Sens. Environ. **115**, 2104-2115 (2011).

11. A. Tonizzo, M. Twardowski, S. McLean, K. Voss, M. Lewis, C. and Trees, "Closure and uncertainty assessment for ocean color reflectance using measured volume scattering functions and reflective tube absorption coefficients with novel correction for scattering," Appl. Opt. **56**, 130 – 146 (2017),
12. M. Berger, J. Moreno, J. A. Johannessen, P. F. Levelt, and R. F. Hanssen, "ESA's sentinel missions in support of Earth system science," Remote Sens. Environ. **120**, 84–90 (2012).
13. C. Del Castillo, *Pre-Aerosol, Clouds, and ocean Ecosystem (PACE) Mission science definition team report* (2012), *available at* https://pace.oceansciences.org/docs/pace_sdt_report_final.pdf.
14. B. A. Franz, S. W. Bailey, P. J. Werdell, and C. R. McClain, "Sensor-independent approach to the vicarious calibration of satellite ocean color radiometry," Appl. Opt. **46**, 5068–5082 (2007).
15. S. W. Bailey, S. B. Hooker, D. Antoine, B. A. Franz, and P. J. Werdell, "Sources and assumptions for the vicarious calibration of ocean color satellite observations," Appl. Opt. **47**(12), 2035–2045 (2008).
16. G. Zibordi, F. Mélin, K. J. Voss, B. C. Johnson, B. A. Franz, E. Kwiatkowska, J.-P. Huot, M. Wang, and D. Antoine, "System vicarious calibration for ocean color climate change applications: Requirements for *in situ* data," Remote Sens. Environ. **159**, 361–369 (2015).

1. Introduction

Satellite ocean color radiometric products, such as the water-leaving radiance, L_w, or the related remote sensing-reflectance, R_{RS}, are the fundamental quantities used to generate geo-physical data products (e.g., chlorophyll concentration, *Chla*). Accuracy requirements set for these derived products [1,2] bound uncertainty requirements for satellite radiometric data.

Presently, post-launch system vicarious calibration (SVC) [2] is the only viable approach allowing satellite radiometric data to meet the level of uncertainty that satisfies requirements for ocean color products. The SVC process implies the use of highly accurate *in situ* radiometric measurements. *In situ* radiometric data are also frequently applied to investigate uncertainties affecting satellite products through validation exercises.

Markedly, both validation and SVC applications rely on matchups (i.e., time and space coincident) of *in situ* and satellite ocean color radiometric data. This implies a comprehensive assessment of the various sources of uncertainty affecting the *in situ* measurements, which include radiometric, methodological and environmental factors. A source of uncertainty, which causes systematic differences between *in situ* and satellite radiometric data, but is controllable by instrument design, is the diversity of spectral characteristics of *in situ* and satellite ocean color sensors due to the different widths, shapes and center-wavelengths of corresponding spectral bands. This uncertainty can be minimized through the application of corrections (i.e., band-shifting) obtained by modeling the spectral dependence of radiometric quantities such as R_{RS} [3,4]. This solution, however, may still be subject to substantial uncertainties due to the lack of accurate information on seawater optical properties and additionally by incomplete information on the spectral response functions of *in situ* sensors. An alternative solution is given by the statistical reconstruction of R_{RS} from discrete values measured in various spectral bands [5,6]. In this case, the uncertainties affecting the determination of R_{RS} spectra depend on the number of spectral bands, their location and width. As the portion of the uncertainties that are driven by environmental factors and the radiometric calibration process, when combined, can be a large fraction of the desired maximum limit, it is critical that those factors that can be controlled by instrument design be minimized and do not add significantly to the combined uncertainty budget for the *in situ* data.

The problem of spectral differences can be reduced with *in situ* hyperspectral data (i.e., data collected with a relatively large number of narrow spectral bands distributed continuously over the spectrum). In fact, compared to multispectral measurements, *in situ* hyperspectral data allow the determination of R_{RS} in the spectral bands of the satellite sensor with an accuracy increasing with the spectral resolution (defined by the sensor bandwidth $\Delta\lambda_B$ determined by the

full width at half maximum spectral response) and the spectral sampling interval (i.e., the distance between center-wavelengths of adjacent bands $\Delta\lambda_C$) of the *in situ* sensor.

Thus, hyperspectral *in situ* radiometric data can be the optimum solution for SVC data due to the need to minimize this source of uncertainty in the accurate determination of mission specific gain-factors (i.e., *g*-factors) for satellite radiometric data. Specifically, as an extreme case, the accessibility of sub-nanometer radiometric spectra would allow accurate R_{RS} values to be determined for any multispectral or hyperspectral space sensor. In fact, assuming the satellite sensor is comprehensively characterized, *in situ* sub-nanometer spectra would allow the satellite spectral response functions and out-of-band or stray light perturbations to be fully accounted for. However, the technological complexity, and cost, intrinsic in sub-nanometer radiometer systems suggests that there may be a tradeoff between spectral resolution and allowable uncertainty.

The overall objective of this work, which expands on a previous assessment [7], is to investigate the impact of the spectral resolution of *in situ* radiometric data on the determination of R_{RS} at bands representative of current and forthcoming ocean color sensors. The analysis aims at estimating the sole contribution of spectral resolution to the uncertainty budget affecting the comparison of *in situ* and satellite R_{RS}. It specifically focuses on the visible spectral bands of the Ocean Land Color Imager (OLCI) from the European Space Agency (ESA) operating onboard Sentinel-3 since 2016, and of the Plankton, Aerosol, Cloud, ocean Ecosystem (PACE) of the National Aeronautics and Space Administration (NASA) planned for launch in 2022.

2. Data and methods

The study relies on sample R_{RS} spectra from marine waters characterized by varying concentrations of optically significant constituents. These spectra are applied to investigate differences between *in situ* and satellite data solely due to dissimilar spectral bands. Recalling that the analysis is restricted to satellite bands representative of current multispectral and future hyperspectral ocean color systems, the final objective of the work is the definition of requirements for *in situ* hyperspectral sensors supporting validation and SVC applications. It is emphasized that the study is focused on the impact of spectral resolution on *in situ* radiometric measurements and excludes any other source of uncertainty that may affect matchup analysis, or correction schemes that may minimize spectral differences between sensors.

2.1 Data

The study is performed using samples of *in situ* hyperspectral radiometric data representative of various water types. The fundamental quantities are the R_{RS} spectra displayed in Fig. 1 and determined from the ratio of water leaving radiance L_W to downward irradiance E_S. One sample R_{RS} spectra was obtained with the Marine Optical System (MOS) from fixed-depth measurements performed in ultra-oligotrophic waters at the Marine Optical Buoy (MOBY) site with spectral resolution $\Delta\lambda_B$ of 1 nm and a spectral sampling interval $\Delta\lambda_C$ of approximately 0.6 nm [8,9]. Additional sample data are R_{RS} spectra from above-water radiometric measurements performed with RAMSES hyperspectral radiometers in various European seas. These embrace oligotrophic waters in the Western Mediterranean Sea, and optically complex waters in the Western Black and northern Adriatic Seas. RAMSES radiometers, manufactured by TriOS (Rastede, Germany), have a spectral resolution of approximately 10 nm and a nominal spectral sampling interval of 3.3 nm. Clearly, while MOS spectra are suitable to address investigations up to approximately 1 nm spectral resolution, RAMSES data may not fully satisfy requirements to assess R_{RS} spectral matching at resolutions lower than several nanometers. The uncertainties

associated with this limitation, are addressed in the discussion section. It is however anticipated that, while MOS spectra are mostly applied to address both the validation and highly demanding SVC requirements in oligotrophic waters, RAMSES data are only used to draw general conclusions on the less stringent requirements for the validation of satellite products in optically complex waters.

The analysis is restricted to the spectral region between 380 nm and 700 nm for which the considered *in situ* radiometric data exhibit reliable values (i.e., not largely affected by reduced sensitivity of the radiometers or an input signal that is too small), and additionally represent the spectral region of utmost interest for both validation and SVC activities. With respect to this, there are some peculiar features near 400 nm in the spectrum representing ultra-oligotrophic waters as displayed in Fig. 1. These can be explained by slight differences on the order of 0.1 nm in E_S and L_W spectral calibrations in a region characterized by Fraunhofer lines in the solar irradiance. Because of this, results related to such a narrow spectral region need to be considered with some caution.

Details of water bio-optical quantities related to the R_{RS} spectra included in the analysis are summarized in Table 1. These include *Chla*, concentration of total suspended matter, *TSM*, and the absorption coefficient, a, and backscattering coefficient, b_b, at 490 nm of optically significant water constituents. Their values fully support the diversity of cases represented by the R_{RS} spectra considered.

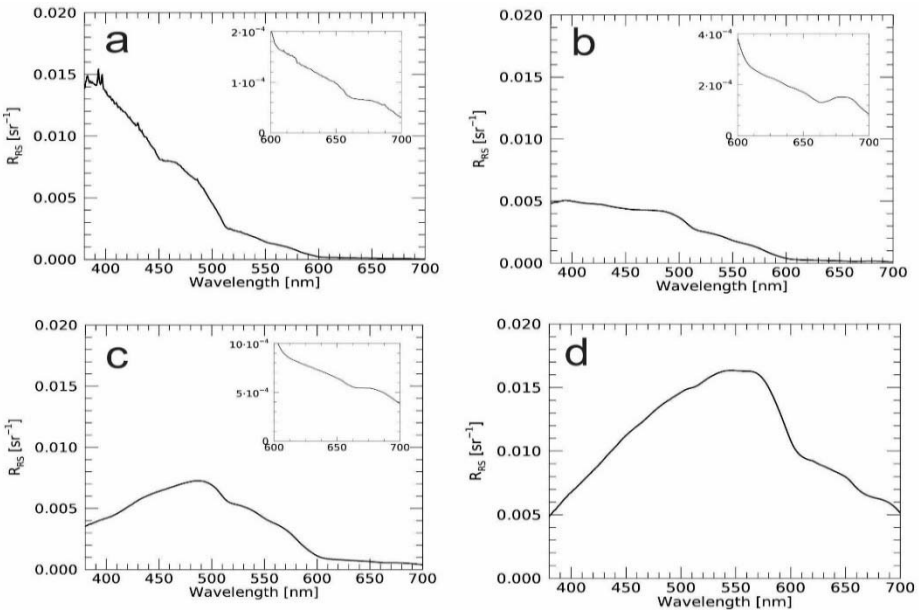

Fig. 1. Sample R_{RS} spectra used in this study. NP (a) and WM (b) refer to the North Pacific Gyre and the Western Mediterranean Sea oligotrophic waters, while WB (c) and NA (d) refer to the Western Black Sea and northern Adriatic optically complex waters. Insets in panels a-c display R_{RS} with scales expanded in the 600-700 nm interval to better visualize spectral features.

Table 1. Bio-optical quantities[a] related to the R_{RS} spectra used in this study: *Chla* and *TSM* indicate the concentration of chlorophyll-a and of total suspended matter, while *a* and b_b indicate the absorption and backscattering coefficients at 490 nm of optically significant constituents, respectively.

Region	Date [dd/mm/yyyy]	Sun zenith [°]	*Chla* [μg l^{-1}]	*TSM* [mg l^{-1}]	*a*(490) [m^{-1}]	b_b(490) [m^{-1}]
North Pacific Gyre (NP)	15/06/2015	4.1	0.13[b]	0.10[b]	0.019[c]	0.0027[c]
Western Med. Sea (WM)	18/04/2014	29.2	0.35	0.24	0.037	0.0027
Western Black Sea (WB)	05/06/2016	45.2	0.27	0.44	0.048	0.0058
North Adriatic Sea (NA)	08/04/2015	54.3	2.68	6.30	0.149	0.0528

[a] from the BioMAP [10] data set.
[b] provided by Stephanie Flora (Moss Landing Marine Labs);
[c] from published values [11], here increased by the pure seawater contribution.

2.2 Spectral bands of satellite sensors

As already mentioned, this study is centered on OLCI [12], representative of current global satellite ocean color sensors, and additionally on PACE [13], which is assumed to be representative of future advanced hyperspectral earth observing systems. While OLCI relies on spectral bands commonly exhibiting 10 nm bandwidth in the visible spectral region (15 nm at 400 nm), PACE will have a large number of bands with 5 nm bandwidth from the ultraviolet to the near-infrared. Consequently, PACE-like bands have been designed by assuming 5 nm bandwidth, an ideal Gaussian spectral response function, and 5 nm spectral sampling interval. It is recognized that this solution produces a sampling of R_{RS} spectra that may differ slightly from actual capabilities of the future space sensor.

The relative spectral response functions for OLCI and PACE-like bands are illustrated in Fig. 2.

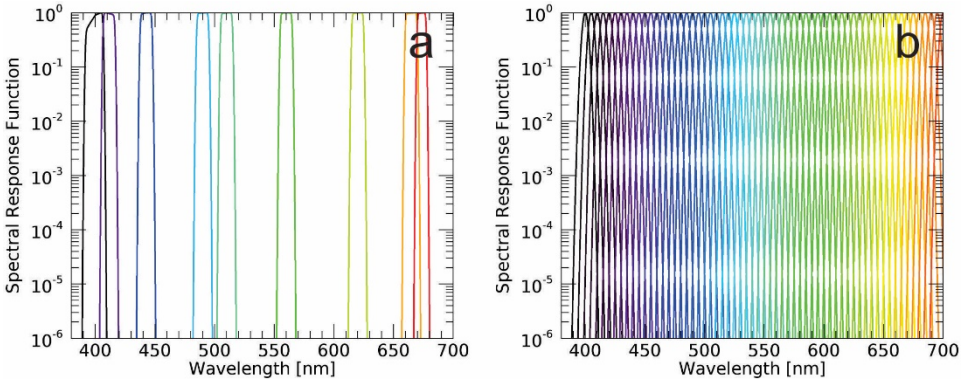

Fig. 2. Relative spectral response functions of the visible OLCI (a) and PACE-like (b) bands.

2.3 Band spectral matching

The spectral matching scheme introduced in this section has been devised to investigate differences between R_{RS} obtained with OLCI or PACE-like sensors, and R_{RS} values reconstructed with *in situ* hyperspectral data having various spectral resolutions and sampling intervals. These differences introduce uncertainties in the SVC process, and are also relevant for the application of *in situ* data to the validation of satellite radiometric products requiring the comparison of satellite and *in situ* R_{RS} values.

It is emphasized that regardless of the focus on R_{RS}, L_W and E_S are processed separately before computing R_{RS} (i.e., $R_{RS} = L_W / E_S$) to fully account for the independence of L_W and E_S measurements from different radiometers.

The flow diagram in Fig. 3 summarizes the matching scheme. The different radiometric quantities identified in the diagram and applied in the following analysis (i.e., L_W, E_S or R_{RS}) are hereafter indicated using the generic variable $\Re$. Specifically,

$\Re^n$: sample L_W and E_S values from MOS or RAMSES hyperspectral sensors;

$\Re^r$: reference L_W and E_S hyperspectral values determined from the resampling at higher spectral resolution (i.e., 0.1 nm) through linear interpolation of the $\Re^n$ sample spectra;

$\Re^s$: satellite-exact radiometric values determined from $\Re^r$ accounting for the spectral response functions of the space sensor S^s;

$\Re^i$: modeled *in situ* hyperspectral values determined from $\Re^r$ accounting for the spectral response functions of the in situ sensor S^i defined using Gaussian functions, and varying the bandwidth and center-wavelength of the hypothetical *in situ* instrument;

$\Re^{r'}$: reconstructed L_W and E_S spectra at 0.1 nm resolution using $\Re^i$;

$\Re^{s'}$: satellite-equivalent radiometric values determined from $\Re^{r'}$ (i.e., from hyperspectral data generated using simulated *in situ* reduced resolution spectra).

Briefly, with reference to the dark-gray path in Fig. 3, satellite-exact $R_{RS}^s(k)$ spectra are computed for each spectral band *k* by relying on sub-nanometer (i.e., 0.1 nm resolution) $\Re^r$ spectra (i.e., L_W^r and E_S^r). In particular, $L_W^s(k)$ and $E_S^s(k)$ data required to compute $R_{RS}^s(k)$ are determined through spectral convolution from:

$$\Re(k) = \frac{\sum_l \Re(l)\, S(k,l)}{\sum_l S(k,l)} \tag{1}$$

where the generic variable $\Re$ indicates $\Re^r$ and S designates the relative spectral response functions S^s of the satellite sensor, with *l* wavelength index for the 0.1 nm increment.

As opposed to $R_{RS}^s(k)$, the determination of $R_{RS}^{s'}(k)$ requires multiple steps. In agreement with the process illustrated by the light-gray path in Fig. 3, first $\Re^r$ spectra are applied to model *in situ* measurements at different spectral resolution $\Re^i$ (i.e., L_W^i and E_S^i) as acquired from ideal hyperspectral radiometers exhibiting Gaussian spectral response functions S^i at spectral bands k^i. This step is again performed through Eq. (1) where the generic variable $\Re$ indicates

$\Re^r$ and S designates the relative spectral response functions S^i of the *in situ* sensor. The derived $\Re^i$ spectra are then deconvolved to reconstruct the $\Re^{r'}$ spectra at 0.1 nm through:

$$\Re^{r'}(l) = \frac{\sum_{k^i} \Re^i(k^i) S^i(k^i, l)}{\sum_{k^i} S^i(k^i, l)}, \tag{2}$$

where S^i is the relative spectral response function of each band k^i of the *in situ* sensor.

The derived $L_W^{r'}$ and $E_S^{r'}$ are finally convolved with the spectral response functions of the satellite sensor S^s to determine the satellite-equivalent $\Re^{s'}(k)$ (i.e., $L_W^{s'}$ and $E_S^{s'}$) required to compute $R_{RS}^{s'}(k)$. Specifically, this last convolution is also performed applying Eq. (1) with the generic variables $\Re$ indicating $\Re^{r'}$ (i.e., $L_W^{r'}$ and $E_S^{r'}$) and S designating the relative spectral response functions S^s of the satellite sensor for each spectral band *k*.

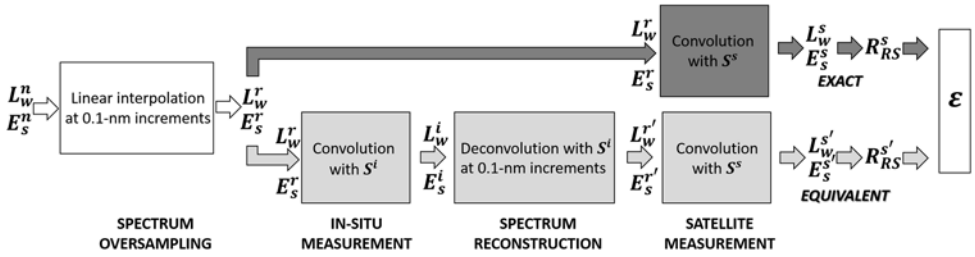

Fig. 3. Flow diagram illustrating the hyperspectral matching scheme. The comparison of satellite-equivalent $R_{RS}^{s'}$ and satellite-exact R_{RS}^{s} values is indicated by ε. See text for a comprehensive description of variables and flow.

3. Results

The comparison of satellite-equivalent $R_{RS}^{s'}$ with respect to the satellite-exact R_{RS}^{s} values are presented for each band *k* through the percent difference ε:

$$\epsilon(k) = 100\left[\frac{\Im(k) - \Im_r(k)}{\Im_r(k)}\right] \tag{3}$$

where $\Im$ indicates $R_{RS}^{s'}$ and $\Im_r$ the reference quantity R_{RS}^{s}.

Table 2 summarizes the various spectral resolution and sampling intervals considered in the analyses for the *in situ* sensor. Most of these configurations mimic spectral features of existing commercial spectrometers.

Results determined for OLCI bands displayed in Fig. 4, indicate values of ε increasing with bandwidth, $\Delta\lambda_B$, and sampling interval, $\Delta\lambda_C$, of the *in situ* sensor. When considering R_{RS} spectra from oligotrophic waters, the values of ε determined with $\Delta\lambda_B$ = 9 nm and $\Delta\lambda_C$ = 3 nm exceed 4 % at 510 nm for NP and 10 % at 673 nm for WM. These latter high values are explained by spectral features located in the vicinity of the specific center-wavelength (note that these differences correspond to very low absolute values of R_{RS} of the order of 10^{-5} sr^{-1}). Still, in the most favorable case given by $\Delta\lambda_B$ = 1 nm and $\Delta\lambda_C$ = 1 nm, ε does not generally exceed 0.1 %.

Table 2. Spectral resolutions $\Delta\lambda_B$ and sampling intervals $\Delta\lambda_C$ considered for the application of the hyperspectral matching scheme.

$\Delta\lambda_B$ [nm]	$\Delta\lambda_C$ [nm]	Comments
1	1	*Comparable to MOS*
2	2	
3	1	
6	2	
9	3	*Comparable to RAMSES*

In contrast to oligotrophic waters, R_{RS} representing optically complex cases generally exhibit values of ε within ±1 % regardless of $\Delta\lambda_B$ and $\Delta\lambda_C$.

Because of the higher resolution of the satellite sensor bands, the same analysis performed for PACE-like bands exhibits larger values of ε than those determined for OLCI in the spectral regions with large changes in the slope of R_{RS}. Specifically, in Fig. 5 the ε values determined with $\Delta\lambda_B$ = 9 nm and $\Delta\lambda_C$ = 3 nm exceed 4 % for oligotrophic waters (e.g., at around 515 nm for NP, and, near 605 nm and 665 nm for both NP and WM). With $\Delta\lambda_B$ = 2 nm and $\Delta\lambda_C$ = 2 nm the value of ε is generally within ±0.5 % in oligotrophic waters and within 0.1 % in optically complex waters.

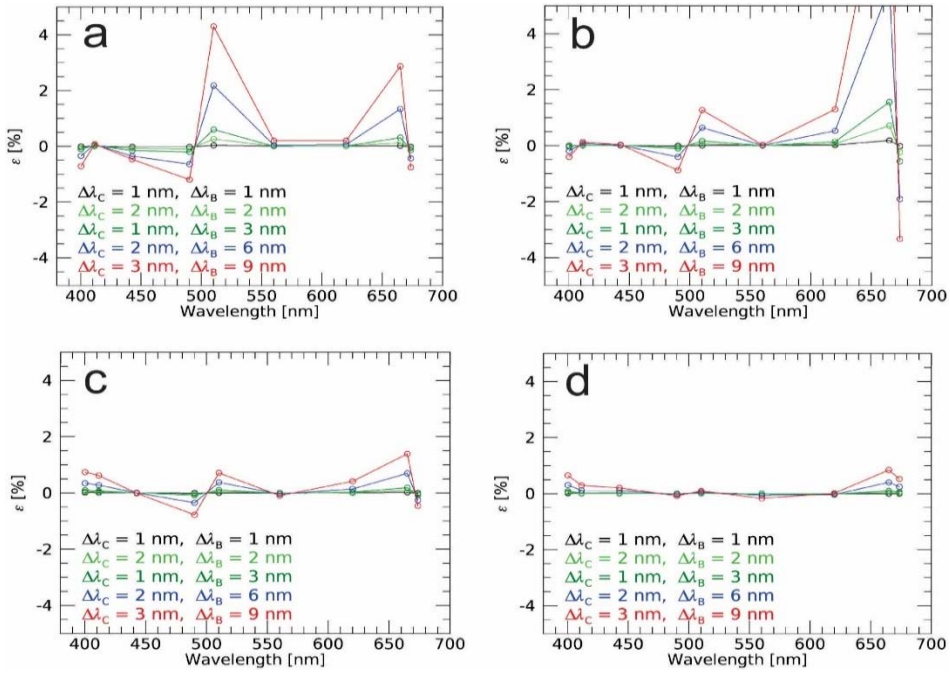

Fig. 4. Percent differences ε between $R_{RS}^{s'}$ and R_{RS}^{s} determined for OLCI bands. Data in different panels refer to the NP (a), WM (b), WB (c) and NA (d) spectra, and are presented at the OLCI center-wavelengths for different bandwidths $\Delta\lambda_B$ and spectral sampling intervals $\Delta\lambda_C$ of the *in situ* hyperspectral sensor.

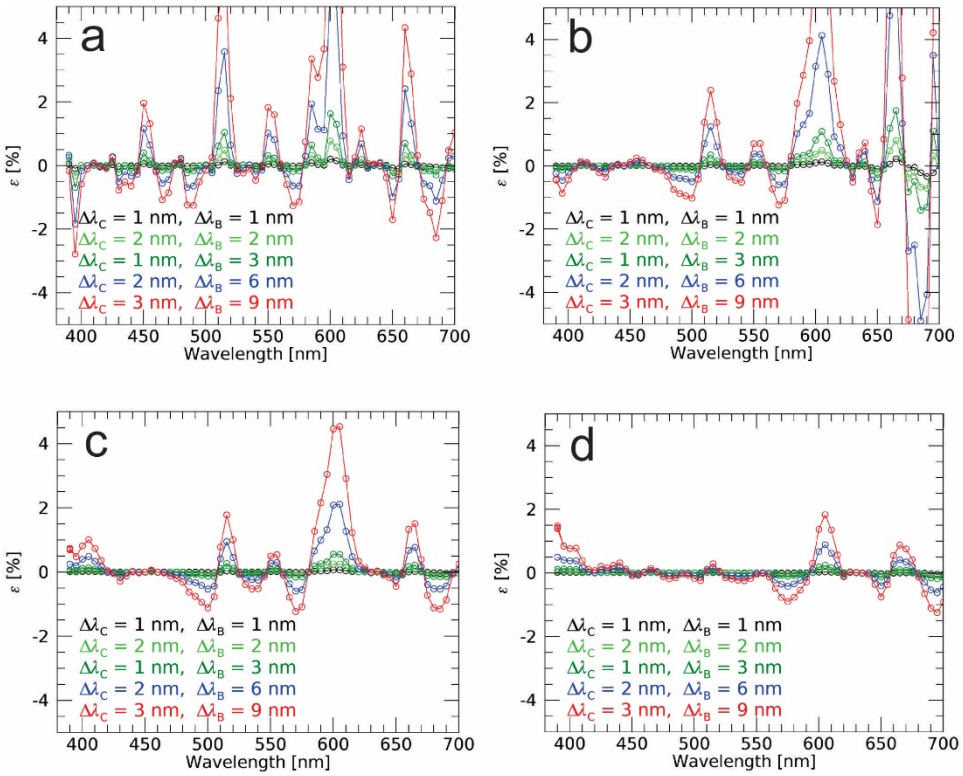

Fig. 5. Percent differences ε between $R_{RS}^{s'}$ and R_{RS}^{s} determined for PACE-like bands. Data in different panels refer to NP (a), WM (b), WB (c) and NA (d) spectra, and are presented at the considered PACE-like center-wavelengths for different bandwidths $\Delta\lambda_B$ and spectral sampling intervals $\Delta\lambda_C$ of the *in situ* hyperspectral sensor.

4. Discussion

The discussion will show how representative the hyperspectral R_{RS} for NP is for that site, the alternative use of L_W instead of R_{RS} for SVC, the uncertainties associated with values of ε determined using RAMSES R_{RS} spectra, and finally the relevance of spectral sampling intervals versus spectral resolution. Accounting for the results from the analyses presented in the previous section and of findings from the discussion topics included in this section, spectral resolution and sampling interval requirements for *in situ* hyperspectral data supporting satellite ocean color validation and SVC applications are summarized assuming strict uncertainty thresholds.

4.1 Stability of R_{RS} for the NP site

This study relies on a few hyperspectral R_{RS} spectra representative of various water types. While it is impossible in one study to include every different water type, it is still expected that these results are useful in outlining the general spectral resolution requirements for *in situ* R_{RS} supporting SVC and validation activities.

Since the NP site has been used extensively for SVC [14], it is important to consider how well the specific hyperspectral R_{RS} spectrum used in this analysis represents the MOBY site. This has been addressed with a statistically significant number (i.e., 103) of MOS spectra collected from 15 May to 28 August 2015 using the same *in situ* sensor applied for producing the spectrum included in this analysis. Using the one spectrum for the NP case is fully supported by the mean μ and standard deviation σ of the ε values displayed in Fig. 6. Specifically, the values of ε shown in Fig. 5(a) appear equivalent to the mean values $\mu(\varepsilon)$ displayed in Fig. 6 for the 103 independent spectra from the same site. Additionally, the related standard deviations $\sigma(\varepsilon)$ exhibit values that, excluding the spectral region nearby 600 nm, do not exceed 0.4 % regardless of the spectral resolution considered for the determination of ε.

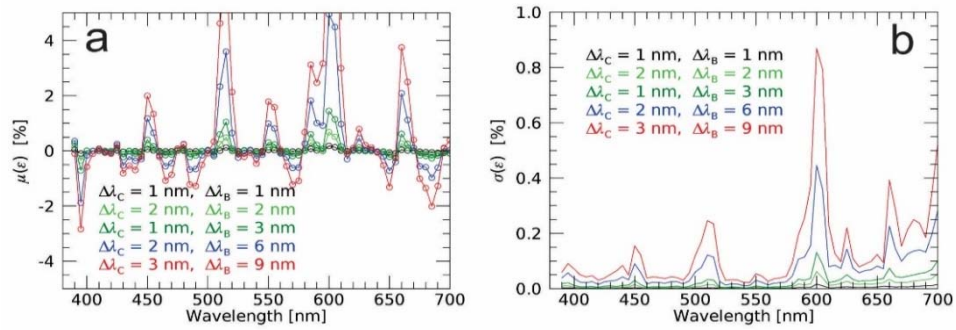

Fig. 6. Mean μ (a) and standard deviation σ (b) values of percent differences ε between $R_{RS}^{s'}$ and R_{RS}^{s} determined for PACE-like bands, and computed with 103 MOS spectra from 15 May to 28 August 2015. Data are presented at the considered PACE-like center-wavelengths for different bandwidths $\Delta\lambda_B$ and spectral sampling intervals $\Delta\lambda_C$ of the *in situ* hyperspectral sensor.

4.2 Accuracy of ε values

The relatively low spectral resolution of RAMSES data for WB, NA, and WM may lead to a misestimate of ε in spectral regions characterized by significant nanometer scaled features. This underestimate has been evaluated with the NP data, which benefit from a higher spectral resolution with respect to the other cases and additionally exhibit more pronounced spectral gradients providing added challenging conditions.

For this analysis, the MOS L_W and E_S data linearly resampled at 0.1 nm were degraded using Eq. (1) to match the RAMSES spectral resolution (i.e., $\Delta\lambda_B$ = 9 nm and $\Delta\lambda_C$ = 3 nm). Then, in agreement with the scheme outlined in Fig. 3, both full resolution and degraded MOS data were applied to calculate $R_{RS}^{s'}$ spectra. The values of ε displayed in Fig. 7 identify the spectral regions for which R_{RS} from the NP site is most affected by a reduction of spectral resolution (e.g., see regions near 385 nm, 510 nm, 600 nm and 660 nm in Fig. 7(b), which exhibit values of ε larger than ±2 % for $\Delta\lambda_B$ = 9 nm and $\Delta\lambda_C$ = 3 nm).

The difference $\Delta\varepsilon$ between ε generated with Eq. (3) using the R_{RS} data that went through the RAMSES spectral response and those obtained without spectral degradation, are displayed in Fig. 8. In particular, Fig. 8(a) shows that in the case of OLCI the most pronounced misestimates of ε as a function of spectral resolution and sampling interval are observed at the 510 nm band, with differences that may reach -0.6 %. These differences are explained by the high gradient in seawater reflectance near this wavelength. In summary, in the case of OLCI bands it can be

assumed that 0.6 % is a tentative estimate of the maximum uncertainty that would affect the previous analysis performed with R_{RS} data from NP, if collected with a spectral resolution of 9 nm and sampling interval of 3 nm (i.e., close to the spectral features of RAMSES data).

In the case of PACE-like bands, the values of $\Delta\varepsilon$ in Fig. 8(b) exceed ±1 % near a few center-wavelengths (i.e., 510 nm, 600 nm, 660 nm and, with some caution, 495 nm) for the lowest spectral resolution and sampling interval (i.e., 9 nm and 3 nm, respectively).

Overall, the previous results confirm misestimates of ε for the analyses performed with RAMSES spectra. It is expected, however, that for optically complex waters (i.e., NA and WB), misestimates will be lower than those quantified through R_{RS} from NP due to R_{RS} naturally exhibiting less pronounced spectral features in these other locations. Thus, it can be assumed that results from the analyses of RAMSES spectra can be applied with some confidence to draw general conclusions in optically complex waters, even though it probably leads to an underestimate of requirements. Nevertheless, the case of the WM oligotrophic waters is more affected by the reduced spectral resolution of RAMSES sensors and these results should only be considered in combination with those determined from R_{RS} related to NP.

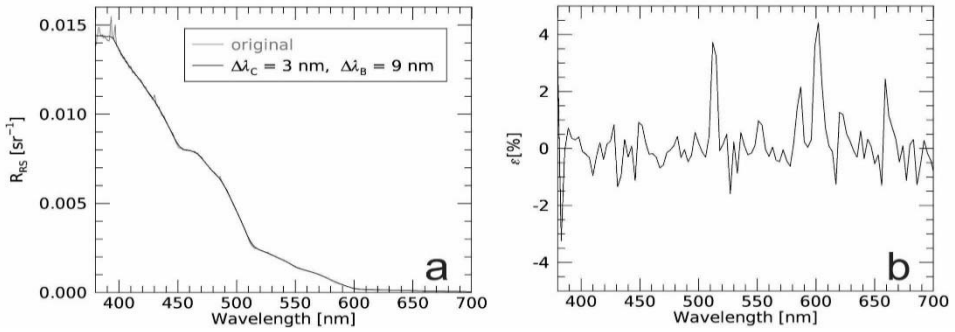

Figure 7. Original (grey line) and spectrally degraded NP R_{RS} data (black line) determined with $\Delta\lambda_C$ = 3 nm and $\Delta\lambda_B$ = 9 nm (a), and percent differences ε between degraded and the original high resolution spectra (b).

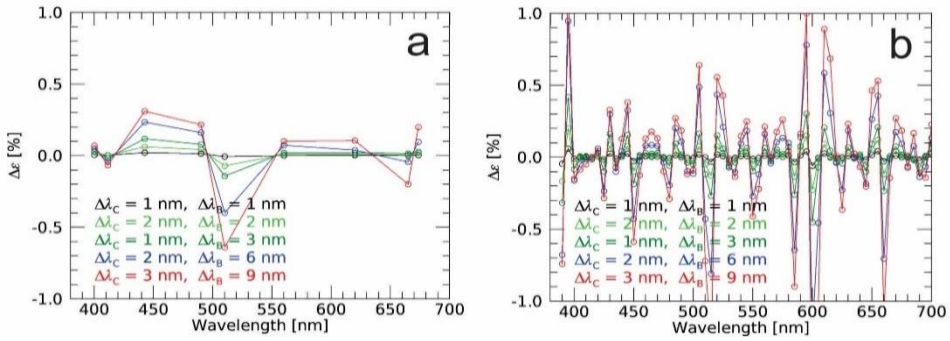

Figure 8. Differences $\Delta\varepsilon$ between values of ε determined from $R_{RS}^{s'}$ and R_{RS}^{s} for the OLCI (a) or PACE-like (b) bands, with reduced resolution (i.e., $\Delta\lambda_B$ = 9 nm and $\Delta\lambda_C$ = 3 nm) and full resolution NP spectra.

It is emphasized that the relatively low impact of spectral degradation resulting from the previous analysis is largely explained by the "smoothness" of the R_{RS} spectrum obtained through

the normalization of L_W to E_S. In fact, this process removes the high spectral resolution features due to the solar spectrum and atmospheric absorption that affect L_W. Consequently, the same conclusions achieved for R_{RS} do not likely apply to RAMSES L_W spectra.

4.3 L_W versus R_{RS}

The overall analysis has been based on R_{RS} data that are the target quantity for most ocean color applications. However, SVC is often performed using L_W data [14,15]. This alternative solution avoids dealing with uncertainties of computed or measured downward irradiance E_S, but increases the spectral resolution requirements for *in situ* radiometry due to the higher spectral complexity of the L_W compared with the R_{RS} spectra. This is shown in Fig. 9 by the percent differences ε computed using Eq. (3) with $\Im$ indicating $L_W^{s'}$ and $\Im_r$ the reference quantity L_W^s from NP spectra (the same analysis is not presented for RAMSES data due to their relatively low spectral resolution). These ε values, when compared to those displayed in Fig. 4(a), do not show a significant impact of the use of L_W or R_{RS} on spectral resolution requirements for multispectral satellite sensors such as OLCI, when excluding the bands in the blue spectral region. Similarly, the values of ε determined for the PACE-like bands exhibit a marked increase in the blue spectral region near 395 nm, 400 nm and 430 nm, when compared to those shown in Fig. 5(a). This is fully explained by the pronounced spectral features of L_W in the blue spectral region. The comparison of Fig. 10 with Fig. 7, which display full resolution and spectrally degraded data for both L_W and R_{RS} together with the related values of ε, shows the higher spectral complexity of L_W and the importance of using higher resolutions *in situ* sensors for applications requiring L_W with respect to R_{RS}.

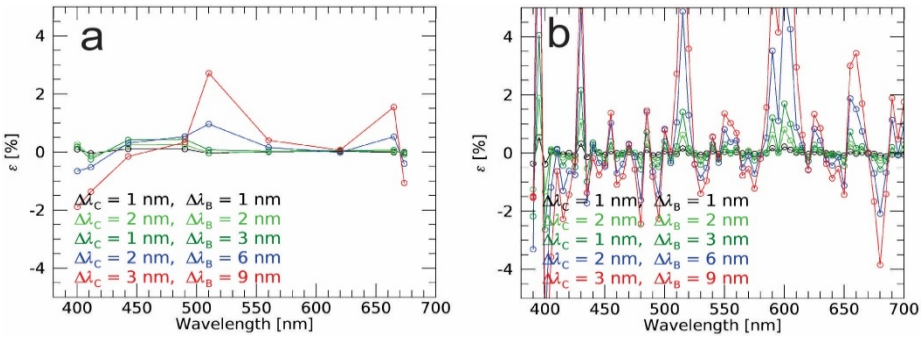

Fig. 9. Percent differences ε between $L_W^{s'}$ and L_W^s determined with NP spectra for OLCI (a) or PACE-like (b) bands. Data are presented at the considered OLCI or PACE-like center-wavelengths for different simulated bandwidths $\Delta\lambda_B$ and spectral sampling intervals $\Delta\lambda_C$ of the *in situ* hyperspectral sensor.

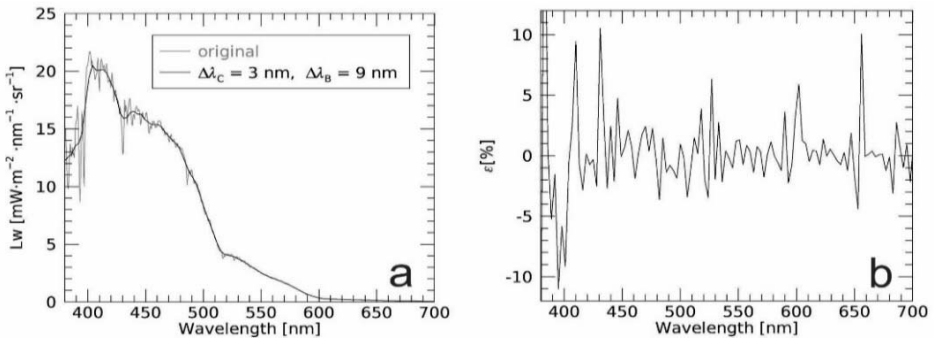

Fig. 10. Original (grey line) and spectrally degraded NP L_w data (black line) determined with $\Delta\lambda_C$ = 3 nm and $\Delta\lambda_B$ = 9 nm (a), and percent differences ε between degraded and the original high resolution spectra (b).

4.4 Spectral sampling interval versus resolution

Spectral resolutions $\Delta\lambda_B$ and sampling intervals $\Delta\lambda_C$ considered in the previous analysis are limited to a few cases guided by the specifications of existing spectrometers. When looking at results presented in Figs. 4 and 5, the configuration defined by $\Delta\lambda_B$ = 2 nm and $\Delta\lambda_C$ = 2 nm exhibits a slightly better performance than that given by $\Delta\lambda_B$ = 3 nm and $\Delta\lambda_C$ = 1 nm. This clearly indicates the importance of spectral resolution over sampling interval in requirements for hyperspectral ocean color sensors. This is fully confirmed by the additional analysis presented in Fig. 11 and performed for the NP case by setting $\Delta\lambda_B$ = 6 nm, or alternatively $\Delta\lambda_B$ = 3 nm, with $\Delta\lambda_C$ varying from 1 nm to $\Delta\lambda_B$ in 1 nm increments. These results indicate that when $\Delta\lambda_C$ approaches or is lower than $\Delta\lambda_B$ /2, differences with respect the reference configuration defined by $\Delta\lambda_C$ = 1 nm become irrelevant (i.e., drop within ±0.01 %). This implies that in agreement with Nyquist sampling theory, oversampling with $\Delta\lambda_C$ lower than approximately $\Delta\lambda_B$/2 does not lead to any significant increase in accuracy.

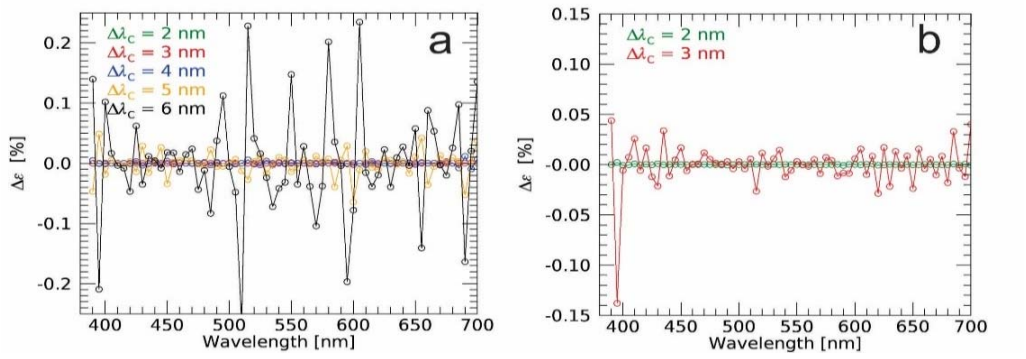

Fig. 11. Differences $\Delta\varepsilon$ between values of ε determined from $R_{RS}^{s'}$ and R_{RS}^{s} at the PACE-like bands, with reduced and full resolution (i.e., with $\Delta\lambda_C$ = 1 nm and $\Delta\lambda_B$ = 1 nm) NP spectra. Specifically, data in the various panels refer to $\Delta\varepsilon$ for various spectral degradation defined assuming fixed bandwidths (i.e., $\Delta\lambda_B$ = 6 nm (a) and $\Delta\lambda_B$ = 3 nm (b)) and different spectral sampling intervals $\Delta\lambda_C$.

4.5 Uncertainty requirements

The Implementation Plan for the Global Observing System for Climate (GCOS [1]) indicates a 5 % uncertainty requirement for ocean color radiometric data products (i.e., L_W) in the blue-green spectral regions, and additionally the need for 0.5 % radiometric stability per decade.

Considering that uncertainties affecting *in situ* radiometric data [9] result from a number of contributions (e.g., calibration, environmental and superstructure perturbations, and data reduction through subsurface extrapolation, self-shading, correction for bidirectional effects), it is important that the maximum difference due to spectral matching is well below the target uncertainty defined for validation and SVC. Accounting for expected uncertainty budgets of highly accurate radiometric measurements [16] and recognizing that accuracy requirements are much more demanding for SVC than for validation, strict thresholds of ε within ±1 % and of ε within ±0.5 % are applied in the following analysis for validation and SVC activities performed with R_{RS}, respectively. It is underlined that the small values chosen for ε are justified by the fact that perturbations introduced by spectral resolution contribute as additive terms (i.e., biases) to the uncertainty budget of each specific mission, and consequently may directly affect the 0.5 % GCOS stability requirement per decade. Additionally, while some of the other contributions to the overall uncertainty budget are difficult to minimize (e.g., environmental effects), the one solely due to spectral resolution can be reduced to negligible values by instrument design.

Thus, emphasizing that the spectral matching problem is addressed from the pure radiometric point of view without considering any potential correction for the *in situ* values (e.g., band-shifting), spectral resolution requirements for both validation and SVC applications are determined from the results summarized in the previous sections. Specifically, assuming that the spectral sampling interval $\Delta\lambda_C$ is close to or lower than half the spectral resolution (i.e., $\Delta\lambda_C \leq \Delta\lambda_B/2$), results from Figs. 4-5 lead to the subsequent requirements solely based on R_{RS} data.

For SVC activities, which are commonly performed in oligotrophic waters [15] and consequently by solely considering findings from the analysis of R_{RS} from ultra-oligotrophic waters, the following general conclusions can be drawn with ε within ±0.5 % in the blue-green spectral region:

- A spectral resolution better than 3 nm is required for *in situ* hyperspectral sensors in the case of satellite multispectral sensors (as shown for OLCI bands in Fig. 4 (a));
- Conversely, a spectral resolution better than 1 nm is recommended for *in situ* sensors in the case of satellite hyperspectral sensors (as shown for PACE-like bands in Fig. 5 (a)). The previous requirement can be relaxed to 2 nm when excluding spectral regions near 510 nm, 600 nm and, with caution, at 395 nm.

For validation activities performed with R_{RS} setting ε within ±1 % in the blue-green spectral region:

- The spectral resolution of *in situ* hyperspectral sensors should be better than 3 nm in oligotrophic waters in the case of satellite multispectral sensors. The requirements can be relaxed to a spectral resolution better than approximately 9 nm for optically complex waters (as shown for OLCI bands in Fig. 4).
- The spectral resolution of *in situ* hyperspectral sensors should also be better than 3 nm in oligotrophic waters in the alternative case of satellite hyperspectral sensors. Excluding bands near 600 nm, spectral resolution better than 6 nm may satisfy requirements for optically complex waters (as shown for PACE-like bands in Fig. 5).

It is important to remember, however, that the previous spectral resolution requirements defined for optically complex waters may be somewhat underestimated having been determined using *in situ* hyperspectral data with relatively low spectral resolution. Obviously, a different target ε would imply more or less stringent requirements. Additionally, the use of L_W instead

of R_{RS} , would increase requirements ultimately indicating the need for sub-nanometer resolution in the blue spectral region for hyperspectral sensors such as PACE.

5. Summary and conclusions

An estimate of the uncertainties (actually biases) affecting comparisons of *in situ* and satellite radiometric matchups has been derived as a function of spectral band characteristics of *in situ* sensors. This analysis, that has relevance for SVC applications and satellite ocean color validation relying on the use of *in situ* R_{RS} data, has been developed using *in situ* hyperspectral radiometric data representative of different water types: oligotrophic and optically complex. These spectra have been used to construct hyperspectral data characterized by different spectral resolution and sampling intervals, successively applied to quantify differences between *in situ* and satellite R_{RS} values.

Results obtained for the OLCI visible bands, indicate that differences may reach several percent in oligotrophic waters with spectral resolution and sampling intervals of 9 nm and 3 nm, respectively. Considering the same resolution and sampling interval, differences are always within ±1 % in optically complex waters.

In the case of PACE-like visible bands defined by 5 nm width, Gaussian spectral response and 5 nm sampling interval, differences may also exhibit values exceeding several percent as a function of the water type and spectral resolution of the *in situ* sensor.

The analysis has also shown that the sampling interval of the *in situ* hyperspectral sensors should be close to half the spectral resolution and that, in agreement with the Nyquist sampling theory, any oversampling does not provide significant benefits.

An attempt to define requirements for the spectral resolution of *in situ* hyperspectral radiometers supporting validation and SVC applications through R_{RS} spectra led to diverse requirements. Setting the target difference to ±1 % in the blue-green spectral region for this one factor, validation activities in oligotrophic waters require spectral resolutions better than 3 nm for both OLCI and PACE-like bands. Spectral resolution requirements in optically complex waters, which are likely underestimated, result in values of 6 nm for PACE-like bands and 9 nm for OLCI.

SVC applications, restricted to oligotrophic waters, imply a higher accuracy when compared to validation activities. Assuming a maximum difference of ±0.5 % between *in situ* and satellite R_{RS} data in the blue-green spectral region, the analysis performed for OLCI indicates the need for hyperspectral *in situ* data to be collected with a spectral resolution better than 3 nm. In the case of PACE, the spectral resolution needs to be lower than 1 nm, or alternatively 2 nm when excluding spectral regions nearby 510 nm, 600 nmand likely 395 nm.

When using L_W instead of R_{RS} , the study also indicates more stringent requirements for hyperspectral *in situ* data due to the added spectral features of the incident solar irradiance spectrum and atmospheric absorption, which are minimized in R_{RS} by the normalization of L_W with respect to the downward irradiance E_S .

These stringent requirements on spectral resolution of *in situ* hyperspectral sensors result from the adoption of strict uncertainty requirements for satellite radiometric products. Thus it is recognized that a relaxation of spectral resolution requirements is feasible for non-critical applications of *in situ* data such as validation activities performed in challenging measurement conditions (e.g., high spatial inhomogeneity of seawater optical properties, low sun elevations, non-oceanic aerosols), where other factors dominate the quality of the matchup analysis.

Funding
Joint Research Centre (JRC); National Oceanic and Atmospheric Administration (NOAA) (NA15OAR4320064, NOAA2012-09-0004); National Aeronautics and Space Administration (NASA) (NNX14AP63G).

Acknowledgments
The authors would like to thank Stephanie Flora for providing the MOS data essential for the analysis presented in the work and additionally some of the data presented in Table 1.

Certain commercial instruments and suppliers are identified in this paper to foster understanding. Such identification does not imply recommendation or endorsement by any of the Institutions involved in the study, nor does it imply that the equipment identified is necessarily the best available for the purpose.

Annex 3

An evaluation of marine regions relevant for ocean color system vicarious calibration. Reprinted from *Remote Sens. Environ.* 190, 122–136.

Remote Sensing of Environment 190 (2017) 122–136

Contents lists available at ScienceDirect

Remote Sensing of Environment

journal homepage: www.elsevier.com/locate/rse

An evaluation of marine regions relevant for ocean color system vicarious calibration

Giuseppe Zibordi *, Frédéric Mélin

European Commission, Joint Research Centre, Ispra, Italy

ARTICLE INFO

Article history:
Received 22 May 2016
Received in revised form 17 November 2016
Accepted 27 November 2016
Available online xxxx

Keywords:
Ocean color
System vicarious calibration

ABSTRACT

System Vicarious Calibration (SVC) is the fundamental process commonly implemented to meet uncertainty requirements in satellite ocean color data. It is performed by applying gain factors, *g*-factors, to the pre-launch calibration coefficients of the space sensor already corrected for sensitivity decay with time. Mission specific *g*-factors are determined from top-of-the-atmosphere data computed by propagating highly accurate in situ values of the water-leaving radiance, L_w, to the satellite sensor. Values of L_w from marine regions characterized by oligotrophic/mesotrophic waters and maritime aerosols, high environmental stability and spatial homogeneity, low cloudiness and absence of any source of land contamination, are essential to determine *g*-factors applicable to the creation of Climate Data Records (CDRs) from multiple ocean color missions. Accounting for the location of existing and potential new SVC fixed sites, marine regions satisfying SVC requirements for the generation of CDRs have been identified through the analysis of satellite data from recent ocean color missions.

© 2016 The Author(s). Published by Elsevier Inc. This is an open access article under the CC BY license (http://creativecommons.org/licenses/by/4.0/).

1. Introduction

System Vicarious Calibration (SVC) is the indirect calibration of satellite ocean color sensors that minimizes the combined effects of atmospheric correction and sensor calibration uncertainties on derived radiometric data. SVC is performed to meet uncertainty requirements in data products such as the spectral water leaving radiance L_w determined from the top-of-atmosphere radiance L_T (Gordon, 1987, 1998): it is accomplished by applying gain factors, *g*-factors, to pre-launch spectral calibration coefficients already corrected for sensitivity change with time (e.g., Eplee et al., 2001; Franz et al., 2007; Werdell et al., 2007; Bailey et al., 2008; Mélin and Zibordi, 2010).

Values of *g*-factors are determined by the ratio of simulated to measured top-of-the-atmosphere spectral L_T values, where the simulated ones are derived by propagating accurate in situ L_w to the satellite level. Unique to SVC is the use of the same models and algorithms embedded in the atmospheric correction process for the determination of satellite-derived radiometric data. Thus SVC is a relative radiometric calibration specific for each mission, i.e., for each ocean color sensor and atmospheric correction framework.

It is emphasized that SVC implies availability of highly accurate in situ L_w data in the visible spectral region. This is as opposed to the near-infrared bands where modeled L_T values with uncertainties up to a few percent (which may imply extremely high relative uncertainties in the corresponding L_w) do not significantly affect the SVC process (Wang and Gordon, 2002).

In addition to the accuracy of in situ L_w data, a number of features specific to the measurement site such as small environmental variability (i.e., a high intra-annual stability), high spatial homogeneity, mesotrophic/oligotrophic waters, maritime aerosols and lack of any land perturbation (Zibordi et al., 2015), are also fundamental requirements for ocean color SVC supporting climate change applications. This implies that not all individual in situ measurements or series of measurements, regardless of their level of accuracy, meet SVC needs for the construction of Climate Data Records (CDRs) from multiple ocean color missions.

The objective of this study is to identify marine regions satisfying SVC requirements for the construction of CDRs. By using time-series of satellite ocean color global data products, the study investigates the fulfilment of the requirements mentioned above for a number of regions already hosting SVC fixed sites or for which new sites are under consideration.

This work adds to ongoing investigations like those on data merging (e.g., Maritorena et al., 2010) or on the effects of biases affecting independent missions (e.g., Mélin, 2016), all contributing to the international effort to create ocean color CDRs by benefitting from global long-term missions such as the Joint Polar Satellite System (JPSS) from the National Oceanic and Atmospheric Administration (NOAA) started in 2011, Sentinel-3 from the European Space Agency (ESA) started in 2016, the Global Change Observation Mission-Climate (GCOM-C) from the Japan Aerospace Exploration Agency (JAXA) scheduled from 2017, and the

* Corresponding author.
E-mail address: giuseppe.zibordi@jrc.ec.europa.eu (G. Zibordi).

http://dx.doi.org/10.1016/j.rse.2016.11.020
0034-4257/© 2016 The Author(s). Published by Elsevier Inc. This is an open access article under the CC BY license (http://creativecommons.org/licenses/by/4.0/).

Plankton Aerosols Clouds and ocean Ecosystems (PACE) from the National Aeronautics and Space Administration (NASA) scheduled from 2022.

2. Background

The water-leaving radiance L_w is the primary satellite-derived radiometric quantity from which high-level data products such as the remote sensing reflectance R_{rs} or chlorophyll-a concentration *Chla* are determined. This has led to the inclusion of L_w among the oceanic Essential Climate Variables (ECV) in association with uncertainty requirements of 5% in the blue-green spectral regions and radiometric stability better than 0.5% per decade (WMO, 2011). SVC is the technique commonly used to address such requirements. However, while the 5% uncertainty can be met with moderate efforts using alternative sources of in situ data, the 0.5% stability requirement is only achievable at the expense of extraordinary efforts through the application of state of the art radiometry and at sites exhibiting high intra-annual stability and spatial homogeneity of marine and atmospheric optical properties (Zibordi et al., 2015). This comprehensive framework is required by the need to ensure the same high precision to *g*-factors determined for successive missions. In fact, changes with time of uncertainties characterizing in situ measurements or observation conditions, may affect the precision of *g*-factors determined during the different time intervals of independent missions. This need for high precision ultimately favors SVC sites exhibiting: *i.* a high spatial homogeneity that minimizes the impact of the different geometric resolutions characterizing in situ and satellite observations; and *ii.* a high intra-annual stability of the marine and atmospheric optical properties that minimizes uncertainties due to the varying performance of the atmospheric correction process across different observation conditions. It must be additionally noted that a high intra-annual stability is commonly associated with low concentrations of seawater optically significant constituents typical of oligotrophic waters (Iverson et al., 2000). This implies a low bio-optical complexity that improves modeling accuracy (e.g., while removing the effects of the non-isotropic distribution of the in-water light field in satellite data to match satellite and in situ viewing geometries) and that consequently increases the precision of *g*-factors.

Overall, general requirements for in situ data supporting SVC for ocean color climate applications (see Zibordi et al., 2015) are summarized by the need for long-term, hyperspectral, traceable and highly accurate measurements performed at sites:

1. Located in a region chosen to maximize the number of high-quality matchups by trading off factors such as best viewing geometry, sun-glint avoidance, low cloudiness, and additionally set away from any continental contamination and at a distance from the mainland to safely exclude adjacency effects in satellite data;
2. Exhibiting known or accurately modelled optical properties coinciding with maritime atmosphere and oligotrophic/mesotrophic waters, to represent the majority of world oceans and minimize relative uncertainties in computed *g*-factors;
3. Characterized by high spatial homogeneity and small environmental variability, of both atmosphere and ocean, to increase precision of computed *g*-factors.

It is mentioned that the work by Zibordi et al. (2015) indicates that the creation of CDRs from independent ocean color missions should ideally rely on the application of the same atmospheric correction process and on time-series of in situ L_w data from a single reference SVC site. However, the work also recognizes that strategies to support long-term climate investigations recommend redundancy of in situ SVC measurement sites (IOCCG, 2012). This implies establishing multiple SVC sites: i. relying on in situ radiometry systems equivalent in terms of data accuracy and long-term performance; ii. and located in regions also exhibiting ideal and likely similar measurement conditions.

The high cost of establishing and maintaining over decades SVC sites meeting the requirements for the creation of CDRs from multiple ocean color missions, nevertheless, suggests a careful evaluation of suitable marine regions without neglecting the fundamental necessity to benefit from logistical support from infrastructures located at nearby islands or coastal locations.

3. Regions, data and methods

3.1. Marine regions

As already anticipated, the regions considered in this analysis (see Table 1), are those related to fixed sites already in use for ocean color SVC or alternatively potential SVC sites under consideration because of their atmospheric and marine optical properties expected to be representative of the world oceans.

The regions hosting established SVC sites include: the North Pacific Ocean (NPO) with the Marine Optical Buoy (MOBY) site managed by the US National Oceanic and Atmospheric Administration (NOAA; Clark et al., 1997, 2002, 2003); the Arabian Sea (ASea) with the Kavaratti Site managed by the Indian Space Research Organization (ISRO; Shukla et al., 2013); the Ligurian Sea (LSea) with the BOUée pour l'acquiSition d'une Série Optique à Long termE (BOUSSOLE) site managed by the French Laboratoire d'Océanographie de Villefranche (LOV; Antoine et al., 2008b). The regions for which the setting up of new SVC sites has been a matter of discussion within the scientific community comprise: the Mediterranean Sea (MSea) near the Island of Crete; the Caribbean Sea (CSea) near Puerto Rico Islands; the North Atlantic Ocean (NAO) near Azores Islands; and the Eastern Indian Ocean (EIO) near Rottnest Island off Perth. In addition to the previous regions, the South Pacific Gyre (SPG) is also included as a virtual reference region due to its highly oligotrophic waters and its expected high temporal stability (Twardowski et al., 2007).

It is noted that the considered regions are characterized by Case-1 waters (i.e., exhibit optical properties that can be described as a function of *Chla*, only), which are representative of the most common oceanic waters. It is also pointed out that all regions, with the exception of the virtual SPG one, are located nearby islands or coastal locations favouring maintenance services of the offshore SVC measurement infrastructure, but also at distances from the coast minimizing land contamination such as adjacency effects in satellite data (Bulgarelli et al., 2014).

It is finally recognized that the regions included in this study are not likely to reflect all those potentially suitable for ocean color SVC. Still, not excluding alternatives, the regions considered provide an overview of the marine/atmospheric optical properties of those potential SVC sites currently considered of major relevance to support the creation of ocean color CDRs.

3.2. Remote sensing data and methods

The accuracy of ocean color data products is related to a number of factors encompassing the overall calibration of the space sensor and atmospheric correction scheme applied in conjunction with the embedded marine/atmospheric models and algorithms. These factors may certainly lead to the generation of data products with uncertainties varying from region to region as a function of different marine/atmospheric optical properties or observation/illumination geometries (Mélin et al., 2016).

The Sea-Viewing Wide Field-of-View Sensor (SeaWiFS, Hooker et al., 1992) ocean color data products, besides constituting one of the longest time-series from a single mission, are among those most investigated and exploited. In particular they benefitted from a number of incremental improvements in data processing and related models/algorithms (e.g., Gordon and Wang, 1994; Wang et al., 2005; Franz et al., 2007; Ahmad et al., 2010; Hu et al., 2012b), and additionally were the foundation of extensive and geographically distributed validation exercises for

Table 1
Reference locations of the various marine regions considered in the following analysis.

Acronym	Region	Lon	Lat	Notes
SPG	South Pacific Gyre	−125.0	−25.0	Virtual site
NPO	North Pacific Ocean	−157.8	19.4	Near the MOBY Site operated by NOAA
MSea	Mediterranean Sea	25.0	34.0	Potential site near Crete Island
CSea	Caribbean Sea	−67.0	17.5	Potential site near Puerto Rico Islands
ASea	Arabian Sea	72.0	10.0	Near the Kavaratti Site operated by ISRO
NAO	North Atlantic Ocean	−28.5	39.0	Potential site near Azores Islands
LSea	Ligurian Sea	8.0	43.5	Near the BOUSSOLE Site operated by LOV
EIO	Eastern Indian Ocean	114.5	−32.0	Potential site near Rottnest Island

radiometric and derived marine products (e.g., Gregg and Casey, 2004, Mélin et al., 2005, Bailey and Werdell, 2006, Zibordi et al., 2006, Antoine et al., 2008a, Hu et al., 2013) as well as for the aerosols (e.g., Wang et al., 2005, Mélin et al., 2013a, b). Specifically, Hu et al. (2013) and Mélin et al. (2016) confirmed the capability of SeaWiFS to meet the 5% uncertainty requirement in the blue bands in oligotrophic waters, even though often reaching values of 10–15% in the green bands.

The previous elements indicate confident applicability of SeaWiFS marine/atmospheric data products to open sea investigations (e.g., Gregg et al., 2003; McClain et al., 2004; Gregg, 2008; Vantrepotte and Mélin, 2011). Thus, by relying on this evidence, the analysis on the atmospheric and marine bio-optical properties of the regions included in this study is carried out with data from the SeaWiFS mission (1997–2010) with the assumption that any geographically dependent uncertainty does not affect basic findings.

The following analysis is performed using SeaWiFS Level-2 daily 1-km spatial resolution and Level-3 monthly averages 24th-degree spatial resolution products, both from the R2014.0 reprocessed data distributed by the US National Aeronautics and Space Administration (NASA).

Time-series of monthly averages of atmospheric and marine data products are applied to investigate the climatology of atmospheric/marine bio-optical properties. The list of these quantities is presented in Table 2: i. R_{rs} relevant to characterize the water type associated with each region and to address the impact of the in situ radiometric signal in the uncertainty of *g*-factors; ii. diffuse attenuation coefficient at 490 nm, $K_d(490)$, and concentration of chlorophyll-*a*, *Chla*, relevant to discuss the climatology of marine bio-optical properties; iii. aerosol optical thickness at 865 nm, $\tau_a(865)$, and the Ångström exponent, α, relevant to discuss the climatology of atmospheric optical properties.

Instead of monthly averages, time series of daily full resolution R_{rs} and derived data products are used to evaluate the potential of each region to contribute to the construction of in situ and satellite matchups for ideal observation conditions (e.g., when exhibiting high spatial homogeneity and not affected by clouds, high glint, high viewing angle). In view of discussing the effects of different viewing geometries, analyses are also extended to data from a number of ocean color sensors, all processed with the same system (i.e., the SeaWiFS Data Analysis System (SeaDAS) version 7.2 or above).

4. Analysis of monthly averaged data

This section aims at providing a comprehensive overview of the marine and atmospheric optical properties for the various regions included in the study. The climatology of relevant optical properties has been determined using mean values from monthly averages of the 5 × 5 data elements centered at each region included in the analysis (the use of mean instead of the alternative median, ensures consistency with the input Level-3 monthly averages). Data have been retained when at least one of the data elements exhibits a valid value.

4.1. Climatology of marine bio-optical properties: R_{rs} spectra and time-series of $R_{rs}(555)$, $K_d(490)$ and Chla

Mean R_{rs} spectra and standard deviations determined over the entire SeaWiFS mission are presented for the different marine regions identified in Fig. 1. Spectra show a range of cases varying from those representative of oligotrophic waters to those typical of mesotrophic waters (see Fig. 2). The highest values are found in the oligotrophic waters of the South Pacific Gyre (SPG) and of the North Pacific Ocean (NPO). On average the lowest R_{rs} spectra are found in the Ligurian Sea (LSea) and North Atlantic Ocean (NAO), while slightly higher R_{rs} are observed for the Arabian Sea (ASea) and Eastern Indian Ocean (EIO) waters. At 412 nm, the R_{rs} values of the Mediterranean Sea (MSea) and Caribbean Sea (Csea) are approximately twice that of the LSea mesotrophic region.

Standard deviations σ of R_{rs} in Fig. 2 largely vary from region to region and are likely explained by seasonal cycles. Despite the bluest waters, SPG exhibits values of σ much higher than those determined for NPO.

Notable is also the difference in the slope of R_{rs} in the blue spectral interval at MSea with respect to the other oligotrophic regions. This feature that also characterizes the LSea mesotrophic waters, is confirmed by field measurements (Zibordi et al., 2011). Explanation is likely given by the presence of an excessive amount of yellow substance in the Mediterranean Sea waters with respect to comparable oceanic areas (Morel and Gentili, 2009). An alternative hypothesis is the presence of submicron Saharan dust that increases absorption in the blue and backscattering in the green parts of the spectrum (Claustre et al., 2002).

It is noted that radiometric data from mesotrophic rather than oligotrophic waters, minimize uncertainties in *g*-factors when using an equivalent number of in situ data and assuming comparable uncertainties (see discussion in Zibordi et al., 2015). This may suggest preference for mesotrophic rather than oligotrophic regions. However, the more advantageous L_w spectral values obtainable in mesotrophic waters may be outclassed by the higher intra-annual stability and spatial homogeneity typical of oligotrophic waters, both creating observation conditions favoring precision of *g*-factors.

Table 2
Quantities investigated at each region of interest.

Acronym	Quantity	Relevance
R_{rs}	Remote Sensing Reflectance	To address water type
$K_d(490)$ and *Chla*	Diffuse attenuation coefficient at 490 nm and Chlorophyll-a concentration[1]	To discuss climatology of marine bio-optical properties
$\tau_a(865)$ and α	Aerosol optical thickness at 865 nm and Ångström exponent	To discuss climatology of atmospheric optical properties
θ_0	Sun zenith	To address seasonal variability of illumination conditions

[1] *Chla* determined with the Hu et al. (2012b) color index algorithm for values lower than approximately 0.25 μg l^{-1} and the O'Reilly et al. (2000) band ratio for higher concentrations.

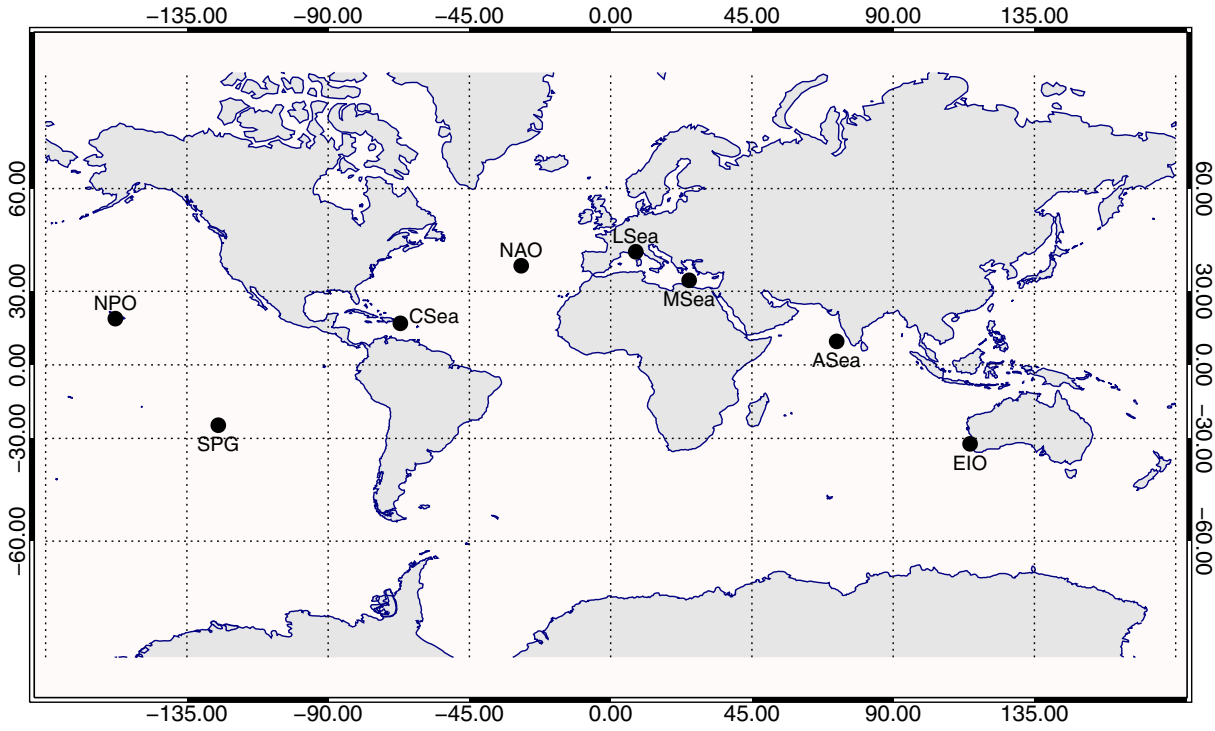

Fig. 1. Map of the marine regions of interest (see Table 1 for details).

Figs. 3–5 show the time-series of $R_{rs}(555)$, $K_d(490)$ and *Chla* for the regions considered. While the quantities $K_d(490)$ and *Chla* are bio-optical indicators suitable to evaluate the intra-annual variability of the region, R_{rs} at the 555 nm band is included to investigate the existence of potential uncorrelated changes in the concentration of optically significant constituents. This specific capability is offered by the small dependence of $R_{rs}(555)$ on *Chla* in Case-1 waters (see the slight differences among $R_{rs}(555)$ displayed in Fig. 2 for the various marine regions representing different bio-optical regimes).

The time-series of $R_{rs}(555)$ show the highest intra-annual stability for SPG, NPO and CSea regions with standard deviations σ of 0.12–0.14 × 10^{-3} sr^{-1}. Larger changes are observed for ASea, LSea and NAO with values of σ in the range of 0.24–0.30 × 10^{-3} sr^{-1}. Intermediate values with σ = 0.16 × 10^{-3} sr^{-1} are shown by MSea and EIO. However, it could be that part of the observed variability is produced by seasonal changes in illumination conditions (i.e., changes in θ_0) not fully removed by the atmospheric correction process.

The time-series of $K_d(490)$ also show the lowest and most stable values for the SPG and NPO regions. Specifically, SPG exhibits mean value of 0.022 m^{-1} and NPO of 0.029 m^{-1}, both with σ = 0.002 m^{-1}. Close values are shown by MSea with a mean of 0.032 m^{-1} and σ = 0.005 m^{-1}, and also by CSea with a mean of 0.036 m^{-1} and σ = 0.007 m^{-1}. Higher values characterize EIO, ASea and NAO with a mean in the range of 0.040–0.048 m^{-1} and σ in the range of 0.008–

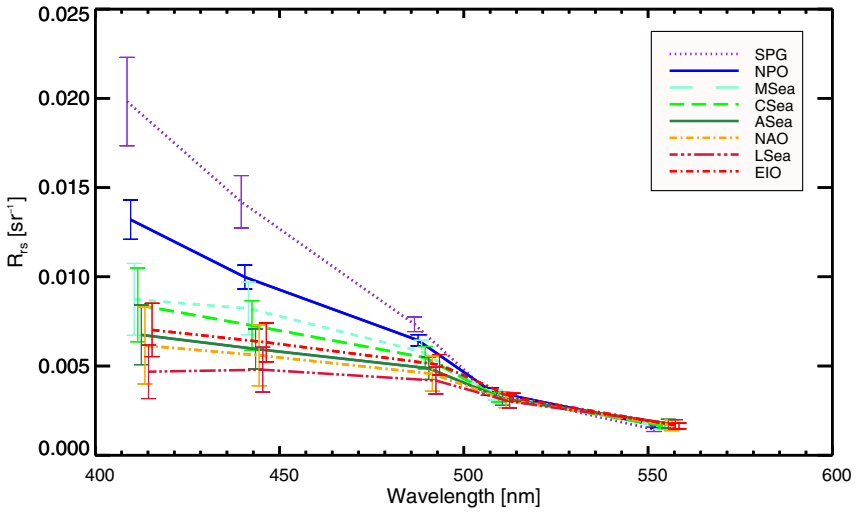

Fig. 2. Mean values of R_{rs} determined from the entire SeaWiFS mission at the 412–555 nm bands for the considered marine regions. Error bars indicate ±1σ. Spectra are incrementally shifted by 2 nm to increase readability of the figure while values at the 670 nm band, which are almost nil for all the regions, are not plotted.

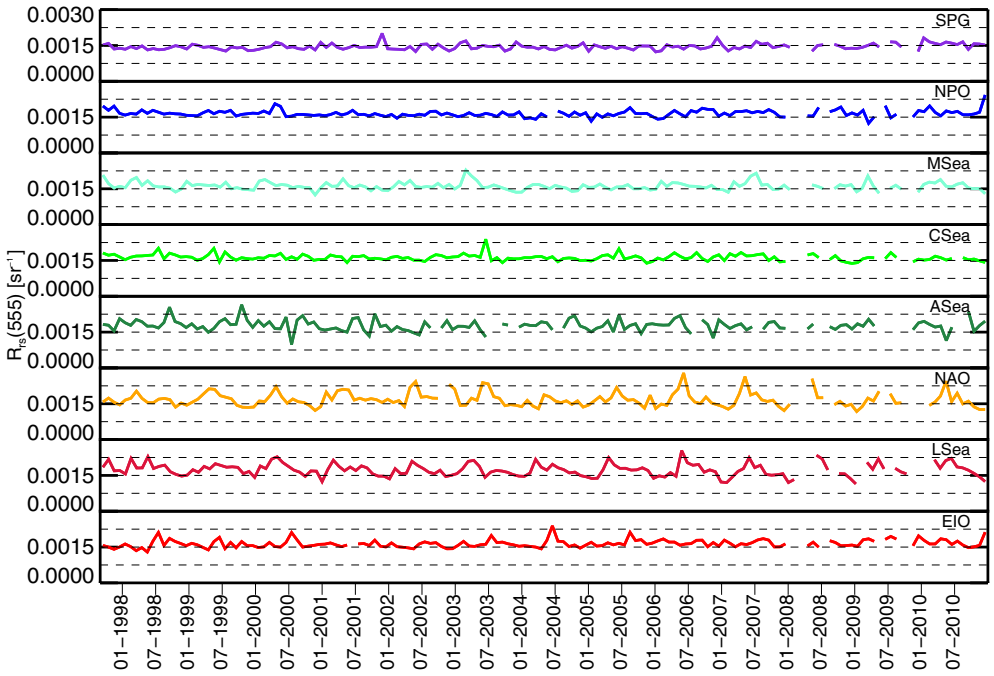

Fig. 3. Time-series of monthly values of $R_{rs}(555)$ for the various regions of interest.

0.017 m^{-1}. LSea exhibits the largest values with a mean of 0.056 m^{-1} and $\sigma = 0.018$ m^{-1}.

Consistent with $K_d(490)$, *Chla* time-series exhibit the lowest and most stable values for SPG and NPO with means of 0.03 and 0.07 μg l^{-1}, respectively, and σ of 0.01–0.02 μg l^{-1}. In agreement with the oligotrophic nature of the Eastern Mediterranean basin (e.g., Bosc et al., 2004), MSea also exhibits low and relatively stable values with mean of 0.11 μg l^{-1} and $\sigma = 0.04$ μg l^{-1}. Larger values characterize the CSea and EIO regions with means of 0.14 and 0.18 μg l^{-1}, respectively, both with $\sigma = 0.06$ μg l^{-1}. The largest values are then observed for ASea, NAO and LSea with means in the range of 0.21–0.33 μg l^{-1} and σ of 0.10–0.25 μg l^{-1}.

Fig. 6 displays the annual climatology of $K_d(490)$. LSea and NAO exhibit the highest seasonal variability with σ of 0.016 and 0.015 m^{-1}, respectively. SPG and NPO show the lowest, with σ of approximately 0.001 m^{-1}. All the other regions exhibit values of σ in the range of 0.005–0.007 m^{-1}.

In summary, excluding SPG, unequivocally NPO exhibits the least pronounced annual cycles and the clearest waters. Additional regions that also exhibit a low intra-annual variability of bio-optical properties are MSea and CSea. Among these, MSea is characterized by the lowest mean values and seasonal variability for both $K_d(490)$ and *Chla*. The largest mean values and variabilities for both $K_d(490)$ and *Chla* are observed for LSea.

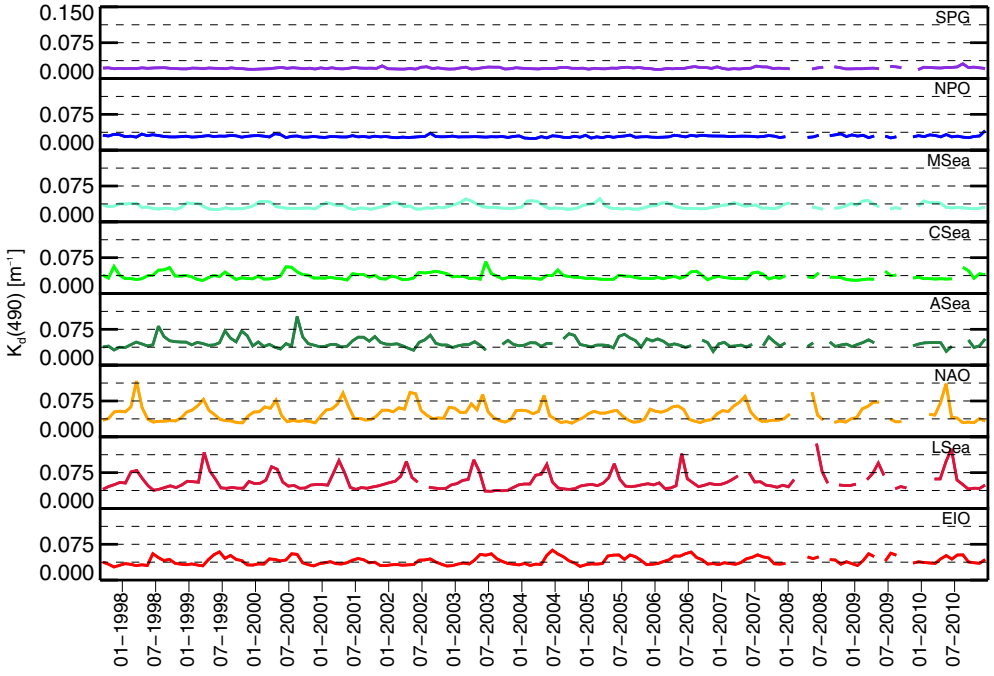

Fig. 4. Time-series of monthly values of $K_d(490)$ for the various regions of interest. Increase of $K_d(490)$ in Case-1 waters indicates increase in *Chla*.

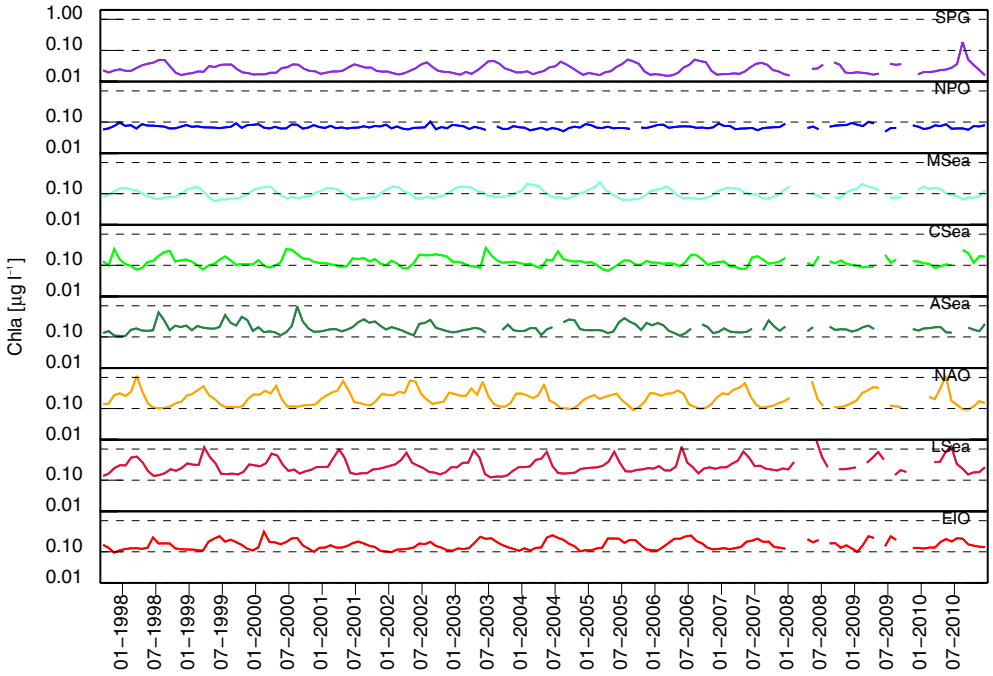

Fig. 5. Time-series of monthly values of *Chla* (in logarithmic scale) for the various regions of interest.

4.2. Climatology of atmospheric optical properties: time-series of $\tau_a(865)$ and α

The atmospheric optical properties are illustrated in Figs. 7 and 8 through $\tau_a(865)$ that provides information on the aerosol load, and through α chosen to describe the aerosol type. The lowest mean values and seasonal variabilities of $\tau_a(865)$ are those determined at EIO, LSea, NAO, SPG and MSea with means in the range of 0.05–0.07 and σ of 0.02–0.03 (admittedly, the relative values of τ_a may change between sites at shorter wavelengths as a function of α). Slightly higher temporal variabilities are noted for NPO with mean value of 0.09, and $\sigma = 0.03$. The highest values are observed for CSea and ASea with means of 0.10 and 0.13, respectively, both with σ of 0.05. The higher summer values at CSea are consistent with an influx of dust aerosols crossing the Atlantic Ocean towards the Caribbean Sea with possible contributions from biomass burning in South America (e.g., Colarco et al., 2003; Prospero et al., 2014; Yu et al., 2015).

Looking at α, the SPG, CSea and NPO regions exhibit mean values in the range of 0.5–0.8, with σ of 0.20–0.24, coherent with dominant marine aerosols (Smirnov et al., 2002, 2003, 2009). Slightly higher values are observed for EIO, NAO, and ASea with means in the range of 0.80–0.99 and σ of 0.28–0.32. Over a background of marine aerosols, the region of the Azores (i.e., NAO) can be subject to episodic influx of African desert dust (Chazette et al., 2001), while the annual cycle observed at ASea is coherent with the oscillations affecting the Arabian

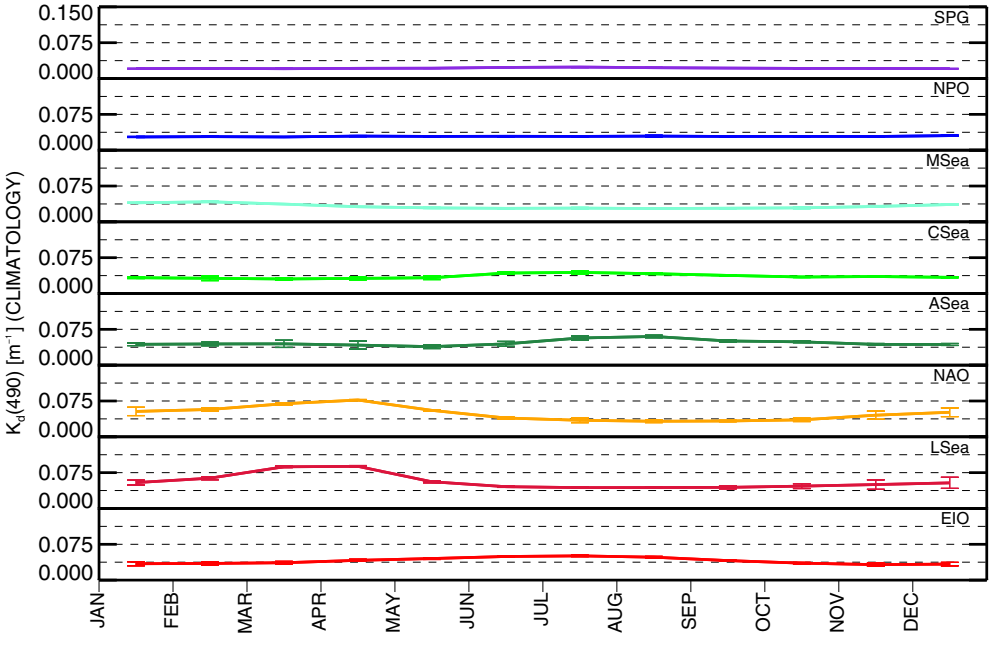

Fig. 6. Monthly climatology of $K_d(490)$ for the various regions of interest.

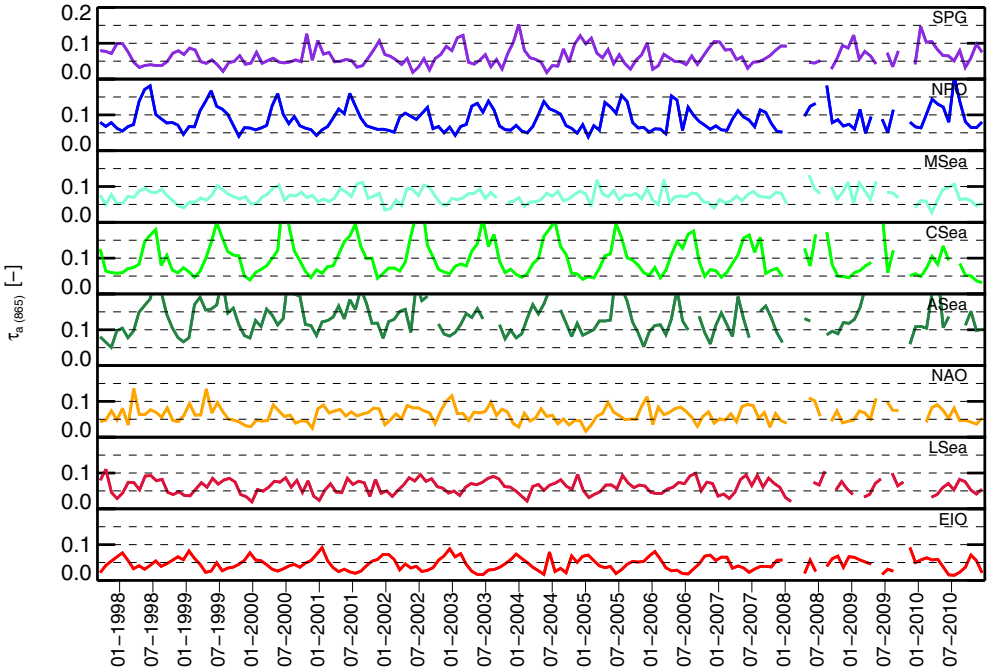

Fig. 7. Time-series of monthly values of $\tau_a(865)$ for the various regions of interest.

Sea (see Holben et al., 2001 for the Maldives) with summer monsoon events leading to low α due to aerosols dominated by sea-salt and dust (Vinoj and Satheesh, 2003), and winter monsoon events leading to high α determined by aerosols from the Indian sub-continent (Ramanathan et al., 2001). The highest values but also the lowest seasonal variabilities are observed at MSea and LSea with means of 1.14 and 1.40, respectively, both with $\sigma = 0.22$. These values indicate aerosol significantly affected by continental origin at LSea and to a lesser extent at MSea. Actually, all the Mediterranean Sea is under the influence of aerosols from diverse sources, including marine, continental of various types, desert dust and biomass burning (Lelieveld et al., 2002; Pace et al., 2006; Sciare et al., 2008). It is mentioned that the values of α for MSea are coherent with field measurements performed at the Island of Crete (Bryant et al., 2006; Kalivitis et al., 2007). However, annual means of field observations (Smirnov et al., 2009) as well as validation statistics (Mélin et al., 2013b) suggest that α determined from SeaWiFS data might be somewhat overestimated around Rottnest Island (EIO).

The annual climatology of $\tau_a(865)$ is illustrated in Fig. 9. It indicates the highest intra-annual variability for CSea with $\sigma = 0.045$ and the lowest for NAO with $\sigma = 0.011$. When looking at the annual climatology for α displayed in Fig. 10, LSea, CSea, NPO and MSea show the lowest variability with σ in the range of 0.11–0.15. Differently, ASea and EIO exhibit the highest values with σ of 0.25 and 0.27, respectively.

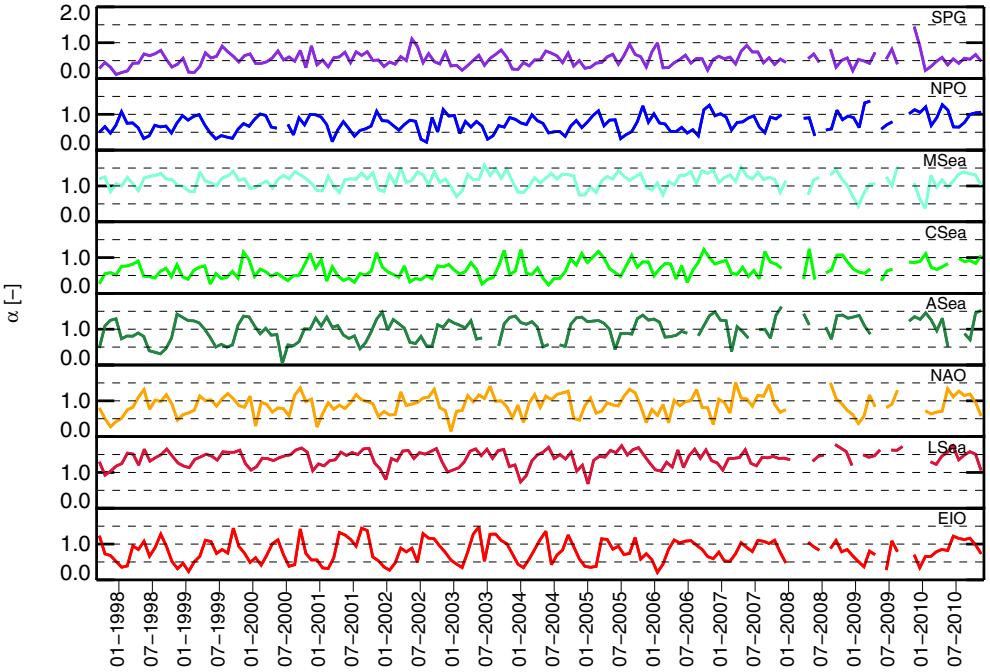

Fig. 8. Time-series of monthly values of α determined from near-infrared spectral bands for the various regions of interest.

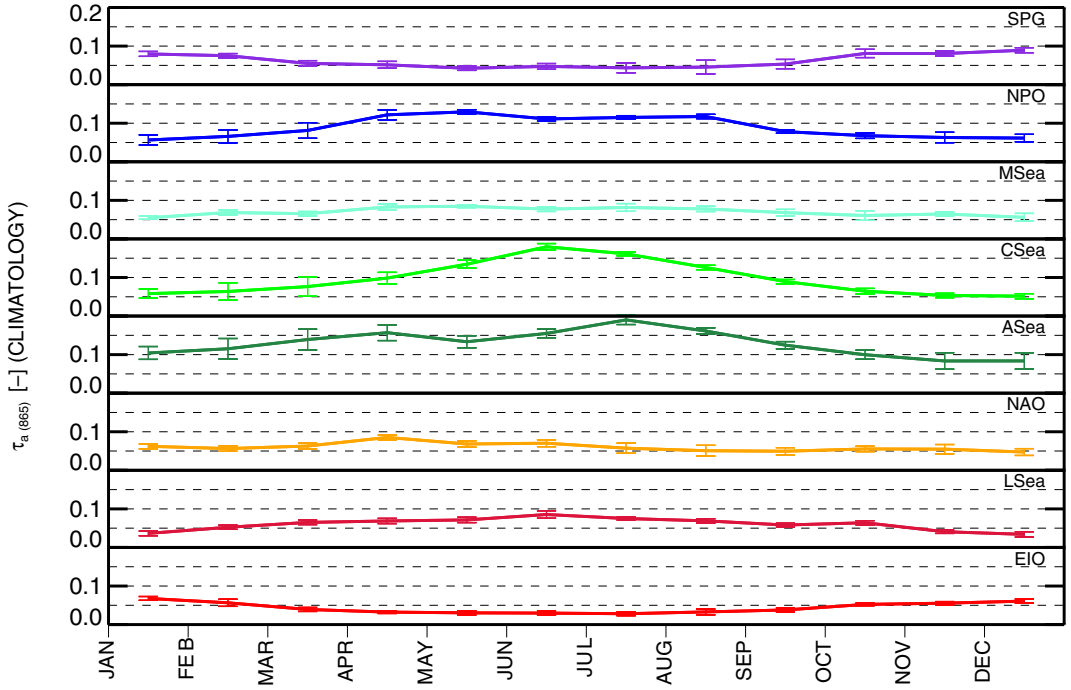

Fig. 9. Monthly climatology of $\tau_a(865)$ for the various regions of interest.

Overall, excluding SPG, the lowest and most stable values of $\tau_a(865)$ are observed at NAO, EIO, MSea and LSea. In contrast, again excluding SPG, the regions showing dominance of maritime aerosol characterized by low α and intra-annual variability are CSea (with exceptions in summer) and NPO.

4.3. Illumination: θ_0

Seasonal changes in the illumination conditions are illustrated in Fig. 11 through values of the sun zenith angle θ_0. The continuous lines indicate θ_0 at local noon, while the dashed lines indicate values at approximately ± 2 h from local noon chosen to cover a realistic interval of satellite overpass times. As expected, in agreement with latitude values, the lowest annual changes in θ_0 at local noon are observed for the ASea, CSea and NPO regions with values within 2–43°. Values of θ_0 in the range of 9–57° characterize EIO and MSea, while LSea and NAO exhibit values in the range of 16–67°.

These data indicate that the geometrical component of illumination (i.e., θ_0) is an additional source of optical stability for sites like MOBY or Kavaratti. Large changes in θ_0 may certainly decrease precision of *g*-

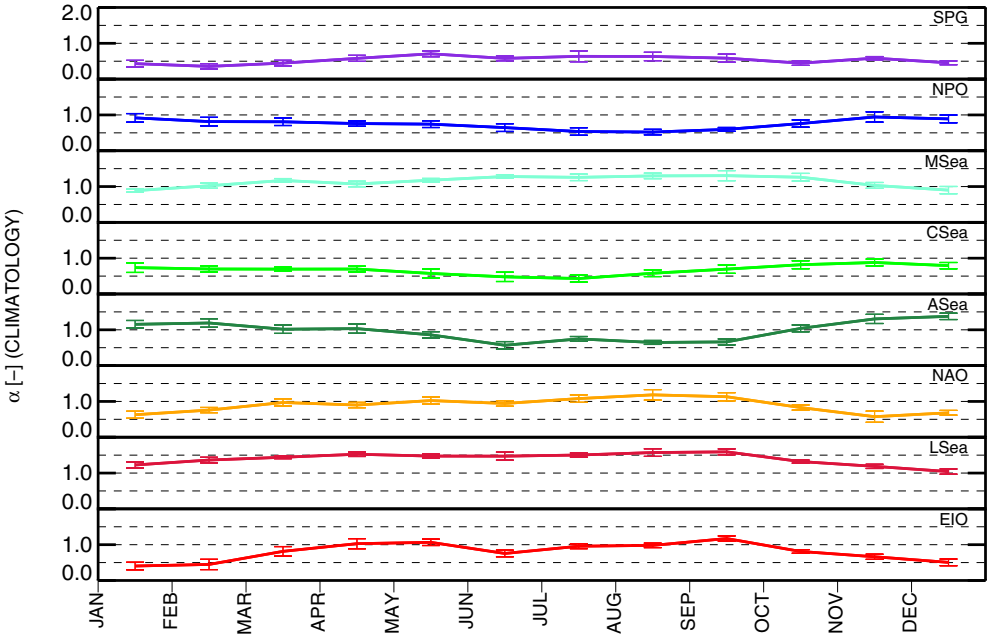

Fig. 10. Monthly climatology of α for the various regions of interest.

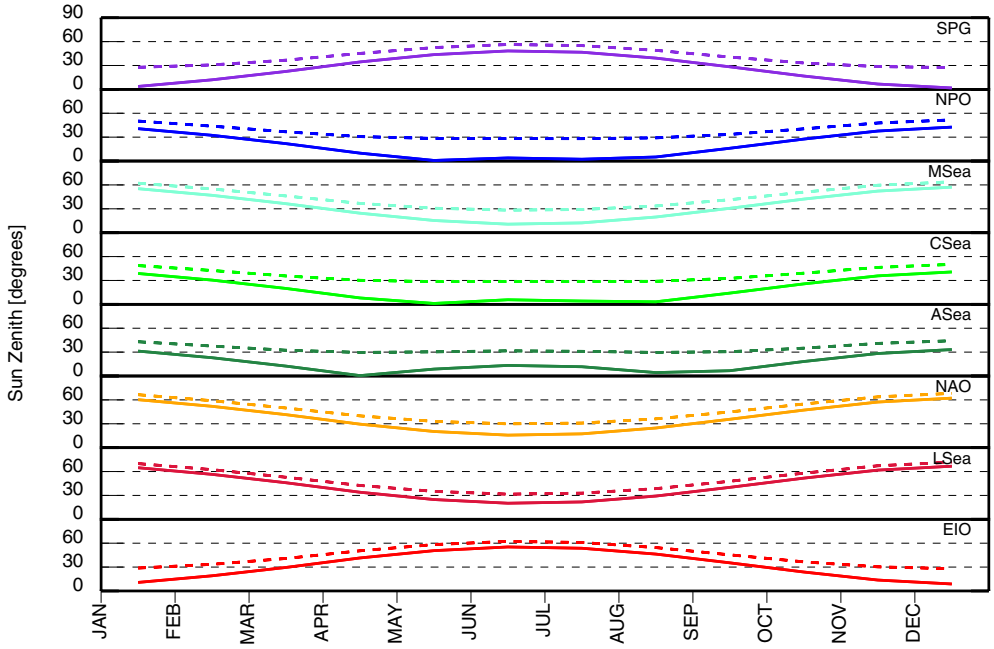

Fig. 11. Intra-annual variations of θ_0 at the regions of interest. The continuous lines indicate the values of θ_0 at local noon, while the dashed lines indicate the values of θ_0 at approximately ± 2 h from local noon.

factors and become the source of differences among SVC sites. However, it must be also recognized that large variations in θ_0 may offer the capability to comprehensively and systematically investigate the effects of illumination conditions and consequently of bi-directional effects, as needed to improve data processing by minimizing related sources of uncertainty.

5. Analysis of daily full-resolution data products

In order to investigate the characteristics of the study regions in more detail and particularly to address their potential for match-up collection, the analysis is extended to SeaWiFS Level-2 full resolution daily data (so-called Local Area Coverage data). Additionally, to discuss matchup rates as a function of mission-specific features (orbit, overpass time, width of the viewing swath, …), statistical analyses are also performed with Level-2 data from the Moderate Resolution Imaging Spectroradiometer (MODIS) onboard the Aqua platform, MEdium Resolution Imaging Spectrometer (MERIS) onboard the Envisat platform, and Visible Infrared Imaging Radiometer Suite (VIIRS) onboard the Suomi National Polar-Orbiting Partnership (Suomi NPP) spacecraft. The period of analysis is 5-year (limited to 4 for VIIRS) typical of mission lifetimes, specifically 1999–2003 for SeaWiFS, 2003–2007 for MODIS and MERIS, and 2012–2015 for VIIRS.

The SPG site is excluded from this analysis due to the relatively low number of full resolution data available for SeaWiFS and additionally by the difficulty to establish an SVC site in the region.

5.1. Cloud, high glint and high viewing angle flags

Effects of a number of exclusion flags determined by SeaDAS are investigated to discuss the probability of gathering high quality matchups of satellite and in situ data at the marine regions considered. The analysis indicates that flags responsible for at least 90% of the exclusions incurred by the application of all SeaDAS Level-2 default flags (see http://oceancolor.gsfc.nasa.gov/cms/atbd/ocl2flags), are those for screening cloud/ice contamination, high glint perturbations and high viewing angles effects. In the following analysis the limit for the satellite zenith angle is set to 60° (equal to the current SeaDAS default value). It is however mentioned that early SVC exercises were performed with an angle limit of 56° (Franz et al., 2007) and that a recent assessment of satellite derived R_{rs} indicated zenith angle dependences above 40° (Barnes and Hu, 2016).

Note that the three main flags applied in the following analysis are largely independent of the algorithms associated with the atmospheric correction process: they specifically depend on geometry (viewing angle), geometry and wind (glint) and on conservative tests applied to top-of-atmosphere Rayleigh-corrected radiance for cloud screening (which may be additionally triggered by bright waters or thick aerosol plumes (Banks and Mélin, 2015)). These elements attribute relevance to the resulting statistics beyond the application of any specific atmospheric correction scheme.

It is noted that high viewing angles and, to a lesser extent glint perturbation, are related to the instrument design and not solely to regional geophysical features. Still, the analysis of high glint and high viewing angle flagged data is considered relevant to illustrate typical cases directly applicable to future missions. In fact, it is evident that for matchup collection, MERIS is hindered by the smaller viewing swath (i.e., 1150 km) and the lack of tilt capability when compared to SeaWiFS having a larger swath (i.e., 2800 km) and a tilted view to reduce the probability of glint conditions (Gregg and Patt, 1994).

Considering that satellite observations are rejected if at least one of the 5×5 Level-2 elements centered at the considered region is affected by the specific exclusion flag(s), results from the analyses of SeaWiFS, and additionally of MODIS, MERIS and VIIRS data, are summarized in Table 3. Data related to cloud/ice flagging indicate that MSea followed by LSea and EIO, are the regions least affected by cloudiness. Specifically, MSea exhibits a rejection rate in the range of 53–63% across the different satellite data products. This significantly contrasts with the much higher values of 77–94% determined for ASea. It is also noted that NPO exhibits a rejection rate in the range of 72–84%.

In agreement with expectations, results from the analysis of high glint flagging vary from sensor to sensor and exhibit the lowest rejection rate in the range of 0–4% for SeaWiFS that benefits of tilt capability. The highest rejection rate that varies from 12 to 40% is observed for MERIS due to the small viewing swath in association with its early overpass time (however, when considering the generally lower rejection

Table 3
Fraction of satellite observations (in %) affected by cloud/ice (F_C), high glint (F_G), and high viewing angle (F_V) flags, or by all together (Q_F), computed over the period considered for the various regions. The analysis relies on full resolution Level-2 data from the SeaWiFS, MODIS, MERIS and VIIRS ocean color sensors. Data were excluded when at least one of the 5 × 5 elements centered at the specific region was affected by the exclusion flag (s). The number of satellite observations per site and per sensor is given in Tables 4 and 5.

	SeaWiFS				MODIS				MERIS				VIIRS			
	F_C	F_G	F_V	Q_F	F_C	F_G	F_V	Q_F	F_C	F_G	F_V	Q_F	F_C	F_G	F_V	Q_F
NPO	77.4	1.8	35.5	84.8	83.5	14.9	15.3	86.4	71.6	33.9	0.0	82.2	80.9	11.7	31.6	88.6
MSea	53.5	0.2	31.6	65.4	63.3	12.3	17.0	72.9	53.5	25.6	0.0	68.1	56.1	10.0	28.5	73.4
CSea	74.7	4.4	37.7	84.2	78.2	18.5	14.3	82.4	68.9	37.0	0.0	84.9	74.0	13.8	31.8	85.3
ASea	88.6	3.3	42.0	92.6	91.1	21.2	14.3	92.5	76.8	40.2	0.0	87.8	93.6	14.9	27.9	96.4
NAO	84.5	0.0	29.8	87.9	83.6	11.8	16.0	87.5	72.5	25.2	0.0	80.4	83.4	8.4	26.7	89.1
LSea	61.9	0.0	30.3	69.1	67.4	3.7	21.0	72.6	61.6	12.0	0.0	66.4	66.2	3.2	25.0	73.5
EIO	65.1	0.8	44.0	79.2	65.5	13.6	12.4	74.3	67.6	19.7	0.0	76.3	62.1	11.1	28.9	78.4

rate for clouds observed for MERIS, an interplay between glint and cloud flagging is likely to occur). Overall results indicate that, on average and regardless of the sensor, LSea appears to be the region least affected by glint while ASea located close to the equator is the most.

As expected, the high viewing angle flag largely affects SeaWiFS data with rejection rate of 30–44% due to the large viewing swath and its tilted view, while MERIS data are not at all affected due to the smaller swath.

When considering the combined effects of the previous three main flags, regardless of the sensor, MSea and LSea are the regions exhibiting the lowest rejection rates varying in the range of 65–74%. For comparison, NPO exhibits a rejection rate in the range of 85–89%.

As already anticipated the above results are definitely site and mission dependent. In fact, even assuming equivalent space sensors, the overpass time would have an impact on the daily percent observations due to glint and cloudiness affecting the same regions differently during the day (Feng and Hu, 2016).

5.2. Spatial homogeneity

Spatial homogeneity in the regions of interest is investigated through the coefficient of variation C_V (i.e., the ratio between standard deviation and the related mean) of the 5 × 5 Level-2 satellite derived R_{rs} values centered at the reference location. By restricting the analysis to cases in which all the 5 × 5 data elements are not affected by any of the SeaDAS Level-2 processing default flags, a region is heuristically considered spatially homogeneous when C_V is lower than 0.2 at the 443, 490 and 555 nm bands.

Results from the analysis of approximately 2000–3000 potential SeaWiFS observations per region over 5 years, are summarized in Table 4 (the number of observations varies from region to region and depends on latitude, onboard automatic recording over some sites and coverage provided by ground receiving stations). These results indicate that the Mediterranean regions (i.e., MSea and LSea) show the highest potential for matchups (i.e., observations not affected by default flags) with acceptance rates of 33 and 29%, respectively. In contrast ASea, NAO, CSea and NPO exhibit values ranging from 6 to 12%, while EIO reaches rates of 18%.

The test on homogeneity leads to an acceptance rate varying from 88% at NPO up to 97% at MSea with respect to cases not affected by the default flags. It is mentioned that the application of the more severe threshold $C_V < 0.1$ would decrease the previous acceptance rate to 79% at NPO and to 91% at MSea.

It is also recalled that the homogeneity test applied to R_{rs} data is mostly intended to ensure better comparability between in situ and satellite observations performed at very different spatial resolutions. Nevertheless, atmospheric optical properties around the SVC site may also exhibit spatial inhomogeneity. Its impact has been evaluated through the application of an additional homogeneity test to $\tau_a(865)$ from the 5 × 5 data elements centered at the reference location. Results obtained from the application of the threshold $C_V < 0.2$ to $R_{rs}(443)$, $R_{rs}(490)$ and $R_{rs}(555)$, and of the additional threshold $C_V < 0.3$ to $\tau_a(865)$, indicate a mean decrease of approximately 3% in the acceptance rate of matchups (the threshold of 0.3 applied to $\tau_a(865)$ has been simply chosen to satisfy the much larger variation coefficients characterizing $\tau_a(865)$ with respect to $R_{rs}(443)$, $R_{rs}(490)$ and $R_{rs}(555)$, as documented by the mean and standard deviation values later presented in Table 6). This result indicates a correlation between the spatial variability of R_{rs} and that of aerosol optical properties at the small scale considered, and suggests that the sole homogeneity test applied to R_{rs} may satisfy the need to flag cases affected by spatial inhomogeneity around SVC sites.

The analysis on SeaWiFS data is complemented by the determination of observations exhibiting a restricted range of sun zenith values (Table 4). Results obtained from the identification of those cases satisfying a threshold of $\theta_0 \le 45°$ (versus a limit of 70° associated with the default processing flag) show that the sun zenith at NPO, CSea and ASea does not exceed the threshold applied, and also confirm an expected increase of threshold effects with latitude (with LSea being the most affected).

Fig. 12 illustrates the temporal distribution of SeaWiFS observations not affected by default flags and passing the spatial homogeneity test. Notable is the regular seasonal distribution of potential matchups at MSea, LSea, EIO and to a lesser extent at NAO, with peaks centered during local summer. Conversely, NPO, CSea and ASea exhibit a higher occurrence of data during winter likely explained by a more pronounced summer cloudiness (especially for CSea and ASea).

While analyzing Table 5 with the number of matchups for other missions, it should be noted the generally larger number of observations (i.e., N) of VIIRS available over 4 years when compared to those of MODIS over 5 years justified by the different viewing swaths (i.e., 3000 km versus 2300 km, respectively). Results in Table 5 show a lower number of non-flagged cases (M) with respect to those determined for SeaWiFS, a finding indicating a reduction in the capability of producing high quality matchups by MODIS, MERIS and VIIRS with respect to SeaWiFS. This can be explained by a lower number of available data (particularly for MERIS because of a smaller swath) and by a different performance of processing flags on data products from the various sensors.

Table 4
SeaWiFS Level-2 full-resolution data over a 5-year period (1999–2003) included in the statistical analysis and of those passing different quality tests for the various regions. N indicates the number of available observations, M is the number of cases remaining after applying the SeaDAS default exclusion flags, and M_{CV} indicates the number of cases that also passed the homogeneity test defined by a variation coefficient $C_V < 0.2$ determined from the 5 × 5 values of R_{rs} at the 443, 490 and 555 nm bands. Finally, M_{SZ} indicates the number of cases with respect to M, for which $\theta_0 \le 45°$.

	N	M	M vs N [%]	M_{CV}	M_{CV} vs M [%]	M_{SZ}	M_{SZ} vs M [%]
NPO	1768	212	12.0	187	88.2	211	99.5
MSea	2472	821	33.2	798	97.2	680	82.8
CSea	2071	242	11.7	218	90.1	242	100.0
ASea	1842	114	6.2	103	90.4	114	100.0
NAO	2796	274	9.8	256	93.4	211	77.0
LSea	3024	873	28.9	827	94.7	575	65.9
EIO	2101	382	18.2	367	96.1	309	80.9

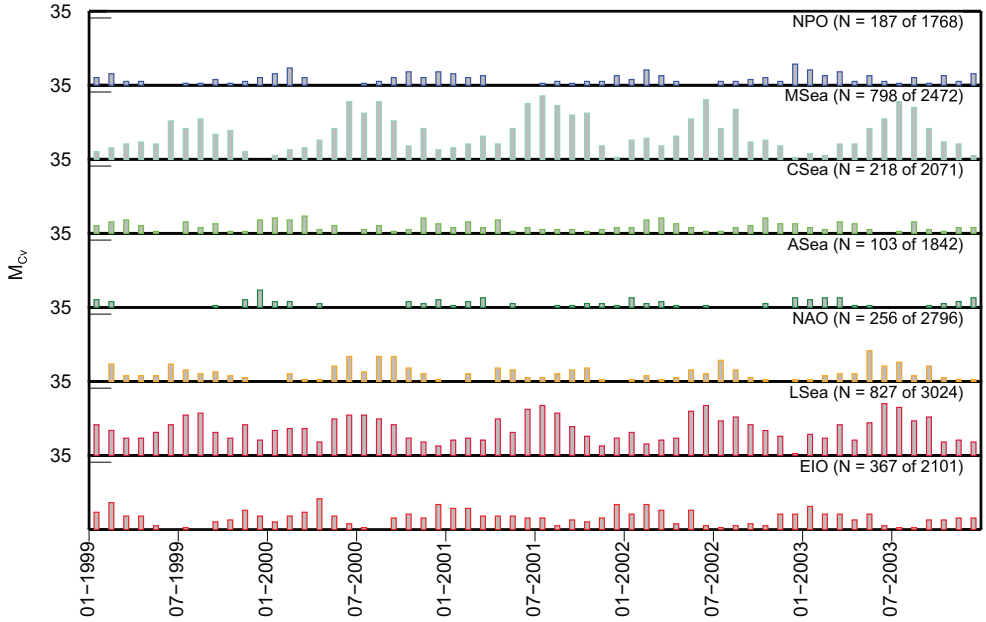

Fig. 12. Number of SeaWiFS observations M_{CV} remaining after applying the default exclusion flags and passing the spatial homogeneity test (i.e., $C_V < 0.2$ for R_{rs} at the 443, 490 and 555 nm bands) for the 5-year period considered. Assuming no more than one daily observation, the maximum value of M_{CV} would not exceed 31 (for convenience the maximum value on the y-axes has been set to 35).

Finally, the comparison of Table 4 with Table 5 indicates a generally higher number of cases removed by the homogeneity test when applied to SeaWiFS data as opposite to radiometric products from other ocean color sensors. This is very likely explained by a lower signal-to-noise ratio characterizing SeaWiFS radiometric data with respect to that of other sensors (Hu et al., 2012a).

6. Identification of prime SVC regions

The objective of this work is to identify the location of potential SVC sites suitable to support ocean color missions contributing to the creation of CDRs. While the analysis based on Level-3 data was expected to document the climatology of each marine region of interest, the actual identification of prime SVC sites is conditioned by the analysis of in situ and satellite matchups gathered from Level-2 products. Thus, in view of supporting the following investigation on relevance and also equivalence of SVC sites, results from the statistical analysis of marine/atmospheric 5-year SeaWiFS Level-2 daily full-resolution products are summarized in Table 6 for each region through mean m and standard deviation σ. These data provide an overview at the spatial scale of matchups on relevant bio-optical quantities and on their intra-annual variability (or conversely stability).

Values in Table 6 may show differences from those determined from the Level-3 monthly averaged data used to investigate the climatology of bio-optical atmospheric/marine quantities. These differences, in addition to a diverse spatial resolution and time binning, are also explained by the different quality control applied: more inclusive in the case of Level-3 products, driven by the objective to maximize the number of data products applicable for climatology analysis (i.e., retaining each valid Level-3 data element); and otherwise exclusive in the case of Level-2 products, finalized to the objective of preserving only those satellite observations applicable to the identification of high quality matchups (i.e., retaining only those cases for which all the 5 × 5 Level-2 data elements centered at the region of interest satisfy specific quality criteria).

The work of Zibordi et al. (2015) shows that the MOBY site in the NPO region, when compared to a number of alternative data sources, exhibits high capability to meet requirements for long-term stability essential for the creation of CDRs from multiple ocean color missions. This is explained by an outstanding effort to characterize, calibrate and maintain field radiometers in view of minimizing sources of uncertainties in derived in situ L_w data (Brown et al., 2007), together with a restricted range of illumination conditions, favourable marine/atmospheric optical properties and low intra-annual variability.

Results from Sections 4 and 5, definitely confirm the unique features of NPO with respect to any other region among those considered: maritime aerosols and oligotrophic waters exhibiting high intra-annual optical stability in addition to low sun zenith variations. Thus, the MOBY site remains a perfect candidate for SVC in support of climate applications, and can be considered a reference when looking for additional or alternative SVC sites relevant for the creation of CDRs.

Table 5
MODIS, MERIS and VIIRS full-resolution observations N for the various regions and various sensors over the period considered, together with those observations M not affected by the SeaDAS default exclusion flags, and those observations M_{CV} passing the homogeneity test.

	MODIS			MERIS			VIIRS		
	N	M	M_{CV}	N	M	M_{CV}	N	M	M_{CV}
NPO	1708	132	132	760	118	117	1726	89	89
MSea	1922	447	441	888	223	221	1899	325	324
CSea	1591	202	202	740	107	105	1722	116	114
ASea	1589	69	66	737	73	71	1622	28	28
NAO	1977	158	158	991	110	105	2093	108	106
LSea	2165	482	477	1045	288	276	2272	397	394
EIO	1819	397	395	861	199	196	1910	266	266

6.1. Equivalence of measurement conditions across regions

It is recalled that equivalence of measurement conditions across marine regions is an element expected to minimize differences in g-factors regardless of the geographic location of the SVC site. However, despite the importance of this ideal requirement, the identification of multiple SVC sites may imply trading-off some of the criteria associated with the marine/atmospheric properties. For instance, with reference to results from the climatology analysis and also to data in Table 6, MSea followed by CSea and EIO are the regions that most compare with NPO in terms of intra-annual stability and mean values of the

Table 6
Mean m and standard deviation σ of SeaWiFS Level-2 non-flagged data products (M) utilized to complement the climatology analysis of the marine/atmospheric properties at the regions considered: $R_{rs}(412)$ and $R_{rs}(555)$ are units of $sr^{-1} \times 10^{-3}$, $k_d(490)$ in units of m^{-1}, *Chla* in units of $\mu g\ l^{-1}$, $\tau_a(865)$ and α both dimensionless, and θ_0 in units of degrees.

		$R_{rs}(412)$		$R_{rs}(555)$		$k_d(490)$		*Chla*		$\tau_a(865)$		α		θ_0	
	M	m	σ	m	σ	m	σ	m	σ	m	σ	m	σ	m	σ
NPO	212	12.9	1.45	1.54	0.29	0.027	0.004	0.07	0.01	0.07	0.04	0.88	0.40	29.5	12.3
MSea	821	9.48	2.38	1.51	0.33	0.029	0.006	0.09	0.03	0.08	0.05	1.22	0.41	26.8	14.2
CSea	242	8.64	2.31	1.54	0.23	0.033	0.009	0.13	0.07	0.08	0.05	0.69	0.42	23.8	12.7
ASea	114	6.57	1.19	1.62	0.30	0.043	0.011	0.19	0.11	0.11	0.05	1.14	0.29	24.2	9.3
NAO	274	6.46	2.11	1.68	0.41	0.047	0.020	0.25	0.22	0.06	0.04	1.09	0.45	31.7	14.2
LSea	873	5.09	2.03	1.65	0.41	0.051	0.020	0.28	0.23	0.07	0.04	1.45	0.37	38.7	15.9
EIO	382	7.51	1.81	1.53	0.25	0.036	0.008	0.15	0.05	0.05	0.03	0.76	0.55	28.3	14.7

considered marine bio-optical quantities (i.e., $k_d(490)$ and *Chla*). When looking at $R_{rs}(555)$, CSea and EIO show variabilities (quantified by σ) lower than those observed at NPO, while ASea and MSea exhibit slightly higher values. At 412 nm, the lowest variability (better indicated by the coefficient of variation, σ/m, due to the wide range of $R_{rs}(412)$ values) shows the lowest values for NPO, followed by ASea, EIO, MSea and CSea.

When looking at the atmospheric optical quantities, the lowest intra-annual variability of both $\tau_a(865)$ and α is observed at ASea and LSea. However, both regions exhibit values of α indicating contamination by continental aerosols more marked for LSea (and also seen for MSea). On the other hand, despite a lower intra-annual stability, CSea and EIO show mean values of α approaching those of NPO. It is however remarked that while CSea (see Fig. 9) is characterized by a relatively high seasonal variability of $\tau_a(865)$, EIO (see Fig. 10) exhibits a more pronounced seasonal variability of α.

Finally, in addition to differences in sun zenith angles θ_0 also given Table 6, elements worth mentioning are the ozone concentration O_3 and the wind speed W_S across the considered marine regions. In fact, O_3 strongly varies with latitude and may diversely affect the accuracy of the atmospheric correction process. Similarly, a different W_S may diversely perturb the reflectance of the sea surface and additionally the performance of measuring systems at sea (e.g., optical buoys).

Statistical analysis performed with ancillary data from SeaWiFS Level-2 products non flagged by the SeaDAS default exclusion flags, shows mean values of O_3 varying from 253 and 259 DU at ASea and NPO, and up to 308 and 320 DU at NAO and LSea, respectively. Equivalent analysis performed on W_S ancillary data (originated by the US National Centers for Environmental Prediction (NCEP)) exhibits mean values in the range of 3–6 m s^{-1} with σ generally within 1.5–2.5 m s^{-1}. More specifically, ASea, LSea and NPO show the lowest values (i.e., 3.2, 3.3, and 3.9 m s^{-1}, respectively), while CSea, MSea, NAO and EIO exhibit the highest (i.e., 4.6, 5.3, 5.5 and 6.0 m s^{-1}, still below the 12 m s^{-1} threshold ensuring application of the SeaDAS whitecap correction).

Considering the previous differences among θ_0, O_3 and W_S from the various regions, a thorough evaluation of their impact on g-factors would require dedicated theoretical investigations, which are beyond the objective of this work. Because of this, the following investigation on best suitability of regions for SVC is restricted to *Chla*, $\tau_a(865)$ and α.

6.2. Prime SVC regions

Assuming in situ L_w measurements are regularly available at each location considered, Table 7 presents the number of potential high quality matchups (i.e., applicable for SVC) between SeaWiFS and in situ data over a 5-year period, as identified through the application of very stringent criteria associated with oligotrophic conditions and clear marine atmosphere: *Chla* ≤ 0.1 $\mu g\ l^{-1}$ or $\tau_a(865) \le 0.1$ or $\alpha \le 1.0$, or all of them. These thresholds have been chosen to tentatively reflect the statistical values determined for the NPO reference region and thus to implicitly identify cases characterized by oligotrophic conditions and maritime aerosols (Smirnov et al., 2003) as well as a small seasonal variability and a low marine bio-optical complexity. The use of the thresholds selected, implicitly favoring regions exhibiting high intra-annual stability, is thus expected to supersede any other index derived from the regional climatology of the relevant geophysical quantities.

Results show a dramatic decrease of the number of matchups when all quality criteria are applied. In particular, despite the low number of overall potential matchups (i.e., $M_{CV} = 187$) with respect to those available for other regions (e.g., $M_{CV} = 798$ for MSea or 828 for LSea), NPO exhibits the highest number of high quality matchups (i.e., $M_{Q1} = 75$). In addition to NPO, those regions showing an appreciable number of potential high quality matchups are MSea, CSea and EIO with M_{Q1} equal to 59, 48 and 42, respectively.

The number of potential high quality matchups obtained for NPO is fully supported by those determined from the application of MOBY data to SeaWiFS SVC. In fact, the number of 15 high quality matchups per year for NPO is comparable to the approximately 17 per year (i.e., 150 over a 9-year period) actually identified by Franz et al. (2007) for MOBY applying slightly different selection criteria. It is however

Table 7
SeaWiFS Level-2 observations M_{CV} over the 5-year period considered, not affected by SeaDAS Level-2 default exclusion flags and passing the spatial homogeneity test, applied to investigate cases for which the 5 × 5 elements representing each region exhibit mean: *Chla* ≤ 0.1 $\mu g\ l^{-1}$, *Chla* ≤ 0.2 $\mu g\ l^{-1}$, $\tau_a(865) \le 0.10$, $\tau_a(865) \le 0.15$ and $\alpha \le 1.0$. M_{Q1} indicates the number of potential high quality matchups identified through the application of combined tests on mean *Chla* ≤ 0.1 $\mu g\ l^{-1}$, mean $\tau_a(865) \le 0.10$ and mean $\alpha \le 1.0$ (M_{Q1}/year is the related number of potential high quality matchups per year). Differently, M_{Q2} indicates results from the application of combined tests on mean *Chla* ≤ 0.2 $\mu g\ l^{-1}$, mean $\tau_a(865) \le 0.15$ and mean $\alpha \le 1.0$ (M_{Q2}/year, indicates the related potential number of matchups per year).

	M_{CV}	*Chla* ≤ 0.1	*Chla* ≤ 0.2	$\tau_a(865) \le 0.10$	$\tau_a(865) \le 0.15$	$\alpha \le 1.0$	M_{Q1} (M_{Q1}/year)	M_{Q2} (M_{Q2}/year)
NPO	187	182	187	153	177	107	75 (15.0)	98 (19.6)
MSea	798	572	794	570	714	212	59 (11.8)	147 (29.4)
CSea	218	79	197	164	195	172	48 (9.6)	141 (28.2)
ASea	103	0	80	37	83	21	0 (0.0)	13 (2.6)
NAO	256	3	156	219	246	102	1 (0.2)	56 (11.2)
LSea	827	0	400	668	790	87	0 (0.0)	36 (7.2)
EIO	367	53	328	337	363	235	42 (8.4)	220 (44.0)

recognized that the consistency of results across the various regions may be affected by geographical differences in the accuracy of data products. A specific case is that of *Chla* that is likely overestimated at MSea and LSea as a result of the application of global bio-optical algorithms (Morel and Gentili, 2009).

The numbers in Table 7, much smaller than the potential matchups determined solely applying the SeaDAS default exclusion flags in combination with the spatial homogeneity test, confirm the multi-annual effort generally required to produce mission specific *g*-factors qualified for the construction of CDRs.

Nevertheless, the need for a statistically significant number of matchups per mission (e.g., Franz et al., 2007), may suggest to increase their number by relaxing some of the thresholds applied to geophysical quantities. Results in Table 7 indicate that the potential for matchups at some regions can vastly increase through the application of less restrictive criteria. Examples are EIO and CSea, which exhibit typical *Chl*a values higher than those of regions like NPO or MSea (see Table 6). Thus, when relaxing the exclusion criteria and thus accepting mean values of $Chla \leq 0.2\ \mu g\ l^{-1}$ and also of $\tau_a(865) \leq 0.15$, the number of potential matchups may massively increase for some regions (e.g., EIO). Nevertheless, the increase can be relatively moderate for others (e.g., NPO).

The choice of relaxing the selection criteria would, however, affect the desirable equivalence of multiple SVC sites. Besides, differences in the intra-annual variability of marine and atmospheric optical quantities at the diverse regions could unevenly impact the precision of *g*-factors across missions relying on different SVC sites.

Table 8 shows that the number of high quality potential matchups (i.e., M_{Q1}) determined for MODIS, MERIS and VIIRS with the application of strict thresholds to geophysical quantities over the period considered, significantly varies from mission to mission, but in general exhibits regional values much lower than those determined for SeaWiFS. This result, fully supported by the number of matchups obtained through the sole application of default flags and homogeneity tests, may be additionally explained by the effects of thresholds in combination with systematic differences among data products. Still, regardless of the number of high quality matchups, notable is the consistency of M_{Q1} rates across the different regions. In fact, in all cases NPO (except for VIIRS) shows the best performance, followed by MSea, CSea and EIO in decreasing order. The very different number of potential matchups obtained for VIIRS at MSea when compared to those determined for MODIS is probably explained by the systematically lower mean regional values of α determined for the former (i.e., 1.04 ± 0.48) with respect to those computed for the latter (i.e., 1.34 ± 0.43).

In agreement with results from the analysis of SeaWiFS data, when relaxing the exclusion criteria for the selection of potential matchups for other sensor data by accepting mean values of $Chla \leq 0.2\ \mu g\ l^{-1}$ and of $\tau_a(865) \leq 0.15$, their number (i.e., M_{Q2}) largely increases for all sensors with respect to M_{Q1}. Still these numbers are usually lower than those determined for SeaWiFS.

For completeness, the effects of applying the SeaDAS default limit value of 60° to the satellite zenith angle has also been investigated with the SeaWiFS dataset. The use of a 40° limit, that could further increase the quality of matchups and ideally make this quality more comparable across satellite sensors exhibiting different viewing swaths, was shown to lead to a reduction of M_{Q1} in the range of 45–75%. This large reduction appears to favor MSea with respect to NPO, but does not affect the overall relative ranking of the other marine regions.

7. Conclusions

Restating the fundamental importance of establishing SVC sites in regions that may benefit by logistical support from nearby islands or coastal locations, the study shows the difficulty in identifying regions located in different seas and characterized by ideal and likely equivalent measurement conditions: oligotrophic/mesotrophic waters and maritime aerosols in conjunction with low cloudiness, and high intra-annual stability and spatial homogeneity.

By relying on existing or potential fixed SVC sites (see Table 1), the study confirms the ideal location of the MOBY site associated with NPO. In fact, when looking at the marine optical properties (e.g., $K_d(490)$) as derived from SeaWiFS Level-3 monthly average 24-th degrees products, NPO exhibits the least pronounced seasonal cycles. Additional regions characterized by high intra-annual stability are MSea and CSea, followed by EIO. It must be noted that the application of criteria favoring high intra-annual stability in the selection of SVC regions, may privilege low latitude with respect to higher latitudes regions, despite a lower number of overpasses and higher glint perturbations.

On the atmospheric side, Level-3 data exhibit the lowest and likely most stable values of $\tau_a(865)$ at EIO, slightly increasing for LSea, NAO, MSea and NPO. Maritime aerosols empirically identified by mean values of α lower than 1, and also exhibiting high intra-annual stability, are determined at CSea and NPO. Still maritime aerosols, but affected by higher seasonal variability, are observed at EIO. MSea and LSea exhibit mean monthly values of α higher than 1 (i.e., 1.14 at MSea and 1.40 at LSea), but both characterized by high intra-annual stability.

From the analysis of Level-2 daily 1-km products, results indicate that MSea followed by LSea and EIO are the regions least affected by cloudiness with rejection rates due to cloud flagging in the range of 53–78% depending on region and satellite overpass. The spatial homogeneity, as determined from the analysis of the coefficient of variation C_V computed at the 443, 490 and 555 nm bands from the 5×5 values of R_{rs} centered at each location of interest, appears high for all the regions considered. Specifically, by solely considering observations passing tests from SeaDAS default exclusion flags, acceptance rates determined by $C_V < 0.2$ vary from 88% at NPO to 97% at MSea.

In view of drawing conclusions for the practical identification of SVC sites satisfying requirements for the creation of ocean color CDRs, the occurrence of ideal conditions equivalent to those observed at NPO

Table 8
MODIS, MERIS and VIIRS Level-2 observations, M_{CV}, not affected by exclusion flags and passing the spatial homogeneity test for the various regions over the number of years considered. M_{Q1} indicates potential high quality matchups obtained by applying combined tests on mean $Chla \leq 0.1\ \mu g\ l^{-1}$, mean $\tau_a(865) \leq 0.1$ and mean $\alpha \leq 1.0$ (M_{Q1}/year, indicates the related potential number of high quality matchups per year). M_{Q2} refers to cases determined through combined tests on mean $Chla \leq 0.2\ \mu g\ l^{-1}$, mean $\tau_a(865) \leq 0.15$ and mean $\alpha \leq 1.0$ (M_{Q2}/year, indicates the related potential number of matchups per year).

	MODIS			MERIS			VIIRS		
	M_{CV}	M_{Q1} (M_{Q1}/year)	M_{Q2} (M_{Q1}/year)	M_{CV}	M_{Q1} (M_{Q1}/year)	M_{Q2} (M_{Q2}/year)	M_{CV}	M_{Q1} (M_{Q1}/year)	M_{Q2} (M_{Q2}/year)
NPO	132	31 (6.2)	54 (10.8)	117	27 (5.4)	45 (9.0)	88	21 (5.3)	33 (8.3)
MSea	441	14 (2.8)	61 (12.2)	221	17 (3.4)	65 (13.0)	324	44 (11.0)	106 (26.5)
CSea	202	6 (1.2)	95 (19.0)	105	14 (2.8)	54 (10.8)	113	13 (3.3)	58 (14.5)
ASea	66	0 (0.0)	4 (0.8)	71	0 (0.0)	3 (0.6)	28	0 (0.0)	2 (0.5)
NAO	158	1 (0.2)	31 (6.2)	105	7 (1.4)	22 (4.4)	105	5 (1.3)	38 (9.5)
LSea	475	0 (0.0)	25 (5.0)	276	1 (0.2)	26 (5.2)	394	0 (0.0)	57 (14.3)
EIO	393	5 (1.0)	129 (25.8)	195	16 (3.2)	73 (14.6)	266	7 (1.8)	128 (32.0)

has been investigated through the construction of potential in situ and satellite matchups. This has been performed using a number of strict quality tests applied to marine and atmospheric optical Level-2 data products passing the SeaDAS default flagging and spatial homogeneity checks, assuming that geographical differences in the accuracy of data products do not question basic conclusions. Summary results based on SeaWiFS Level-2 data and quality tests based on mean values of $Chla \le 0.1$ μg l^{-1}, $\tau_a(865) \le 0.1$ and $\alpha \le 1.0$ from the 5×5 data elements centered at each region, indicate the possibility of obtaining 15 high quality matchups per year at NPO (consistent with the number of approximately 17 actually determined at the MOBY site), approximately 12 at MSea, 10 at CSea and 8 at EIO. The smaller number of potential high quality matchups at MSea, when compared to NPO, is explained by the rejection of cases affected by non-maritime aerosol. Conversely, in the case of CSea and EIO it is explained by rejections due to $Chla > 0.1$ μg l^{-1}. It must be emphasized that the previous number of matchups might however vary to some extent if a different atmospheric correction or regional bio-optical algorithms are adopted.

The study has also investigated the impact of lessening the criteria for the construction of matchups by using alternative thresholds such as $Chla \le 0.2$ μg l^{-1} and $\tau_a(865) \le 0.15$. The increase in the number of potential matchups obtainable at regions like EIO or CSea is striking. However, in spite of the benefit of a larger number of matchups, the relaxation of selection criteria diminishes the equivalence of observation conditions among SVC sites. Yet, this reduced equivalence should not significantly impact the capability to satisfy the 5% requirement on L_w uncertainty. Contrarily, it could lessen the capability of SVC sites to meet the 0.5% per decade radiometric stability requirement due to a lower intra-annual environmental stability and likely a higher bio-optical complexity of the sites.

The same analysis performed with MODIS, MERIS and VIIRS Level-2 data provides a lower number of high quality matchups per year for all sensors, probably explained by systematic differences among products. Still the number of potential MODIS, MERIS and VIIRS matchups reflects the performance rate among marine regions determined with SeaWiFS data. It is also emphasized that the four ocean color missions considered offer a representative set of possible instrument and orbital characteristics. This suggests that conclusions from the study might be applicable to new or upcoming sensors such as the Ocean and Land Colour Instrument (OLCI) on-board the Sentinel-3 platforms.

In conclusion, the analysis on potential high quality matchups confirms the superior location of the MOBY site in the northern Pacific Ocean for SVC. While recognizing that no site is superior for all criteria reviewed in the analysis, it nonetheless suggests that the Eastern Mediterranean Sea near the Island of Crete exhibits best equivalence with NPO and could be considered as a further site for SVC complying with requirements for the creation of CDRs. Additional sites, even though exhibiting a lower capability of producing high quality matchups per year are the Caribbean Sea and the Indian Ocean near Rottnest Island.

It is finally restated that the previous findings are based on the analysis of optical properties of a limited number of SVC fixed sites already in place or under discussion, thus they do not exclude alternatives. In addition, it is also recognized that a theoretical investigation based on the application of actual atmospheric correction codes (e.g., SeaDAS) would likely help to better define thresholds for geophysical parameters satisfying SVC requirements.

Acknowledgments

The authors would like to thank the Ocean Biology Processing Group of the National Aeronautics and Space Administration for the distribution of the satellite ocean color products.

Special appreciation is expressed to Mirko Marioni for the diligent extraction and handling of satellite data.

Finally, K.J. Voss and two anonymous reviewers are sincerely thanked for their comments and suggestions that helped to improve the quality of the work.

References

Ahmad, Z., Franz, B.A., McClain, C.R., Kwiatkowska, E.J., Werdell, J., Shettle, E.P., et al., 2010. New aerosol models for the retrieval of aerosol optical thickness and normalized water-leaving radiances from the SeaWiFS and MODIS sensors over coastal regions and open oceans. Appl. Opt. 49, 5545–5560.

Antoine, D., D'Ortenzio, F., Hooker, S.B., Bécu, G., Gentili, B., Tailliez, D., Scott, A.J., 2008b. Assessment of uncertainty in the ocean reflectance determined by three satellite ocean color sensors (MERIS, SeaWiFS and MODIS-A) at an offshore site in the Mediterranean Sea (BOUSSOLE project). J. Geophys. Res. 113 (C7), C07013.

Antoine, D., Guevel, P., Deste, J.F., Bécu, G., Louis, F., Scott, A.J., Bardey, P., 2008a. The "BOUSSOLE" buoy-a new transparent-to-swell taut mooring dedicated to marine optics: design, tests, and performance at sea. J. Atmos. Oceanic Technol. 25, 968–989 (2008a).

Bailey, S.W., Werdell, P.J., 2006. A multi-sensor approach for the on-orbit validation of ocean color satellite data products. Remote Sens. Environ. 102, 12–23.

Bailey, S.W., Hooker, S.B., Antoine, D., Franz, B.A., Werdell, P.J., 2008. Sources and assumptions for the vicarious calibration of ocean color satellite observations. Appl. Opt. 47, 2035–2045.

Banks, A.C., Mélin, F., 2015. An assessment of cloud masking schemes for satellite ocean colour data of marine optical extremes. Int. J. Remote Sens. 36 (3), 797–821.

Barnes, B.B., Hu, C., 2016. Dependence of satellite ocean color data products on viewing angles: a comparison between SeaWiFS, MODIS, and VIIRS. Remote Sens. Environ. 175, 120–129.

Bosc, E., Bricaud, A., Antoine, D., 2004. Seasonal and interannual variability in algal biomass and primary production in the Mediterranean Sea, as derived from 4 years of SeaWiFS observations. Glob. Biogeochem. Cyles 18 (1), GB1005. http://dx.doi.org/10.1029/2003GB002034.

Brown, S.W., Flora, S.J., Feinholz, M.E., Yarbrough, M.A., Houlihan, T., Peters, D., Kim, K.Y.S., Mueller, J.L., Johnson, B.C., Clark, D.K., 2007. The Marine Optical BuoY (MOBY) radiometric calibration and uncertainty budget for ocean color satellite sensor vicarious calibration. SPIE Conference Proceedings Remote Sensing. International Society for Optics and Photonics, p. 67441M.

Bryant, C., Eleftheriadis, K., Smolik, J., Zdimal, V., Mihalopoulos, N., Colbeck, I., 2006. Optical properties of aerosols over the eastern Mediterranean. Atmos. Environ. 40 (32), 6229–6244.

Bulgarelli, B., Kiselev, V., Zibordi, G., 2014. Simulation and analysis of adjacency effects in coastal waters: a case study. Appl. Opt. 53, 1523–1545.

Chazette, P., Pelon, J., Moulin, C., Dulac, F., Carrasco, I., Guelle, W., Bousquet, P., Flamant, P.-H., 2001. Lidar and satellite retrieval of dust aerosols over the Azores during SOFIA/ASTEX. Atmos. Environ. 35 (25), 4297–4304.

Clark, D.K., Feinholz, M.E., Yarbrough, M.A., Johnson, B.C., Brown, S.W., Kim, Y.S., Barnes, R.A., 2002. Overview of the radiometric calibration of MOBY. SPIE Proceedings Earth Observing Systems VI. 4483, pp. 64–76.

Clark, D.K., Gordon, H.R., Voss, K.J., Ge, Y., Broenkow, W., Trees, C., 1997. Validation of atmospheric correction over the oceans. J. Geophys. Res. 102 (D14), 17209–17217.

Clark, D. K., Yarbrough, M. A., Feinholz, M., Flora, S., Broenkow, W., Kim, Y. S., Johnson, B. C., Brown, S. W., Yuen, M. & Mueller, J. L. (2003). A radiometric buoy for performance monitoring and vicarious calibration of satellite ocean color sensors: measurement and data analysis protocols, In Ocean Optics Protocols for Satellite Ocean Color Sensor Validation. J.L. Mueller, G.S. Fragion and V.R. McClain. (NASA/TM-2003-211621/Rev4-Vol. IV, Greenbelt, MD).

Claustre, H., Morel, A., Hooker, S.B., Babin, M., Antoine, D., Oubelkheir, K., Bricaud, A., Leblanc, K., Quéguiner, B., Maritorena, S., 2002. Is desert dust making oligotrophic waters greener? Geophys. Res. Lett. 29 (10):1469. http://dx.doi.org/10.1029/2001GL14056.

Colarco, P.R., Toon, O.B., Reid, J.S., Livingston, J.M., Russell, P.B., Redemann, J., Schmid, B., Maring, H.B., Savoie, D., Welton, E.J., Campbell, J.R., Holben, B.N., Levy, R., 2003. Saharan dust transport to the Caribbean during PRIDE: 2. Transport, vertical profiles, and deposition in simulations of in situ and remote sensing observations. J. Geophys. Res. Atmos. 108 (D19):8590. http://dx.doi.org/10.1029/2002JD002659.

Eplee, R.E., Robinson, W.D., Bailey, S.W., Clark, D.K., Werdell, P.J., Wang, M., Barnes, R.A., McClain, C.R., 2001. Calibration of SeaWiFS. II. vicarious techniques. Appl. Opt. 40, 6701–6718.

Feng, L., Hu, C., 2016. Comparison of Valid Ocean observations between MODIS Terra and Aqua over the global oceans. IEEE Trans. Geosci. Remote Sens. 54 (3), 1575–1585.

Franz, B.A., Bailey, S.W., Werdell, P.J., McClain, C.R., 2007. Sensor-independent approach to the vicarious calibration of satellite ocean color radiometry. Appl. Opt. 46, 5068–5082.

Gordon, H.R., 1987. Calibration requirements and methodology for remote sensors viewing the ocean in the visible. Remote Sens. Environ. 22, 103–126.

Gordon, H.R., 1998. In orbit calibration strategy for ocean color sensors. Remote Sens. Environ. 63, 265–278.

Gordon, H.R., Wang, M., 1994. Retrieval of water-leaving radiance and aerosol optical thickness over the oceans with SeaWiFS: a preliminary algorithm. Appl. Opt. 33, 443–452.

Gregg, W.W., 2008. Assimilation of SeaWiFS ocean chlorophyll data into a three-dimensional global ocean model. J. Mar. Syst. 69 (3), 205–225.

Gregg, W.W., Conkright, M.E., Ginoux, P., O'Reilly, J.E., Casey, N.W., 2003. Ocean primary production and climate: global decadal changes. Geophys. Res. Lett. 30 (15).

Gregg, W.W., Casey, N.W., 2004. Global and regional evaluation of the SeaWiFS chlorophyll data set. Remote Sens. Environ. 93, 463–479.
Gregg, W.W., Patt, F.S., 1994. Assessment of tilt capability for spaceborne global ocean color sensors. IEEE Trans. Geosci. Remote Sens. 32, 866–877.
Holben, B.N., Smirnov, A., Eck, T.F., Slutsker, I., Abuhassan, N., Newcomb, W.W., Schafer, S., Chatenet, B., Lavenu, F., Kaufman, Y.J., Vande Castle, J., Setzer, A., Markham, B., Clark, D., Frouin, R., Halthore, R., Karneli, A., O'Neill, N.T., Pietras, C., Pinker, R.T., Voss, K., Zibordi, G., 2001. An emerging ground-based aerosol climatology - aerosol optical depth from AERONET. J. Geophys. Res. 106 (D11), 12067–12097.
Hooker, S.B., Esaias, W.E., Feldman, G.C., Gregg, W.W., McClain, C.R., 1992. In: Hooker, S.B., Firestone, E.R. (Eds.), An Overview of SeaWiFS and Ocean Color. NASA Tech. Memo. 1992–104566 vol. 1. NASA Goddard Space Flight Center, Greenbelt, MD.
Hu, C., Feng, L., Lee, Z., Davis, C.O., Mannino, A., McClain, C.R., Franz, B.A., 2012a. Dynamic range and sensitivity requirements of satellite ocean color sensors: learning from the past. Appl. Opt. 51 (25), 6045–6062.
Hu, C., Lee, Z., Franz, B., 2012b. Chlorophyll algorithms for oligotrophic oceans: a novel approach based on three-band reflectance difference. J. Geophys. Res. Oceans 117 (C1).
Hu, C., Feng, L., Lee, Z., 2013. Uncertainties of SeaWiFS and MODIS remote sensing reflectance: implications from clear water measurements. Remote Sens. Environ. 133, 168–182.
IOCCG White Paper, 2012. International Network for Sensor Inter-comparison and Uncertainty Assessment for Ocean Color Radiometry (INSITU-OCR): Working Toward Consistency and Accuracy in the Development of Essential Climate Variables From Multiple Missions. Available at. http://www.ioccg.org/groups/INSITU-OCR_White-Paper.pdf.
Iverson, R.L., Esaias, W.E., Turpie, K., 2000. Ocean annual phytoplankton carbon and new production, and annual export production estimated with empirical equations and CZCS data. Glob. Chang. Biol. 6, 57–72.
Kalivitis, N., Gerasopoulos, E., Vrekoussis, M., Kouvarakis, G., Kubilay, N., Hatzianastassiou, N., Vardavas, I., Mihalopoulos, N., 2007. Dust transport over the eastern Mediterranean derived from total ozone mapping spectrometer, aerosol robotic network, and surface measurements. J. Geophys. Res.-Atmos. 112 (D3).
Lelieveld, J., Berresheim, H., Borrmann, S., Crutzen, P.J., Dentener, F.J., Fischer, H., Feichter, J., Flatau, P.J., Heland, J., Holzinger, R., Korrmann, R., Lawrence, M.G., Levin, Z., Markowicz, K.M., Mihalopoulos, N., Minikin, A., Ramanathan, V., de Reuss, M., Roelofs, G.J., Scheeren, H.A., Sciare, J., Schlager, H., Schultz, M., Siegmund, P., Steil, B., Stephanou, E.G., Stier, P., Traub, M., Warneke, C., Williams, J., Ziereis, H., 2002. Global air pollution crossroads over the Mediterranean. Science 298 (5594), 794–799.
Maritorena, S., d'Andon, O.H.F., Mangin, A., Siegel, D.A., 2010. Merged satellite ocean color data products using a bio-optical model: characteristics, benefits and issues. Remote Sens. Environ. 114 (8), 1791–1804.
McClain, C.R., Feldman, G.C., Hooker, S.B., 2004. An overview of the SeaWiFS project and strategies for producing a climate research quality global ocean bio-optical time series. Deep Sea Res., Part II 51 (1), 5–42.
Mélin, F., 2016. Impact of inter-mission differences and drifts on chlorophyll-*a* trend estimates. Int. J. Remote Sens. 37, 2061–2079.
Mélin, F., Zibordi, G., 2010. Vicarious calibration of satellite ocean color sensors at two coastal sites. Appl. Opt. 49, 798–810.
Mélin, F., Zibordi, G., Holben, B.N., 2013a. Assessment of the aerosol products from the SeaWiFS and MODIS ocean-color missions. IEEE Geosci. Remote Sens. Lett. 10 (5), 1185–1189.
Mélin, F., Zibordi, G., Carlund, T., Holben, B.N., Stefan, S., 2013b. Validation of SeaWiFS and MODIS aqua/terra aerosol products in coastal regions of European marginal seas. Oceanologia 55 (1), 27–51.
Mélin, F., Berthon, J.-F., Zibordi, G., 2005. Assessment of apparent and inherent optical properties derived from SeaWiFS with field data. Remote Sens. Environ. 97, 540–553.
Mélin, F., Sclep, G., Jackson, T., Sathyendranath, S., 2016. Uncertainty estimates of remote sensing reflectance derived from comparison of satellite data sets. Remote Sens. Environ. 177, 107–124.
Morel, A., Gentili, B., 2009. The dissolved yellow substance and the shades of blue in the Mediterranean Sea. Biogeosciences 6 (2625–2636):2009. http://dx.doi.org/10.5194/bg-6-2625-2009.
O'Reilly, J.E., 24 Coauthors, 2000. In: Hooker, S.B., Firestone, E.R. (Eds.), SeaWiFS Postlaunch Calibration and Validation Analyses, Part 3. NASA Tech. Memo. 2000-206892 Vol. 11. NASA Goddard Space Flight Center, p. 49.
Pace, G., Sarra, A.D., Meloni, D., Piacentino, S., Chamard, P., 2006. Aerosol optical properties at Lampedusa (central Mediterranean). 1. Influence of transport and identification of different aerosol types. Atmos. Chem. Phys. 6 (3), 697–713.
Prospero, J.M., Collard, F.X., Molinié, J., Jeannot, A., 2014. Characterizing the annual cycle of African dust transport to the Caribbean Basin and South America and its impact on the environment and air quality. Glob. Biogeochem. Cyles 28 (7), 757–773.
Ramanathan, V.C.P.J., Crutzen, P.J., Kiehl, J.T., Rosenfeld, D., 2001. Aerosols, climate, and the hydrological cycle. Science 294 (5549), 2119–2124.
Sciare, J., Oikonomou, K., Favez, O., Liakakou, E., Markaki, Z., Cachier, H., Mihalopoulos, N., 2008. Long-term measurements of carbonaceous aerosols in the eastern Mediterranean: evidence of long-range transport of biomass burning. Atmos. Chem. Phys. 8 (18), 5551–5563.
Shukla, A.K., Babu, K.N., Prajapati, R.P., Suthar, N.M., Ajai Sinha, A., Saifee, A.M., Satashia, S.N., Arul Muthiah, M., Venkatesan, R., 2013. An ocean CAL-VAL site at Kavaratti in Lakshadweep for vicarious calibration of OCM-2 and validation of geophysical products—development and operationalization. Mar. Geod. 36, 203–218.
Smirnov, A., Holben, B.N., Kaufman, Y.J., Dubovik, O., Eck, T.F., Slutsker, I., Pietras, C., Halthore, R.N., 2002. Optical properties of atmospheric aerosol in maritime environments. J. Atmos. Sci. 59 (3), 501–523.
Smirnov, A., Holben, B.N., Slutsker, I., Giles, D.M., McClain, C.R., Eck, T.F., ... Quinn, P.K., 2009. Maritime aerosol network as a component of aerosol robotic network. J. Geophys. Res.-Atmos. 114 (D6).
Smirnov, A., Holben, B.N., Dubovik, O., Frouin, R., Eck, T.F., Slutsker, I., 2003. Maritime component in aerosol optical models derived from aerosol robotic network data. J. Geophys. Res. Atmos. 108 (D1). http://dx.doi.org/10.1029/2002JD002701.
Twardowski, M.S., Claustre, H., Freeman, S.A., Stramski, D., Huot, Y., 2007. Optical backscattering properties of the "clearest" natural waters. Biogeosciences 4:1041–1058. http://dx.doi.org/10.5194/bg-4-1041-2007.
Vantrepotte, V., Mélin, F., 2011. Inter-annual variations in the SeaWiFS global chlorophyll a concentration (1997–2007). Deep Sea Res., Part I 58 (4), 429–441.
Vinoj, V., Satheesh, S.K., 2003. Measurements of aerosol optical depth over Arabian Sea during summer monsoon season. Geophys. Res. Lett. 30 (5):1263. http://dx.doi.org/10.1029/2002GL016664.
Wang, M., Gordon, H.R., 2002. Calibration of ocean color scanners: how much error is acceptable in the near infrared? Remote Sens. Environ. 82, 497–504.
Wang, M., Knobelspiesse, K.D., McClain, C.R., 2005. Study of the Sea-viewing Wide Field-of-view Sensor (SeaWiFS) aerosol optical property data over ocean in combination with the ocean color products. J. Geophys. Res. 110, D10S06. http://dx.doi.org/10.1029/2004JD004950.
Werdell, P.J., Bailey, S.W., Franz, B.A., Morel, A., McClain, C.R., 2007. On-orbit vicarious calibration of ocean color sensors using an ocean surface reflectance model. Appl. Opt. 46, 5649–5666 (2007).
World Meteorological Organization (WMO), 2011. Systematic Observation Requirements for Satellite-based Data Products for Climate 2011, Update Supplemental Details to the Satellite-based Component of the Implementation Plan for the Global Observing System for Climate in Support of the UNFCCC (2010 Update). World Meteorological Organization (Report GCOS - 154).
Yu, H., Chin, M., Bian, H., Yuan, T., Prospero, J.M., Omar, A.H., ... Zhang, Z., 2015. Quantification of trans-Atlantic dust transport from seven-year (2007–2013) record of CALIPSO lidar measurements. Remote Sens. Environ. 159, 232–249.
Zibordi, G., Berthon, J.F., Mélin, F., D'Alimonte, D., 2011. Cross-site consistent in situ measurements for satellite ocean color applications: the BiOMaP radiometric dataset. Remote Sens. Environ. 115 (8), 2104–2115.
Zibordi, G., Mélin, F., Berthon, J.-F., 2006. Comparison of SeaWiFS, MODIS, and MERIS radiometric products at a coastal site. Geophys. Res. Lett. L06617. http://dx.doi.org/10.1029/2006GL025778.
Zibordi, G., Mélin, F., Voss, K.J., Johnson, B.C., Franz, B.A., Kwiatkowska, E., Huot, J.P., Wang, M., Antoine, D., 2015. System vicarious calibration for ocean color climate change applications: requirements for in situ data. Remote Sens. Environ. 159, 361–369.

Europe Direct is a service to help you find answers to your questions about the European Union.

Freephone number (*):

00 800 6 7 8 9 10 11

(*) The information given is free, as are most calls (though some operators, phone boxes or hotels may charge you).

More information on the European Union is available on the internet (http://europa.eu).

HOW TO OBTAIN EU PUBLICATIONS

Free publications:

- one copy:
  via EU Bookshop (http://bookshop.europa.eu);
- more than one copy or posters/maps:
  from the European Union's representations (http://ec.europa.eu/represent_en.htm);
  from the delegations in non-EU countries (http://eeas.europa.eu/delegations/index_en.htm);
  by contacting the Europe Direct service (http://europa.eu/europedirect/index_en.htm) or
  calling 00 800 6 7 8 9 10 11 (freephone number from anywhere in the EU) (*).

  (*) The information given is free, as are most calls (though some operators, phone boxes or hotels may charge you).

Priced publications:

- via EU Bookshop (http://bookshop.europa.eu).

KJ-NA-28851-EN-N

JRC Mission

As the science and knowledge service of the European Commission, the Joint Research Centre's mission is to support EU policies with independent evidence throughout the whole policy cycle.

EU Science Hub
ec.europa.eu/jrc

@EU_ScienceHub

EU Science Hub - Joint Research Centre

Joint Research Centre

EU Science Hub

Publications Office

doi:10.2760/145183

ISBN 978-92-79-75340-4